USGS
science for a changing world

Prepared in cooperation with the County of Maui Department of Water Supply

Long-Term Groundwater Availability in the Waiheʻe, ʻĪao, and Waikapū Aquifer Systems, Maui, Hawaiʻi

Scientific Investigations Report 2021–5113

U.S. Department of the Interior
U.S. Geological Survey

Cover. Photograph of Waiheʻe Valley, overlooking Kahului Bay, Wailuku, and Haleakalā (mostly obscured by clouds) in the background. Photograph by Marcus Richter, Mauna Kahālāwai Watershed Partnership, 2018

Long-Term Groundwater Availability in the Waiheʻe, ʻĪao, and Waikapū Aquifer Systems, Maui, Hawaiʻi

By Kolja Rotzoll, Delwyn S. Oki, Adam G. Johnson, and William R. Souza

Prepared in cooperation with the County of Maui Department of Water Supply

Scientific Investigations Report 2021–5113

U.S. Department of the Interior
U.S. Geological Survey

U.S. Geological Survey, Reston, Virginia: 2022

For more information on the USGS—the Federal source for science about the Earth, its natural and living resources, natural hazards, and the environment—visit https://www.usgs.gov or call 1–888–ASK–USGS.

For an overview of USGS information products, including maps, imagery, and publications, visit https://store.usgs.gov.

Suggested citation:
Rotzoll, K., Oki, D.S., Johnson, A.G., and Souza, W.R., 2022, Long-term groundwater availability in the Waiheʻe, ʻĪao, and Waikapū aquifer systems, Maui, Hawaiʻi: U.S. Geological Survey Scientific Investigations Report 2021–5113, 80 p., https://doi.org/10.3133/sir20215113.

Associated data for this publication:
Rotzoll, K., 2022, SUTRA model used to evaluate long-term groundwater availability in the Waiheʻe, ʻĪao, and Waikapū aquifer systems, Maui, Hawaiʻi: U.S. Geological Survey data release, https://doi.org/10.5066/P959B45F.

ISSN 2328-0328 (online)

Acknowledgments

This study was conducted in cooperation with the County of Maui Department of Water Supply (MDWS). The authors are grateful to the following people for supplying data and contributing their expertise: Eva Blumenstein (MDWS) and Patrick Casey, Robert Chenet, and Roy Hardy (Hawai‘i Commission on Water Resource Management). Stephen B. Gingerich and Clifford I. Voss (U.S. Geological Survey) provided constructive technical reviews of the main report. Rodney A. Sheets and Heidi L. Kāne (U.S. Geological Survey) provided insightful technical reviews of the Appendix.

Contents

Acknowledgments iii
Abstract 1
Introduction 2
Purpose and Scope 2
Setting 3
Land Cover 3
Climate 3
Geology 3
Hydrogeologic Framework and Rock Properties 7
Dike-Free Volcanic Rocks 7
Dike-Intruded Volcanic Rocks 7
Sedimentary Rocks 8
Hydraulic Conductivity of the Rocks 8
Dike-Free Volcanic Rocks 8
Dike-Intruded Volcanic Rocks 8
Sedimentary Rocks 8
Effective Porosity, Specific Yield, and Specific Storage 9
Dispersivity 9
Groundwater-Flow System 9
Recharge 10
Water-Budget Recharge Estimates 10
Restored Streamflow 10
Discharge 10
Groundwater Withdrawals 10
Discharge to Streams 10
Freshwater-Lens System 11
Groundwater Levels 11
Freshwater-Lens Thickness 13
Chloride Concentration of Pumped Water 14
Dike-Impounded System 14
Simulation of Groundwater Flow 14
Model Mesh 17
Representation of the System 17
Boundary Conditions 18
Recharge 18
Withdrawals 19
Other Model Properties 22
Initial Conditions and Time Step 22
Estimation of Hydraulic Properties 22
Simulated Historical Conditions 1926–2012 (Calibration) 23
Simulated Future Scenarios 28
Scenario 1—Baseline 28
Scenario 2—Water-Use Permit Rates in ʻĪao Aquifer System, Prorated Pump Capacity in Waiheʻe and Waikapū Aquifer Systems 30

Scenario 3—28.3 Mgal/d Withdrawals from Waiheʻe, ʻĪao, and Waikapū Aquifer System Production Wells 33
Scenario 4—26.9 Mgal/d Withdrawals from Waiheʻe, ʻĪao, and Waikapū Aquifer System Production Wells 35
Scenario 5—27.5 Mgal/d Withdrawals from Waiheʻe, ʻĪao, and Waikapū Aquifer System Production Wells 37
Scenario 6—27.2 Mgal/d Withdrawals from Waiheʻe, ʻĪao, and Waikapū Aquifer System Production Wells 39
Scenario 7—Withdrawals as Scenario 4 and Future Recharge 42
Implications of Scenarios 44
Limitations 44
Summary 44
References Cited 46
Appendix 1. Estimation of Recharge with a Water Budget 49

Figures

1. Map showing location of study area, selected geographic features, wells used in this study, and aquifer systems delineated by the Hawaiʻi Commission on Water Resource Management, central Maui, Hawaiʻi 4
2. Map showing central Maui, Hawaiʻi, average rainfall distribution during 1920–2012 and annual rainfall over Waikapū, ʻĪao, and Waiheʻe aquifer systems 5
3. Generalized surficial geology and geologic features in the study area showing central Maui, Hawaiʻi, and structural contours of the top of Honomanū Basalt/Kula Volcanics and Wailuku Basalt. 6
4. Graphs showing annual reported groundwater withdrawals during 1940–2018 from the Waiheʻe, ʻĪao, and Waikapū aquifer systems, central Maui, Hawaiʻi 11
5. Map showing measured groundwater levels on September 15, 2015, and graphs showing measured groundwater levels in selected wells in the Wailuku area, central Maui, Hawaiʻi 12
6. Graphs showing selected salinity profiles in selected wells in the Wailuku area, central Maui, Hawaiʻi 13
7. Chloride concentration of pumped water from selected wells during 1970–2018 in the Wailuku area, central Maui, Hawaiʻi 15
8. Map showing hydraulic-conductivity zones for the volcanic rocks, sediments, and boundary-condition nodes in the three-dimensional numerical groundwater model, central Maui, Hawaiʻi 16
9. Vertical cross section of model mesh showing geologic units and boundary features 17
10. Simulated water level and 50-percent ocean-water salinity surface altitude in the study area at the end of the historical simulation, central Maui, Hawaiʻi 23
11. Simulated changes in water level and 50-percent ocean-water salinity surface altitude in the study area between 1926 and 2012, central Maui, Hawaiʻi 24
12. Graphs showing measured and simulated groundwater levels at selected wells during 1930–2016 in the Wailuku area, central Maui, Hawaiʻi. 25
13. Measured and simulated salinity profiles in selected wells in the Wailuku area, central Maui, Hawaiʻi 26
14. Graphs showing measured and simulated chloride concentration of pumped water from selected wells during 1970–2012 in the Wailuku area, central Maui, Hawaiʻi 27

15. Simulated change in water level and 50-percent ocean-water salinity surface altitude in the study area for scenario 1 relative to the end of the historical simulation, central Maui, Hawai‘i 30
16. Withdrawal rates and simulated chloride concentrations of pumped water from wells included in scenario 1 31
17. Simulated change in water level and 50-percent ocean-water salinity surface altitude in the study area for scenario 2 relative to scenario 1 32
18. Withdrawal rates and simulated chloride concentrations of pumped water from wells included in scenario 2, central Maui, Hawai‘i 33
19. Simulated change in water level and 50-percent ocean-water salinity surface altitude in the study area for scenario 3 relative to scenario 1, central Maui, Hawai‘i 34
20. Withdrawal rates and simulated chloride concentrations of pumped water from wells included in scenario 3, central Maui, Hawai‘i 35
21. Simulated change in water level and 50-percent ocean-water salinity surface altitude in the study area for scenario 4 relative to scenario 1, central Maui, Hawai‘i. 36
22. Withdrawal rates and simulated chloride concentrations of pumped water from wells included in scenario 4, central Maui, Hawai‘i 37
23. Simulated change in water level and 50-percent ocean-water salinity surface altitude in the study area for scenario 5 relative to scenario 1, central Maui, Hawai‘i 38
24. Withdrawal rates and simulated chloride concentrations of pumped water from wells included in scenario 5, central Maui, Hawai‘i 39
25. Simulated change in water level and 50-percent ocean-water salinity surface altitude in the study area for scenario 6 relative to scenario 1, central Maui, Hawai‘i 40
26. Withdrawal rates and simulated chloride concentrations of pumped water from wells included in scenario 6, central Maui, Hawai‘i 41
27. Simulated change in water level and 50-percent ocean-water salinity surface altitude in the study area for scenario 7 relative to scenario 1, central Maui, Hawai‘i. 42
28. Withdrawal rates and simulated chloride concentrations of pumped water from wells included in scenario 7, central Maui, Hawai‘i 43

Appendix Figures

1.1. Generalized water-budget flow diagrams for non-forest and forest land covers 49
1.2. Map of water-budget study area for the water-budget calculations and boundaries of sixteen aquifer systems on Maui, Hawai‘i 50
1.3. Maps of generalized land cover for water-budget study area on Maui, Hawai‘i 52
1.4. Graph of the percentage of 444-square-mile water-budget study area on Maui, Hawai‘i mapped as sugarcane, agriculture other than sugarcane, developed land cover, and other land cover for eight periods between 1926 and 2017 60
1.5. Graph of crop coefficients used in the water-budget calculation for different growth stages of sugarcane during its 24-month cultivation cycle 62
1.6. Map of septic-effluent rates used in the water-budget calculations for 2010–12 and for parts of census county subdivisions within the water-budget study area on Maui, Hawai‘i 64
1.7. Maps of drainage basins of selected stream-gaging stations and summary statistics of runoff-to-rainfall ratios used in the water-budget calculations for the water-budget study area on Maui, Hawai‘i 66
1.8. Maps of the water-budget study area on Maui, Hawai‘i, showing the distribution of mean annual recharge 74

Tables

1. Recharge input to the boundary-inflow zones shown in figure 8 of the three-dimensional model mesh, central Maui, Hawai‘i 19
2. Values of top and bottom altitudes of open well interval used in the three-dimensional numerical groundwater model, central Maui, Hawai‘i 19
3. Withdrawal rates used in the modeled scenarios for selected production wells in the Waihe‘e, ‘Īao, and Waikapū aquifer systems, central Maui, Hawai‘i 29

Appendix Tables

1.1. Decennial populations for census county subdivisions on Maui, Hawai‘i, 1920–2010 65
1.2. Periods of record used to compute observed seasonal runoff-to-rainfall ratios for drainage basins of selected stream-gaging stations in the water-budget study area on Maui, Hawai‘i, 1926–2012 69
1.3. Selected land-cover parameters used in the water-budget calculations for the water-budget study area on Maui, Hawai‘i 71
1.4. Mean annual water-budget components for the water-budget study area on Maui, Hawai‘i, for nine historical periods between 1926 and 2012 and a hypothetical scenario 73
1.5. Mean annual recharge estimates for 16 aquifers systems in the water-budget study area on Maui, Hawai‘i, for nine historical periods between 1926 and 2012 and for a hypothetical scenario 77

Conversion Factors

U.S. customary units to International System of Units

Multiply	By	To obtain
	Length	
inch (in.)	25.4	millimeter (mm)
foot (ft)	0.3048	meter (m)
mile (mi)	1.609	kilometer (km)
	Area	
square foot (ft^2)	0.09290	square meter (m^2)
square inch (in^2)	6.452	square centimeter (cm^2)
square mile (mi^2)	2.590	square kilometer (km^2)
	Volume	
gallon (gal)	3.785	liter (L)
million gallons (Mgal)	3,785	cubic meter (m^3)
	Flow rate	
foot per day (ft/d)	0.3048	meter per day (m/d)
cubic foot per second (ft^3/s)	0.02832	cubic meter per second (m^3/s)
gallon per minute (gal/min)	0.06309	liter per second (L/s)
gallon per day (gal/d)	0.003785	cubic meter per day (m^3/d)
million gallons per day (Mgal/d)	0.04381	cubic meter per second (m^3/s)
	Mass	
pound, avoirdupois (lb)	0.4536	kilogram (kg)
	Pressure	
atmosphere, standard (atm)	101.3	kilopascal (kPa)
bar	100	kilopascal (kPa)
pound per square foot (lb/ft^2)	0.04788	kilopascal (kPa)
pound per square inch (lb/in^2)	6.895	kilopascal (kPa)
	Density	
pound per cubic foot (lb/ft^3)	16.02	kilogram per cubic meter (kg/m^3)
	Hydraulic conductivity	
foot per day (ft/d)	0.3048	meter per day (m/d)
	Hydraulic gradient	
foot per mile (ft/mi)	0.1894	meter per kilometer (m/km)
	Dynamic viscosity	
Slug per foot per second (slug/ft/s)	47.88	Pascal-sec (Pa-s)

Temperature in degrees Celsius (°C) may be converted to degrees Fahrenheit (°F) as follows:

$$°F = (1.8 \times °C) + 32.$$

Temperature in degrees Fahrenheit (°F) may be converted to degrees Celsius (°C) as follows:

$$°C = (°F - 32) / 1.8.$$

Datum

Vertical coordinate information is referenced to local mean sea level.

Horizontal coordinate information is referenced to the North American Datum of 1983 (NAD 83).

Altitude, as used in this report, refers to distance above the vertical datum.

Supplemental Information

Specific conductance is given in microsiemens per centimeter at 25 degrees Celsius (µS/cm at 25°C).

Concentrations of chemical constituents in water are given in milligrams per liter (mg/L).

State well numbers used by the Hawai'i Commission on Water Resource Management include three digits after the hyphen. For this report, the first digit after the hyphen is invariably zero and was omitted.

Abbreviations

ET	evapotranspiration
MDWS	Maui Department of Water Supply
CWRM	Hawai'i Commission on Water Resource Management
RCP8.5	Representative Concentration Pathway warming scenario during 2071–99 with total radiative forcing of 8.5 Watts per square meter
USGS	U.S. Geological Survey
EPA	U.S. Environmental Protection Agency
TDS	total dissolved solids

Long-Term Groundwater Availability in the Waiheʻe, ʻĪao, and Waikapū Aquifer Systems, Maui, Hawaiʻi

By Kolja Rotzoll, Delwyn S. Oki, Adam G. Johnson, and William R. Souza

Abstract

Groundwater levels have declined since the 1940s in the Wailuku area of central Maui, Hawaiʻi, on the eastern flank of West Maui volcano, mainly in response to increased groundwater withdrawals. Available data since the 1980s also indicate a thinning of the freshwater lens and an increase in chloride concentrations of pumped water from production wells. These trends, combined with projected increases in demand for groundwater in central Maui, have led to concerns over groundwater availability and have highlighted a need to improve general understanding of the hydrologic effects of proposed groundwater withdrawals in the Waiheʻe, ʻĪao, and Waikapū areas of central Maui.

A numerical groundwater model was constructed to simulate the flow and salinity of groundwater in central Maui. The model simulates the effects of changes in groundwater withdrawals and recharge on water levels, freshwater-lens thicknesses, and chloride concentrations of pumped water from production wells. The model incorporates updated water-budget estimates of groundwater recharge from infiltration and direct recharge, seepage in stream channels, and inflow from inland areas. Mean annual groundwater recharge from infiltration and direct recharge was estimated using a daily water-budget model and the most current data, including the distributions of monthly rainfall and potential evapotranspiration, for the study area for nine historical periods from 1926 through 2012: 1926–69, 1970–79, 1980–84, 1985–89, 1990–94, 1995–99, 2000–04, 2005–09, and 2010–12. The water-budget model also estimated groundwater recharge based on one hypothetical scenario that used 1980–2010 rainfall and 2017 land cover. For the nine historical periods, estimated recharge from infiltration and direct recharge within the area of the groundwater model ranged from 30.4 million gallons per day (Mgal/d) during 2010–12 to 98.7 Mgal/d during 1926–69. Variability in recharge during these periods mainly reflects changes in rainfall and irrigation over time. Between 2010 and 2014, streamflow restoration in previously diverted streams resulted in an estimated increase in recharge from seepage in stream channels of about 12.5 Mgal/d. Average groundwater inflow of about 39.6 Mgal/d from inland, dike-intruded areas to the main area of interest was estimated from an existing island-wide numerical groundwater-flow model, which is at a larger scale and incorporates a greater number of simplifying assumptions.

The numerical groundwater model developed for this study was calibrated to 1926–2012 transient water levels, vertical salinity profiles, and chloride concentrations of water pumped by production wells in the study area. The model was then used to evaluate one future recharge and six selected withdrawal scenarios, developed in consultation with the Maui Department of Water Supply, in terms of long-term changes in water level and 50-percent ocean-water salinity surface. The groundwater model was also used to simulate the future salinity of water withdrawn by existing and proposed production wells. The simulations were run to steady-state conditions, providing an estimate of the long-term effects of changes in withdrawal and recharge on the groundwater resource. Results of the simulated future withdrawal scenarios indicate that, relative to 2017–18 rates, the scenarios' long-term effect of increased withdrawals ultimately leads to lower water levels and a higher 50-percent ocean-water salinity surface indicating a thinning of the freshwater lens. Results also indicate that the increased withdrawals produce some groundwater with chloride concentration below 250 milligrams per liter and some groundwater with higher chloride concentration. The amount of drawdown near production wells and the quality of water withdrawn from production wells is dependent on the rate and spatial distribution of the withdrawals.

The model was also used to evaluate how groundwater availability may be affected for a drier recharge scenario based on a published study of future climate. Model results of the future recharge scenario indicate that the rate of groundwater recharge is a controlling factor for (1) water levels, (2) the 50-percent ocean-water salinity surface, and (3) the quality of water withdrawn from production wells in the Wailuku area. Coupled with reduced groundwater recharge (with all other factors remaining equal), the modeled future withdrawals in the scenario would tend to cause lower water levels, a higher 50-percent ocean-water salinity surface, and increased salinity of water withdrawn from production wells.

The three-dimensional numerical groundwater model developed for this study utilizes the latest available hydrologic and geologic information and is a useful tool for understanding

the long-term hydrologic effects of additional groundwater withdrawals in central Maui. The model has several limitations, including its non-uniqueness and inability to account for local-scale heterogeneities. Short-term effects of changes in recharge and withdrawals—and optimization of pumping rates to meet increased demand for water with acceptable salinity—are possible conditions for future simulation analyses.

Introduction

The resident population on the island of Maui, Hawaiʻi, has increased 273 percent from 38,691 in 1970 to 144,444 in 2010 and is expected to increase another 35 percent from the 2010 population to about 195,000 in 2030 (County of Maui, 2012). Groundwater demand for domestic water supply also has increased, and groundwater withdrawals will likely continue to increase in the future in response to the increasing population. Demand for water provided by the County of Maui Department of Water Supply (MDWS) in the central Maui distribution area is expected to increase by 53 percent from about 21.2 million gallons per day (Mgal/d) in 2014 to 32.3 Mgal/d in 2035 (Maui County Department of Water Supply, 2019).

For management purposes, the State of Hawaiʻi Commission on Water Resource Management (CWRM) has divided the island of Maui into 25 management areas called aquifer systems. The aquifer-system boundaries do not necessarily coincide with hydrogeologic barriers to groundwater flow (Mink and Lau, 1990). The Wailuku area of central Maui includes the Waiheʻe, ʻĪao, and Waikapū aquifer systems (fig. 1), which are potential source areas for meeting additional water demand on Maui. New water-supply wells are planned in all three aquifer systems. However, development of additional water supply from wells in the area may lead to increased salinity of water withdrawn from existing and planned wells due to saltwater intrusion into the aquifer systems.

In a freshwater-lens aquifer system, increased withdrawals from the freshwater lens will, in the long term, result in a decline in water levels, a rise in the transition zone between freshwater and saltwater, and a reduction of natural groundwater discharge. Increased withdrawals will ultimately decrease groundwater discharge to the ocean and to low-altitude streams. Increased withdrawals may also cause increased salinity of water withdrawn from wells penetrating the freshwater lens. This study of groundwater availability in the Waiheʻe, ʻĪao, and Waikapū aquifer systems uses a refined and updated version of a previously developed numerical groundwater flow and transport model of the Wailuku area (Gingerich, 2008) to evaluate the effects of additional withdrawals on water levels and salinities of water withdrawn by wells in the study area.

The existing numerical groundwater model (Gingerich, 2008), which used groundwater-recharge estimates from Engott and Vana (2007), was refined and updated for this study to reflect recent hydrologic changes in the area and hydrologic information not previously available. Recent or planned changes that affect hydrologic conditions in the study area include: (1) restoration of about 25 Mgal/d of surface water to streams starting in 2010, which resulted in additional groundwater recharge from stream reaches that lose water; (2) the 2016 shutdown of Shaft 33 (5330–05), which was an important well that had been producing water for about 70 years and which produced on average about 5 Mgal/d in the last 25 years before the shutdown; (3) cessation of sugarcane cultivation in central Maui at the end of 2016, which resulted in reduced irrigation, reduced groundwater recharge in the areas of cultivation, and reduced groundwater withdrawals; and (4) groundwater withdrawal from new and planned wells. Hydrologic information that has become available recently includes: (1) updated groundwater recharge estimates developed using the latest water-budget methods, recently available climate information, and relevant land-cover conditions (Johnson and others, 2018; appendix 1) and recharge estimates for future conditions (Mair and others, 2019); (2) vertical salinity-profile data from deep monitor wells; and (3) a synoptic water-level survey from September 15, 2015, using 22 new and existing wells in the Waiheʻe, ʻĪao, and Waikapū areas (U.S. Geological Survey, 2019). This new hydrologic information provides insight into hydrogeologic conditions in the Wailuku area, including a better understanding of the barrier affecting the north-to-south flow of water between the ʻĪao and Waikapū aquifer systems.

Purpose and Scope

The objective of this study is to characterize the long-term effects of seven future withdrawal and recharge scenarios for the Waiheʻe, ʻĪao, and Waikapū aquifer systems of west Maui on water levels, the depth of the transition zone between freshwater and saltwater, and salinity of water withdrawn by wells. The purpose of this report is to describe an evaluation of groundwater availability in terms of water levels and salinity from production wells in central Maui, Hawaiʻi, for the selected withdrawal scenarios.

Groundwater levels and salinity in central Maui were estimated with a three-dimensional numerical groundwater model capable of simulating density-dependent flow and salinity transport. Estimates of groundwater recharge from beneath the soil root zone, needed as input to the numerical groundwater model, were made using a daily water budget for ten selected subperiods during 1926−2012 and the most current available data, including the distributions of monthly rainfall and potential evapotranspiration (Giambelluca and others, 2013; Giambelluca and others, 2014; Frazier and others, 2016). A two-dimensional, sharp-interface groundwater-flow model covering the entire island (Izuka and others, 2021) was used to estimate subsurface inflows at the boundaries of the updated central Maui groundwater model. Aquifer hydraulic properties for the numerical groundwater model were estimated by trial and error using available water-level and salinity information. Simulated withdrawal scenarios were selected in consultation with MDWS and include: (1) a baseline scenario using average groundwater

recharge (1980−2010 rainfall and 2017 land cover) and average groundwater withdrawals (2017−18); (2) a scenario using average groundwater recharge and withdrawals from existing wells (as of 2019) with simulated withdrawal rates equal to CWRM water-use permit rates; (3) four scenarios using average recharge and selected withdrawals from existing and proposed new wells; and (4) a scenario using reduced recharge and one of the withdrawal scenarios from item (3). The reduced recharge incorporates rainfall projections for a Representative Concentration Pathway warming scenario during 2071–99 with total radiative forcing of 8.5 Watts per square meter (RCP8.5) by the year 2100 and 2017 land cover (Mair and others, 2019).

Setting

The island of Maui is the second largest of the Hawaiian Islands and occupies an area of about 727 square miles (mi^2) (Juvik and Juvik, 1998) between latitude 20°30'–21°05' N and longitude 156°45'–155°55' W (fig. 1). The island is composed mainly of two shield volcanoes (Stearns and Macdonald, 1942): the older West Maui volcano, which rises to an altitude of 5,788 feet (ft) at Puʻu Kukui, and the younger East Maui volcano (Haleakalā), which rises to an altitude of 10,023 ft (Juvik and Juvik, 1998). The two volcanoes are connected by a central isthmus, generally at altitudes less than 300 ft, which is covered with terrestrial and marine sedimentary deposits that have widths up to 5 miles across (Stearns and Macdonald, 1942).

West Maui volcano has been deeply dissected by numerous streams and rivers, including Waikapū Stream and Wailuku[1] and Waiheʻe Rivers. These streams and rivers originate from near the summit of West Maui volcano and flow perennially in their upper reaches because they receive groundwater discharge. The main study area includes the Waiheʻe, ʻĪao, and Waikapū aquifer systems (fig. 1) in the eastern part of West Maui volcano, although areas external to these three aquifer systems are included as part of the numerical groundwater model developed for this study.

Land Cover

Above an altitude of about 600 ft in the study area, forested areas, shrubland, and grassland dominate the landscape. Most of the developed areas in the study area are below an altitude of 300 ft near Kahului, Wailuku, and Waiehu. Throughout much of the 20th century, sugarcane was cultivated in central Maui below an altitude of about 600 ft. Irrigation water for sugarcane was primarily drawn from surface-water sources from east and west Maui streams and secondarily from groundwater sources. Starting in about the 1980s, macadamia nut orchards replaced sugarcane in the northeastern part of the ʻĪao aquifer system. Sugarcane cultivation ceased altogether at the end of 2016, which led to substantial hydrologic changes. For example, irrigation and recharge decreased in areas that no longer were used for sugarcane cultivation. A detailed description of the land-cover changes can be found in appendix 1.

Climate

The climate on Maui is generally characterized by mild temperatures, cool and persistent trade winds, a rainy winter season from October through April, and a dry summer season from May through September (Blumenstock and Price, 1967; Sanderson, 1993). The climate is controlled mainly by topography, the position of the North Pacific anticyclone, and migratory weather systems relative to the island. Annual air temperatures recorded at the Kahului Airport in north-central Maui during 1905–2016 ranged from 67 to 84 °F and averaged 76 °F (Western Regional Climate Center, 2019). During the dry season, persistent northeasterly winds, known locally as trade winds, blow from 80 to 95 percent of the time. During the rainy season, trade winds are less persistent and blow from 50 to 80 percent of the time. Migratory weather systems can bring heavy rains to the island. The dry coastal areas receive much of their rainfall as a result of these systems.

Average annual rainfall during 1920–2012 in west and central Maui ranged from less than 15 inches (in.) near southern coastal areas to more than 330 in. near the summit of West Maui volcano (fig. 2; Frazier and others, 2016). The spatial pattern of rainfall is controlled by the orographic lifting of moisture-laden northeasterly trade winds along the windward slope of West Maui volcano. The moisture-laden air mass cools as it ascends the slopes of the volcano, resulting in condensation, cloud formation, and high rainfall near the topographic crest of the West Maui volcano. Southern coastal areas of west Maui are considerably drier because these areas are in the rain shadows of Haleakalā and West Maui volcano on the leeward side of the island. In the area defined by the Waiheʻe, ʻĪao, and Waikapū aquifer systems, annual rainfall during 1920–2012 varied temporally between 36 and 127 in. and generally increased spatially in a northerly direction, from the Waikapū aquifer system to the Waiheʻe aquifer system. Average annual rainfall during 1920–2012 over the Waiheʻe, ʻĪao, and Waikapū aquifer systems was 73 in. (Frazier and others, 2016).

Above an altitude of about 2,000 ft (fig. 2), rainfall is supplemented by fog drip. Fog drip is a combination of water vapor and precipitation (not measured by rain gages) that is intercepted by vegetation and subsequently drips to the ground surface. Johnson and others (2018) used available information to estimate annual fog drip on windward areas of Maui to be 30 in.

Geology

The geology of Maui has been documented in numerous publications (Stearns and Macdonald, 1942; Yamanaga and Huxel, 1970; Macdonald and others, 1983; Langenheim and

[1]The U.S. Board on Geographic Names approved the name change from ʻĪao Stream to Wailuku River on November 12, 2015.

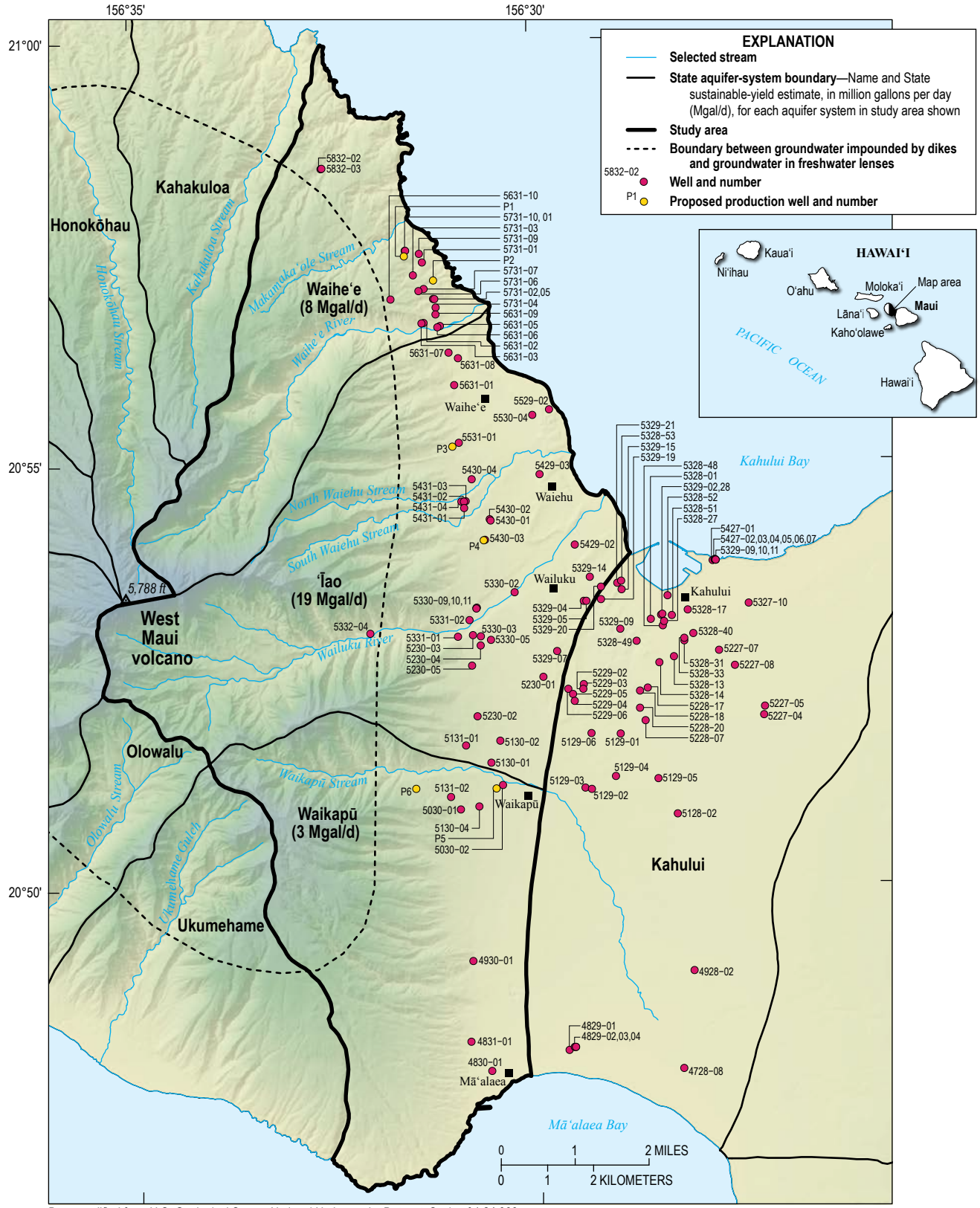

Base modified from U.S. Geological Survey National Hydrography Dataset, Scale of 1:24,000
Shaded relief from U.S. Geological Survey digital elevation model data
Universal Transverse Mercator Projection, Zone 4
North American Datum of 1983

Figure 1. Map showing location of study area, selected geographic features, wells used in this study, and aquifer systems delineated by the Hawai‘i Commission on Water Resource Management, central Maui, Hawai‘i.

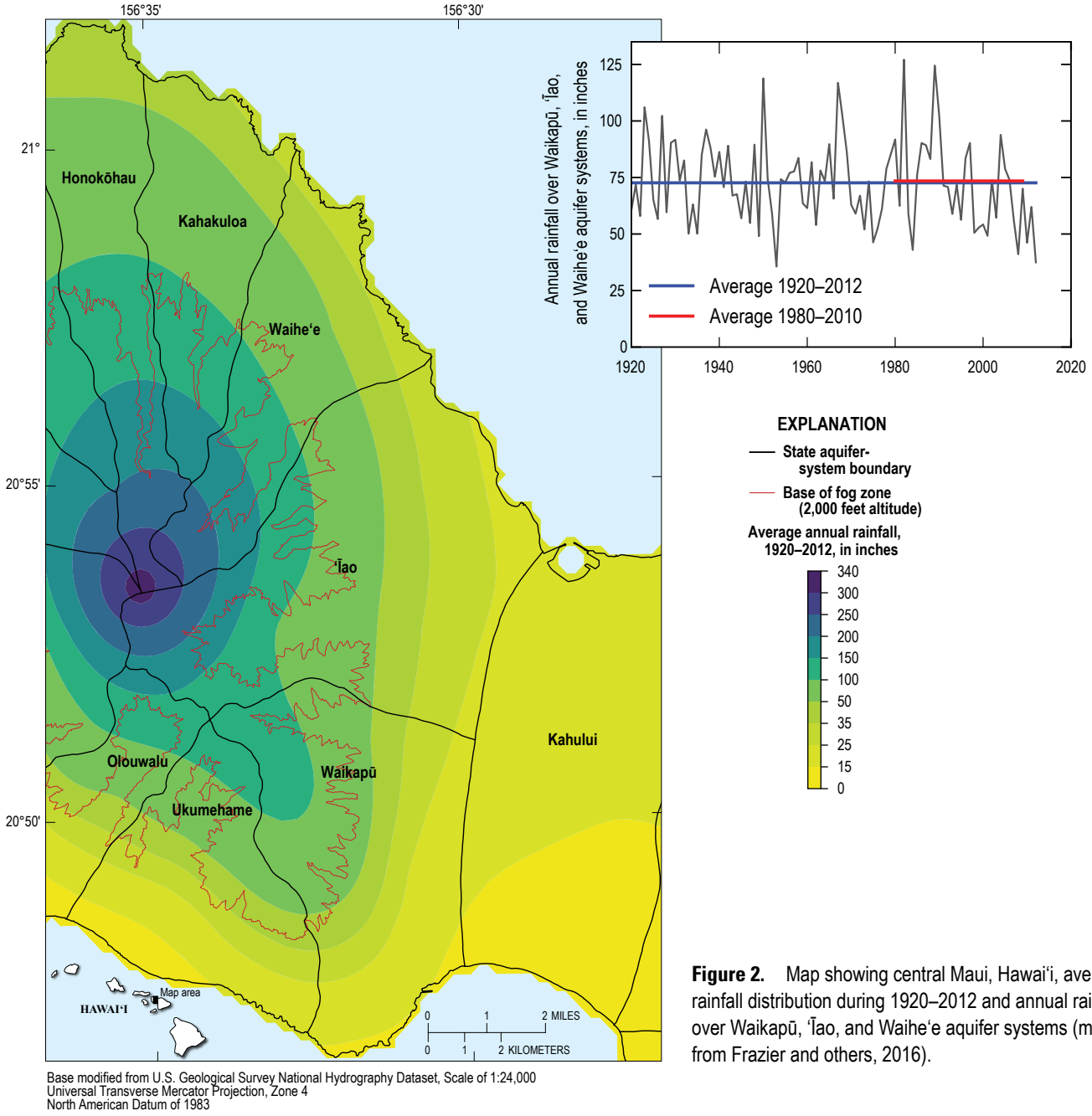

Base modified from U.S. Geological Survey National Hydrography Dataset, Scale of 1:24,000
Universal Transverse Mercator Projection, Zone 4
North American Datum of 1983

Figure 2. Map showing central Maui, Hawai'i, average rainfall distribution during 1920–2012 and annual rainfall over Waikapū, 'Īao, and Waihe'e aquifer systems (modified from Frazier and others, 2016).

Clague, 1987; Sherrod and others, 2007; Izuka and others, 2018) and is briefly summarized here. The rocks of West Maui volcano consist of mostly shield-stage Wailuku Basalt, which is overlain by the post-shield stage Honolua Volcanics and rejuvenated-stage Lahaina Volcanics. The rocks of Haleakalā consist mainly of shield-stage Honomanū Basalt, which is mainly overlain by a thin layer of post-shield stage Kula Volcanics (fig. 3).

The shield stage of volcanic activity represents the most voluminous phase of eruptive activity, during which more than 95 percent of the volcano was formed, mainly by thousands of relatively thin lava flows. Individual lava flows of the shield-stage Wailuku Basalt range in thickness from about 1 to 100 ft, averaging about 15 ft, and dip from 5 to 20 degrees away from their sources (Stearns and Macdonald, 1942). In the central isthmus area, Wailuku Basalt is buried by Honomanū Basalt, Kula Volcanics, and sedimentary deposits (interbedded and at the surface). The original surface of Wailuku Basalt beneath the isthmus can be estimated by projecting the slope of the exposed rocks westward (fig. 3; Gingerich, 2008; Izuka and others, 2018).

The post-shield stage of West Maui volcano is marked by a change in lava chemistry and character that led to the formation of massive lava flows. A sparse red soil as thick

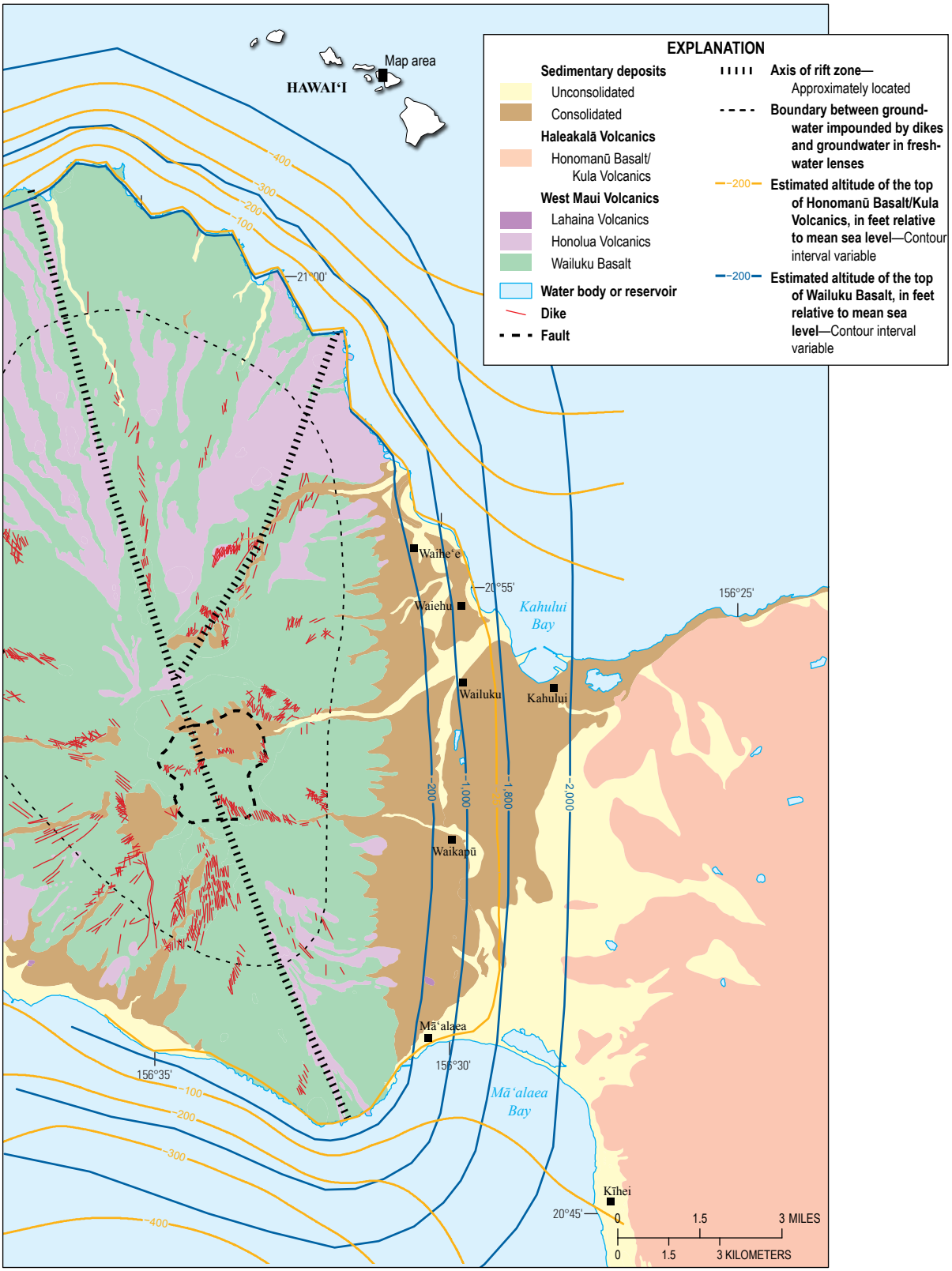

Base modified from U.S. Geological Survey National Hydrography Dataset, Scale of 1:24,000
Universal Transverse Mercator Projection, Zone 4
North American Datum of 1983

Figure 3. Generalized surficial geology and geologic features in the study area (modified from Sherrod and others, 2007) showing central Maui, Hawai‘i, and structural contours of the top of Honomanū Basalt/Kula Volcanics and Wailuku Basalt (modified from Gingerich, 2008; Izuka and others, 2018).

as 5 ft may separate older shield-stage Wailuku Basalt from post-shield stage Honolua Volcanics in places. Individual lava flows of Honolua Volcanics are thicker than those of the Wailuku Basalt and form an incomplete veneer over Wailuku Basalt. Individual lava flows of Honolua Volcanics range in thickness from about 25 to 300 ft, averaging about 75 ft, and dip from 3 to 20 degrees depending on preexisting slopes over which they flowed (Stearns and Macdonald, 1942). The Lahaina Volcanics within the study area is limited to basanite vent deposits near the southeastern part of the Waikapū aquifer system.

Most of the shield- and post-shield stage rocks were erupted from the summit and rift zones (fig. 3). The location of the former summit caldera was identified in the head of Wailuku River valley (otherwise known as ʻĪao Valley) by the presence of breccia, dense horizontal caldera-filling lavas, intrusive structures, hydrothermal alteration, and other features indicative of shield-volcano calderas (Stearns and Macdonald, 1942). Two major rift zones, marked by lines of post-shield cones extending to the northwest and southeast of the caldera, have contributed to the elongation of the shield in those directions.

Erosion has exposed hundreds of dikes in the valleys of West Maui volcano (fig. 3) and thousands of dikes that have yet to be exposed likely exist (Stearns and Macdonald, 1942; Sherrod and others, 2007). Gravity surveys show an anomaly consistent with the presence of intrusive rocks in the central region of the volcano (Kinoshita and Okamura, 1965; Flinders and others, 2013). Intrusive volcanic rocks include near-vertical dikes that formed when magma cooled below the ground surface. The rift zones contain thousands of dikes, with the number increasing toward the caldera and with depth. Additional dikes exist outside the general trends of the rift zones, creating a radial pattern of dikes emanating from the caldera (Macdonald and others, 1983).

The original form of West Maui volcano has been deeply carved by streams radiating from the summit (fig. 1). The largest valleys and canyons are thousands of feet deep. Some of the material eroded from the valleys form large alluvial fans that skirt the volcano, particularly along its margin with the isthmus. Alluvium also partially fills some valleys. The processes of coastal sedimentation and erosion were controlled by sea-level fluctuations during the Pleistocene. These changes in sea level removed soil and cut sea cliffs at some times and locations and caused the deposition of marine sediments, calcareous sand dunes (now consolidated), and gravel terraces at other times and locations. Stearns and Macdonald (1942) classified the sedimentary rocks of Maui into consolidated earthy deposits (older alluvium), calcareous sand dunes, and unconsolidated deposits. The sediments of greatest hydrologic significance are the old, consolidated sediments, which were created during the period of extensive erosion that carved deep valleys in the original volcanoes. Consolidated sediments form deposits in deeply incised valleys and beneath the isthmus of Maui and are hydrologically important because of their relatively low permeability. The valley-fill deposits and underlying weathered rock have been shown to be important features impeding northward and southward groundwater flow from the ʻĪao aquifer system (Gingerich, 2008).

Hydrogeologic Framework and Rock Properties

The three main hydrogeologic units in the study area are (1) the shield-stage, dike-free volcanic rocks from which groundwater is commonly developed and where groundwater levels are less than a few tens of feet above sea level; (2) the dike-intruded rocks where groundwater levels can exceed hundreds of feet above sea level; and (3) the sedimentary rocks and weathered rocks that tend to impede groundwater flow (for example, Izuka and others, 2018). The dike-free volcanic rocks tend to occur below an altitude of about 1,000 ft in the study area. Dike-intruded rocks of West Maui volcano mainly occur in interior areas above an altitude of 1,000 ft, although dikes and vents are also mapped near the coast. Sedimentary rocks cover the dike-free volcanic rocks below an altitude of about 600 ft and occur in stream valleys. In these valleys, sedimentary rocks may be underlain by weathered volcanic rocks and form barriers to lateral groundwater flow through the dike-free volcanic rocks.

Dike-Free Volcanic Rocks

Dike-free volcanic rocks occur on Maui in the form of extrusive lava flows. In general, lava flows that erupted from rift zones during the shield stage of West Maui volcano are about 15 ft thick and are composed either of pāhoehoe, which is characterized by smooth or ropy surfaces, or ʻaʻā, which contains a massive central core sandwiched between rubbly clinker layers (Wentworth and Macdonald, 1953). ʻAʻā flows are typically more abundant at greater distances from eruptive sources (Lockwood and Lipman, 1987). The main developed aquifers of Maui are formed by shield-stage, dike-free volcanic rocks. The post-shield stage Honolua Volcanics overlie shield-stage, dike-free volcanic rocks in parts of the study area and, due to lower permeability, may impede groundwater discharge from the shield-stage, dike-free volcanic rocks, particularly along the northeastern coast of West Maui volcano.

Dike-Intruded Volcanic Rocks

Dikes are thin, near-vertical sheets of dense intrusive volcanic rock that formed when rising magma cut through existing rock and cooled beneath the land surface. Dikes are an important hydrologic control on groundwater because they have low permeability and tend to impede the lateral flow of groundwater, causing groundwater levels to build up behind them. Dikes are commonly exposed by erosion in stream

valleys of older volcanoes (see Takasaki and Mink, 1985), including West Maui volcano. In the central part of a rift zone, dikes can number as many as 1,000 per mile of horizontal distance and compose 10 percent or more of the total rock volume. The central part of a rift zone, where dikes compose 10 percent or more of the total rock volume, is commonly referred to as a dike complex. The number of dikes decreases toward the outer edges of a rift zone within the marginal dike zone, where dikes generally compose less than 5 percent of the total rock volume (Takasaki and Mink, 1985). Wentworth and Macdonald (1953) estimated that 200 dikes are needed to vertically build 1,000 ft of a shield volcano.

Sedimentary Rocks

The sedimentary rocks on Maui are hydrologically important because they tend to impede groundwater flow within and discharge from the dike-free volcanic rocks. Consolidated older alluvium in coastal areas and stream valleys and weathered rocks below the sedimentary rocks are important controls on groundwater flow. Where sedimentary rocks overlie dike-free volcanic rocks near the coast, they form what is known as a caprock, which causes groundwater levels in the dike-free volcanic rocks to be higher than they would be in the absence of a caprock. In stream valleys, sedimentary deposits and underlying weathered rocks can penetrate into the dike-free volcanic rocks, forming valley-fill barriers that affect lateral groundwater flow where the barrier penetrates into the aquifer (Palmer, 1927; Palmer, 1946; Oki, 2005).

Hydraulic Conductivity of the Rocks

Hydraulic conductivity and permeability are quantitative measures of the capacity of a rock to transmit water. The term "permeability" also commonly is used to indicate the ease of fluid movement through a porous rock in a qualitative sense (see Domenico and Schwartz, 1990). The permeability of volcanic rocks depends on several factors, including the presence of clinker zones, voids, fractures, and lava tubes; extent of weathering; and the mode of emplacement.

Dike-Free Volcanic Rocks

In a layered sequence of subaerial, shield-stage lava flows of a Hawaiian volcano, where dike intrusions are absent, the overall permeability generally is high. The main features of lava flows contributing to the high permeability are (1) clinker zones associated with ʻaʻā flows, (2) voids along the contacts between flows, (3) cooling joints normal to flow surfaces, and (4) lava tubes associated with pāhoehoe flows. On the basis of a two-dimensional numerical-model analysis, Izuka and others (2021) estimated the hydraulic conductivity of the dike-free volcanic rocks in the main study area to be 1,600 feet per day (ft/d). On the basis of a three-dimensional numerical-model analysis, Gingerich (2008) estimated the horizontal hydraulic conductivity of the shield-stage, dike-free volcanic rocks of West Maui volcano in the longitudinal direction (corresponding to the direction in which the lava flowed) to range from 300 to about 7,800 ft/d, and about 11,000 ft/d for Honomanū Basalt/Kula Volcanics.

Gingerich (2008) estimated the horizontal hydraulic conductivity of the shield-stage, dike-free volcanic rocks of West Maui volcano and Haleakalā in the transverse direction (corresponding to the lateral direction perpendicular to the lava flow direction) to range from 0.33 to 0.67 times the value in the longitudinal direction. Gingerich (2008) also estimated the vertical hydraulic conductivity (in the direction perpendicular to the plane of the lava flows) of the shield-stage, dike-free volcanic rocks of West Maui volcano to range from 0.38 to about 10 ft/d and for Honomanū Basalt/Kula Volcanics to be about 14 ft/d. These vertical conductivity estimates correspond to anisotropy ratios of 800:1 to 200:1. The vertical anisotropy ratio is the ratio of horizontal hydraulic conductivity in the longitudinal direction to vertical hydraulic conductivity. For the post-shield stage Honolua Volcanics, Gingerich (2008) estimated an isotropic hydraulic-conductivity value of 0.08 ft/d.

Rotzoll and others (2007) used constant-rate and variable-rate aquifer tests to estimate hydraulic-conductivity values of Wailuku Basalt. The median hydraulic conductivity value (from 51 aquifer-test analyses) for the Wailuku Basalt was estimated to be about 1,200 ft/d. Rotzoll and El-Kadi (2008) used a regression between specific capacity and hydraulic conductivity to estimate hydraulic-conductivity values of dike-free volcanic rocks on Maui. The median hydraulic conductivity value (from 218 specific-capacity values) was estimated to be about 1,600 ft/d.

Dike-Intruded Volcanic Rocks

Although most dikes are less than 10 ft thick, they are hydrologically important because of their low permeability and can extend vertically and laterally for thousands of feet. Within a dike complex, dikes intersect at various angles and compartmentalize the more permeable intruded rock, resulting in impoundment of groundwater to high altitudes. Because dikes lower overall rock porosity and permeability, the average hydraulic conductivity of a dike complex decreases as the number of dike intrusions increases. On the basis of a numerical-model analysis, Izuka and others (2021) estimated the overall hydraulic conductivity of the dike complex in the central part of West Maui volcano to be 0.033 ft/d.

Sedimentary Rocks

The permeability of sedimentary deposits can vary widely, from low-permeability compacted older alluvium to higher permeability sand dunes and unconsolidated recent alluvium. Gingerich (2008) assigned values of 17 and 0.38 ft/d for the horizontal (both longitudinal and transverse directions) and vertical hydraulic conductivities, respectively, of sedimentary deposits in a three-dimensional numerical groundwater model that included West Maui volcano. Gingerich (2008) also used values of 6.9 and 0.69 ft/d for the horizontal and

vertical hydraulic conductivities for valley-fill barriers in west Maui. Izuka and others (2021) estimated a vertical hydraulic-conductivity value of 1.6 ft/d for coastal sedimentary deposits in the west region of Maui aquifer systems of concern for this study. Izuka and others (2021) also estimated isotropic horizontal hydraulic-conductivity values from 17 to 490 ft/d for zones used to represent valley-fill barriers in west Maui.

Effective Porosity, Specific Yield, and Specific Storage

The total porosity of an aquifer represents the ratio of the volume of pore space to the total volume of rock and is a dimensionless property of the aquifer. Effective porosity (dimensionless) reflects the part of the total rock porosity that contributes to groundwater flow and generally excludes isolated and dead-end pore spaces. Specific yield (dimensionless) represents the volume of water released by an unconfined aquifer per unit of surface area per unit of decline in the water-table altitude. Specific yield (the drainable volume of the porous medium) and effective porosity (the fraction of the porous medium volume through which flow can easily occur) are closely related parameters. Thus, for the purposes of this study, specific yield is assumed to equal effective porosity. Specific storage is a measure of the compressive storage of the rocks and fluids in the aquifer. The specific yield, effective porosity, and specific storage of an aquifer control the rate at which changes in water levels and salinity occur in response to changes in groundwater withdrawals or recharge. Small values of specific yield or specific storage will cause a rapid water-level response to changes in withdrawal or recharge, whereas large values of specific yield or specific storage will cause a slow water-level response. For central and west Maui, Gingerich (2008) and Gingerich and Engott (2012) estimated the effective-porosity value of the volcanic-rock aquifer to be 0.15, and rock and fluid compressibility values to be 1.2×10^{-7} and 2.14×10^{-8} square feet per pound (ft^2lb^{-1}), respectively.

Dispersivity

In coastal groundwater-flow systems in which freshwater is underlain by saltwater, the mixing of seaward-flowing freshwater with saltwater creates a brackish-water transition zone that separates the freshwater and saltwater. The extent of mixing, called dispersion, is dependent on the groundwater velocity and the aquifer dispersivity, which generally is controlled by aquifer heterogeneities. All other factors being equal, higher dispersivity values result in greater mixing. Dispersion is flow-direction dependent, with greater dispersion (or mixing) expected in the direction of groundwater flow (longitudinal direction) and lower dispersion in directions transverse to the groundwater flow. Furthermore, because of the layered nature of the volcanic-rock aquifers in Hawai‘i, dispersivity values in the roughly horizontal plane of lava flows generally are greater than in the vertical direction, perpendicular to the plane of lava flows. The amount of dispersion that occurs depends on the groundwater-flow velocity and on the values of longitudinal and transverse dispersivities that occur in each local direction of flow. The effective values of dispersivity change depending on the direction of groundwater flow as described in the anisotropic-media dispersion model of Voss and Provost (2010).

Dispersivity-value estimates for Maui are limited. For central and west Maui, Gingerich (2008) estimated longitudinal-dispersivity values of 250, 250, and 25 ft in directions of maximum (horizontal longitudinal) hydraulic conductivity, middle (horizontal transverse) hydraulic conductivity, and minimum (vertical) hydraulic conductivity, respectively. Gingerich (2008) also estimated transverse-dispersivity values of 0.66 ft in all three directions (maximum hydraulic conductivity, middle hydraulic conductivity, and minimum hydraulic conductivity) for volcanic rocks and 3.3 ft (all directions) for sedimentary rocks. For west Maui, Gingerich and Engott (2012) estimated similar longitudinal-dispersivity values of 250, 250, and 25 ft in directions of maximum (horizontal longitudinal) hydraulic conductivity, middle (horizontal transverse) hydraulic conductivity, and minimum (vertical) hydraulic conductivity, respectively, and transverse-dispersivity values of 0.18 ft in all directions.

Groundwater-Flow System

Precipitation is the main source of freshwater on Maui. The precipitation either (1) runs off as surface water to streams, (2) evaporates or is transpired by vegetation, (3) recharges the groundwater system, or (4) is stored in the soil. Groundwater levels are highest in the mountainous interior parts of the island and lowest near the coast. Thus, groundwater flows from the mountainous interior areas (where volcanic dikes are most common) to coastal discharge areas (where the volcanic rocks are mainly dike free). In the mountainous interior areas, volcanic dikes impede groundwater flow, causing groundwater levels to build up behind them. Groundwater in dike-intruded areas may discharge to streams, wells and tunnels, or toward downgradient coastal areas. In the deeply incised valleys of west Maui, springs form where erosion has cut through dike compartments and lowered the land surface such that the water table intersects with the land surface. Groundwater discharge at these springs contributes to the base flow of streams.

Fresh groundwater in the study area occurs mainly in freshwater-lens systems and dike-impounded systems (Yamanaga and Huxel, 1970; Meyer and Presley, 2001; Gingerich, 2008; Izuka and others, 2018). A freshwater-lens system includes a lens-shaped freshwater body, an intermediate transition zone of brackish water, and underlying saltwater. The thickness of the transition zone is dependent on the extent of mixing between freshwater and saltwater. Within the study area, freshwater-lens systems are found in dike-free volcanic rocks of high permeability and sedimentary deposits. A thick wedge of sedimentary deposits forms a confining unit (caprock) over the high-permeability volcanic rocks along the isthmus between West Maui volcano and Haleakalā and impedes the discharge of water from the freshwater-lens system.

Recharge

Groundwater recharge related to direct rainfall infiltration occurs over the entire study area. In addition, groundwater recharge may occur in stream channels where local groundwater levels near the stream channel are lower than the stream altitude. In these cases, some of the streamflow may be lost to the underlying groundwater body.

Water-Budget Recharge Estimates

Recharge estimates from a daily water-budget model were developed for all of Maui using average climate conditions (1978–2007) and 2010 land cover (Johnson and others, 2018). Johnson and others (2018) estimated recharge for average climate conditions (1978–2007) and 2010 land cover in the Waiheʻe, ʻĪao, and Waikapū aquifer systems to be about 22.9, 41.4, and 19.9 Mgal/d, respectively. Expressed as a depth of water uniformly distributed over the Waiheʻe, ʻĪao, and Waikapū aquifer systems, annual recharge is about 38.6, 34.4, and 24.1 in., respectively. For this study (see appendix 1), recharge estimates were updated to reflect 2017 land-cover conditions. For average climate conditions (1980–2010) and 2017 land cover in the Waiheʻe, ʻĪao, and Waikapū aquifer systems, recharge was estimated to be about 22.2, 39.5, and 16.6 Mgal/d, respectively. Recharge also was estimated for nine selected periods: 1926–69, 1970–79, 1980–84, 1985–89, 1990–94, 1995–99, 2000–04, 2005–09, and 2010–12. During these nine periods, recharge ranged from 15.5 to 24.9 Mgal/d in the Waiheʻe aquifer system, from 25.0 to 52.3 Mgal/d in the ʻĪao aquifer system, and from 13.8 to 28.5 Mgal/d in the Waikapū aquifer system.

Restored Streamflow

Prior to 2010, streamflow from four of the main rivers and streams in the study area—the Waiheʻe River, Waiehu Stream, Wailuku River, and Waikapū Stream—was largely diverted. During dry-weather conditions, all streamflow was commonly diverted, leaving downstream reaches dry (Oki and others, 2010). Since about 2010, streamflow has been restored to these rivers and streams in response to the establishment of interim instream-flow standards. The CWRM established interim instream-flow standards of 10, 1.9, 10, and 2.9 Mgal/d, for selected locations on Waiheʻe River, Waiehu Stream, Wailuku River, and Waikapū Stream, respectively (for example, see https://dlnr.hawaii.gov/cwrm/surfacewater/monitoring/). Because of the restored-streamflow conditions, groundwater recharge may occur in reaches that were losing a considerable amount of their flow into the groundwater system and that were previously dry because of diversions. Oki and others (2010) estimated loss rates in these reaches during periods when water was temporarily restored. Loss rates ranged from less than 1 to about 4 Mgal/d per mile of stream reach, depending on the reach considered. Measured loss rates, expressed in terms of percentage of upstream discharge, commonly exceeded 10 percent in reaches of Waiehu Stream, Wailuku River, and Waikapū Stream, but were less than 10 percent in reaches of Waiheʻe River.

On May 7, 2019, the U.S. Geological Survey (USGS) made discharge measurements in Waikapū Stream in the reach between altitudes of about 420 and 35 ft during a period when streamflow was being restored and water from outside the basin also was being discharged from an existing ditch system to the stream. For this reach and under these conditions, the measured loss rate exceeded 40 percent of the discharge at the upstream end of the reach. However, because this reach is mostly in sedimentary deposits, recharge from restored streamflow may not reach the underlying basalt aquifer. The interim instream-flow standards of restored streamflow and the estimated loss rates by Oki and others (2010) were used to estimate additional recharge over streams for the scenarios.

Discharge

Groundwater discharge in the study area occurs in the forms of withdrawals from wells and tunnels, discharge to streams, and discharge to subaerial and submarine coastal springs and seeps. Reported groundwater withdrawals from volcanic rocks of West Maui volcano for 2017–18 averaged about 4.8 Mgal/d for the Waiheʻe aquifer system, 16.5 Mgal/d for the ʻĪao aquifer system, and less than 0.1 Mgal/d for the Waikapū aquifer system (fig. 4).

Groundwater Withdrawals

Groundwater withdrawals in the ʻĪao aquifer system generally increased between the 1940s and 1990s and peaked in the mid-1990s above the CWRM-estimated sustainable-yield value. Since the mid-1990s, groundwater withdrawals have declined to a relatively steady rate less than the CWRM-estimated sustainable-yield value. Prior to the 1990s, a few privately owned wells developed a limited amount of groundwater from the Waiheʻe aquifer system. Groundwater withdrawals in the Waiheʻe aquifer system have been relatively steady since about 2000. Reported groundwater withdrawals in the Waikapū aquifer system started in 2015, although withdrawals have been small compared to the sustainable-yield estimate of that aquifer system or the withdrawals in the ʻĪao and Waiheʻe aquifer system (fig. 4).

Discharge to Streams

The drainage pattern of the stream valleys on west Maui is radial from the summit to the ocean. Most of the streams in the study area drain to the northern coast, although Waikapū Stream drains east and then turns south as it reaches the isthmus. The study-area streams are perennial mainly where they intersect the groundwater table in the dike-impounded system but can also be perennial in losing reaches where streamflow exceeds losses. Where streambeds are above the water table, streamflow infiltration is potentially a source of

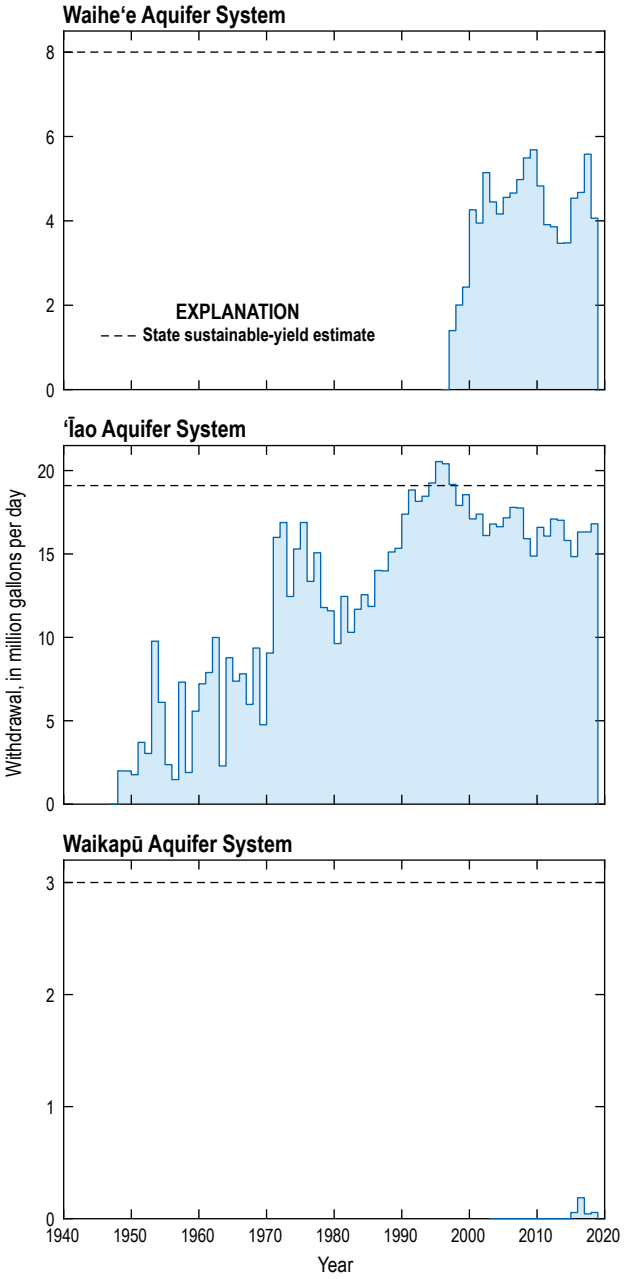

Figure 4. Graphs showing annual reported groundwater withdrawals during 1940–2018 from the Waiheʻe, ʻĪao, and Waikapū aquifer systems, central Maui, Hawaiʻi. Sustainable-yield values as of 2019 (dashed lines) and withdrawal data are from the Hawaiʻi Commission on Water Resource Management. At the time of publication, data had not been published by the Hawaiʻi Commission on Water Resource Management.

recharge to the aquifer (Oki and others, 2010). The infiltration commonly occurs in areas with freshwater-lens systems. Much of the water used to irrigate sugarcane and other agriculture was diverted from the gaining sections of study-area streams with an extensive ditch system (Wilcox, 1996).

The USGS has maintained stream-gaging stations on numerous streams and ditches within the study area (Fontaine, 1996), although the periods of record for some gaging stations are limited. As of 2020, the USGS maintains continuous-record stream-gaging stations on Waiheʻe River (station 16614000) and Wailuku River (station 16604500). For the stream-gaging stations on Waiheʻe River and Wailuku River, Johnson and others (2018) used a computerized hydrograph-separation method to estimate the base-flow component of total streamflow. During water years 1985–2016, average base flows of Waiheʻe River and Wailuku River were estimated to be 29.4 and 18.1 Mgal/d, respectively. These average base-flow values represent an estimate of groundwater discharge to the rivers.

Freshwater-Lens System

A freshwater-lens aquifer system exists as a continuous system in the mainly dike-free volcanic rocks and sedimentary deposits that form a caprock over the volcanic rocks (for example, Meyer and Presley, 2001). The freshwater lens in the study area forms because of the density difference between freshwater and underlying saltwater. A saltwater-circulation system exists beneath the freshwater lens. Saltwater initially flows landward in the deeper parts of the aquifer, then flows upward, and then mixes with seaward-flowing fresher water. This mixing creates the brackish-water transition zone.

The low-permeability sedimentary deposits that form a caprock in northern coastal areas and between West Maui volcano and Haleakalā act as a confining unit that impedes the discharge of fresh groundwater to the ocean. The same deposits impede the discharge of groundwater from the Wailuku area to the Haleakalā Volcanics near the isthmus. The sedimentary caprock also impedes the inflow of saltwater from the ocean into the aquifer. Offshore, the caprock extends beyond the seaward extent of the freshwater lens. Groundwater from the volcanic rocks discharges into the caprock, and the freshwater-lens system in the dike-free volcanic rocks is mainly unconfined inland from the caprock.

Groundwater Levels

The water table of the freshwater-lens system in dike-free volcanic rocks is less than a few tens of feet above sea level. A synoptic survey of groundwater levels in west-central Maui in September 2015 (fig. 5; U.S. Geological Survey, 2019) provided a snapshot of conditions in the aquifer and generally indicated (1) higher water levels in inland areas and lower water levels near the coast, (2) higher water levels in the central part of the surveyed area and lower water levels to the north and south, and (3) a water level greater than 600 ft in the area where groundwater is impounded by dikes (fig. 5). In general, the water-table altitude increases in an inland direction at a rate of about 1 foot per mile, although local variations may exist near areas of converging flow caused by withdrawals from wells. Within the dike-free volcanic rocks, freshwater generally flows from inland areas to coastal discharge areas. Although freshwater flow is predominantly horizontal in the dike-free volcanic rocks, the flow may have an upward component in some areas. Available data indicate

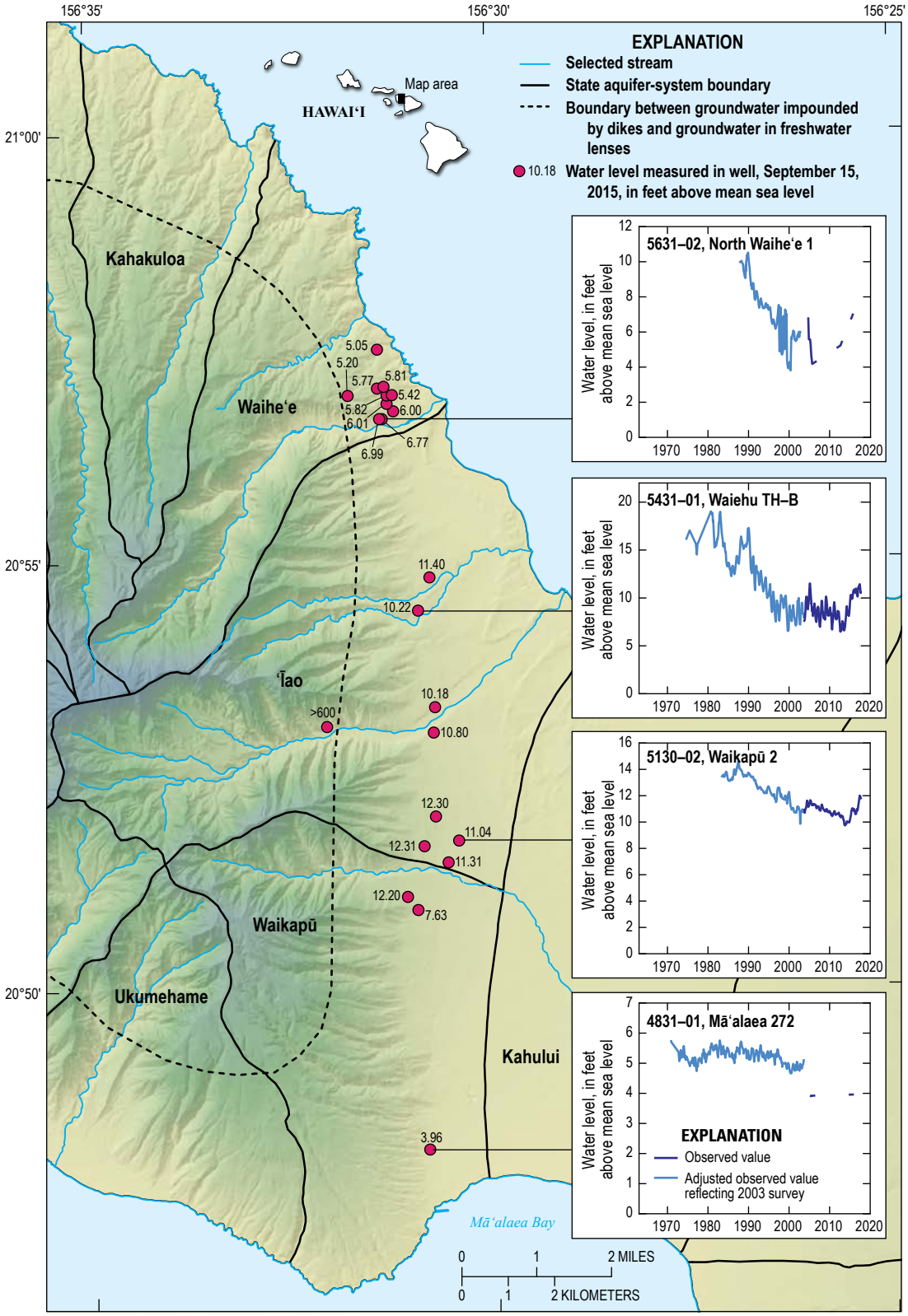

Base modified from U.S. Geological Survey National Hydrography Dataset, Scale of 1:24,000
Shaded relief from U.S. Geological Survey digital elevation model data
Universal Transverse Mercator Projection, Zone 4
North American Datum of 1983

Figure 5. Map showing measured groundwater levels on September 15, 2015, and graphs showing measured groundwater levels in selected wells in the Wailuku area, central Maui, Hawaiʻi (U.S. Geological Survey, 2019).

that groundwater levels in the freshwater-lens system have declined since the 1940s (Gingerich, 2008 or see fig. 12).

In the ʻĪao aquifer system, measured water levels exceeded 30 ft in the 1940s (Gingerich, 2008 or see fig. 12), declined to less than 10 ft during the early 2000s, and were less than 13 ft during the September 2015 synoptic survey. Measured water levels during the September 2015 synoptic survey ranged from about 5 to 7 ft in the Waiheʻe aquifer system and from 4 to 12.2 ft in the Waikapu aquifer system (fig. 5). The synoptic survey also revealed some of the water-level differences indicative of groundwater-flow barriers between wells (for example, 10.22 ft adjacent to 11.40 ft or 12.20 ft adjacent to 7.63 ft).

Freshwater-Lens Thickness

Deep monitor wells are deep open boreholes that penetrate the transition zone and are commonly used in Hawaiʻi to evaluate the thicknesses of the freshwater lens and transition zone. For a salinity profile in a deep open borehole, the altitude of the midpoint of the transition zone is the altitude at which the salinity profile indicates a salinity value about half that of ocean water. For the purposes of this study, ocean water is assumed to have a specific-conductance value of 50,000 microsiemens per centimeter at a reference temperature of 25 °C (fluid specific conductance is an indicator of salinity), and 100 percent ocean-water salinity equates to 100 percent saltwater.

The water level and salinity in the Waiehu Deep Monitor Well (5430–05) have been monitored since 1982. Data from September 2018 indicated a water level of about 12.4 ft and showed the altitude of the midpoint of the transition zone at about −600 ft. The midpoint of the transition zone rose more than 200 ft between 1985 and 2018, which corresponds to a rise of about 6.3 feet per year (ft/yr; fig. 6). The ʻĪao Deep Monitor Well (5230–02) has been monitored since 2006, and data from September 2018 indicated a water level of about 13.2 ft and altitude of the midpoint of the transition zone at about −900 ft. The midpoint of the transition zone rose by about 68 ft between 2006 and 2018, which corresponds to a rise of about 5.5 ft/yr (fig. 6). The Waiheʻe Deep Monitor Well (5631–09) has been monitored since 2011, and data from September 2018 indicated a water level of about 7 ft and altitude of the midpoint of the transition zone at about −330 ft. The midpoint of the transition zone rose by about 26 ft between 2011 and 2018, which corresponds to a rise of about

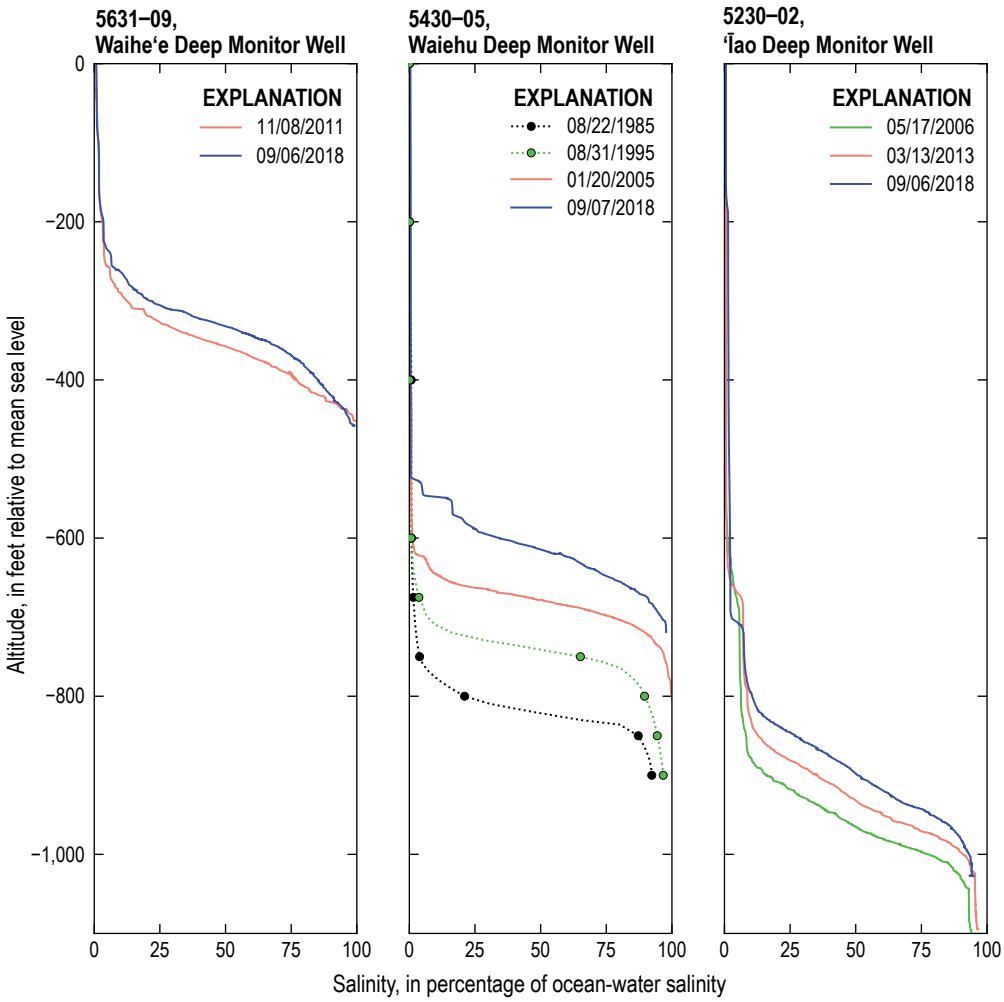

Figure 6. Graphs showing selected salinity profiles in selected wells in the Wailuku area, central Maui, Hawaiʻi. Dotted lines are from a piecewise cubic hermite interpolating polynomial; specific conductance of 50,000 microsiemens per centimeter at 25 degrees Celsius and chloride concentration of 19,500 milligrams per liter correspond to 100 percent salinity. Data from U.S. Geological Survey (5430–05) and Hawaiʻi Commission on Water Resource Management (5230–02, 5430–05, and 5631–09). At the time of publication, data had not been published by the Hawaiʻi Commission on Water Resource Management.

3.8 ft/yr (fig. 6). These data indicate that the freshwater-lens thickness has been decreasing at each of the monitor wells. Data from the ʻĪao and Waiheʻe Deep Monitor Wells were not available during the development of the groundwater-flow model by Gingerich (2008).

For hydrostatic conditions, the altitude at which the brackish water in the transition zone has a salinity about 50 percent that of ocean water (indicating the midpoint of the transition zone) is sometimes estimated from the Ghyben-Herzberg principle. The Ghyben-Herzberg principle describes a freshwater-saltwater equilibrium relation for conditions in which the two fluids do not mix (indicating that there is no transition zone) and freshwater flow is steady and horizontal. For these conditions, the freshwater-lens thickness below sea level is directly proportional to the height of the top of the freshwater above sea level. In principle, at a place where the water table stands 1 ft above sea level, 40 ft of freshwater will be below sea level, and the freshwater lens will therefore be 41 ft thick. This relation exists because ocean water is about one-fortieth denser than freshwater.

In the dike-free volcanic rocks of the Wailuku area, freshwater mixing with underlying saltwater creates a brackish-water transition zone that may be hundreds of feet thick. Because of the presence of this brackish-water transition zone, the Ghyben-Herzberg principle generally overestimates the actual thickness of freshwater in a freshwater-lens system. This generalization may also not be true for cases in which a freshwater-lens system is undergoing change in response to a change in withdrawal or recharge conditions or where groundwater flow has a vertical component. Furthermore, flow in a borehole may cause measured salinity profiles in deep open boreholes to differ from the vertical salinity distribution in the adjacent aquifer (Rotzoll, 2010; Rotzoll, 2012). The Ghyben-Herzberg principle does not accurately predict the altitude of the transition-zone midpoint indicated in deep open boreholes in the study area. The observed transition-zone midpoint is deeper than the midpoint estimated from the Ghyben-Herzberg principle, and the discrepancy is most likely related to the system not being at steady-state conditions and borehole flow.

Chloride Concentration of Pumped Water

Chloride concentration is commonly used as an indicator of salinity, which may increase as a result of saltwater intrusion into a fresh groundwater body. The U.S. Environmental Protection Agency (EPA) secondary standard for chloride concentration in drinking water is 250 milligrams per liter (mg/L; U.S. Environmental Protection Agency, 2020). Water with a chloride concentration above 250 mg/L may have a salty taste. For comparison, the chloride concentration of rainfall is typically less than 10–20 mg/L (Swain, 1973), and that of ocean water about 19,500 mg/L (Wentworth, 1939). The chloride concentration of water pumped from wells in the dike-free volcanic rocks of the Wailuku area has been generally increasing during the period of measurement in most production wells as indicated in figure 7. However, to date, the chloride concentration generally has been less than 200 mg/L except in a few production wells, including Mokuhau 1 to 3 (5330–09 to –11) and Waiehu Heights 1 (5430–01) (fig. 7).

Dike-Impounded System

A dike-impounded system is found in the rift zones and caldera area of West Maui volcano where low-permeability dikes have intruded other rocks. The flow system includes the freshwater body and any underlying brackish water and saltwater. Near-vertical dikes tend to compartmentalize areas of permeable volcanic rocks. Dikes impound water to heights as much as 3,000 ft above sea level in the interior of West Maui volcano as evidenced by tunnels tapping dike compartments (Stearns and Macdonald, 1942). The dike distribution commonly is described as radial; however, a true radial dike distribution without intersecting dikes would not impound groundwater flowing to the coast in the same radial manner. Nevertheless, the evidence supplied from gaining streams, groundwater tunnels, and wells indicate that groundwater is impounded to high levels in the West Maui volcano. Therefore, the extent of the dike-impounded water body is inferred from the dikes exposed in valley walls and water levels in wells (fig. 3; Yamanaga and Huxel, 1970; Izuka and others, 2018).

No data from wells are available for determining the depth to which freshwater extends below sea level within the dike-impounded system. Where erosion or tunneling exposed dike compartments in the stream valleys, groundwater discharges directly to the streams as base flow. Fresh groundwater that does not discharge to streams or that is not withdrawn from wells flows to downgradient areas (freshwater-lens system) where water levels are lower. Although preferential flow to downgradient areas in some parts of the West Maui volcano is likely, no data are available to accurately characterize where these areas might be.

Simulation of Groundwater Flow

A three-dimensional numerical groundwater-flow and salinity-transport model was developed for central Maui using the computer code SUTRA (Voss and Provost, 2010), which simulates density-dependent groundwater flow and salinity transport. For this study, SUTRA was used to represent the mixing of freshwater and saltwater and the formation of a brackish-water transition zone. The groundwater-flow and salinity-transport model of central Maui was developed using temporally varying recharge and withdrawal conditions during 1926–2012. The model accounts for spatially varying hydraulic properties of the geologic materials, recharge, and discharge. The hydraulic properties of the rocks were estimated from available data and were modified by varying them in the model to obtain reasonable agreement between model-calculated and observed water levels, vertical salinity profiles, and salinities of pumped water. Model development also was

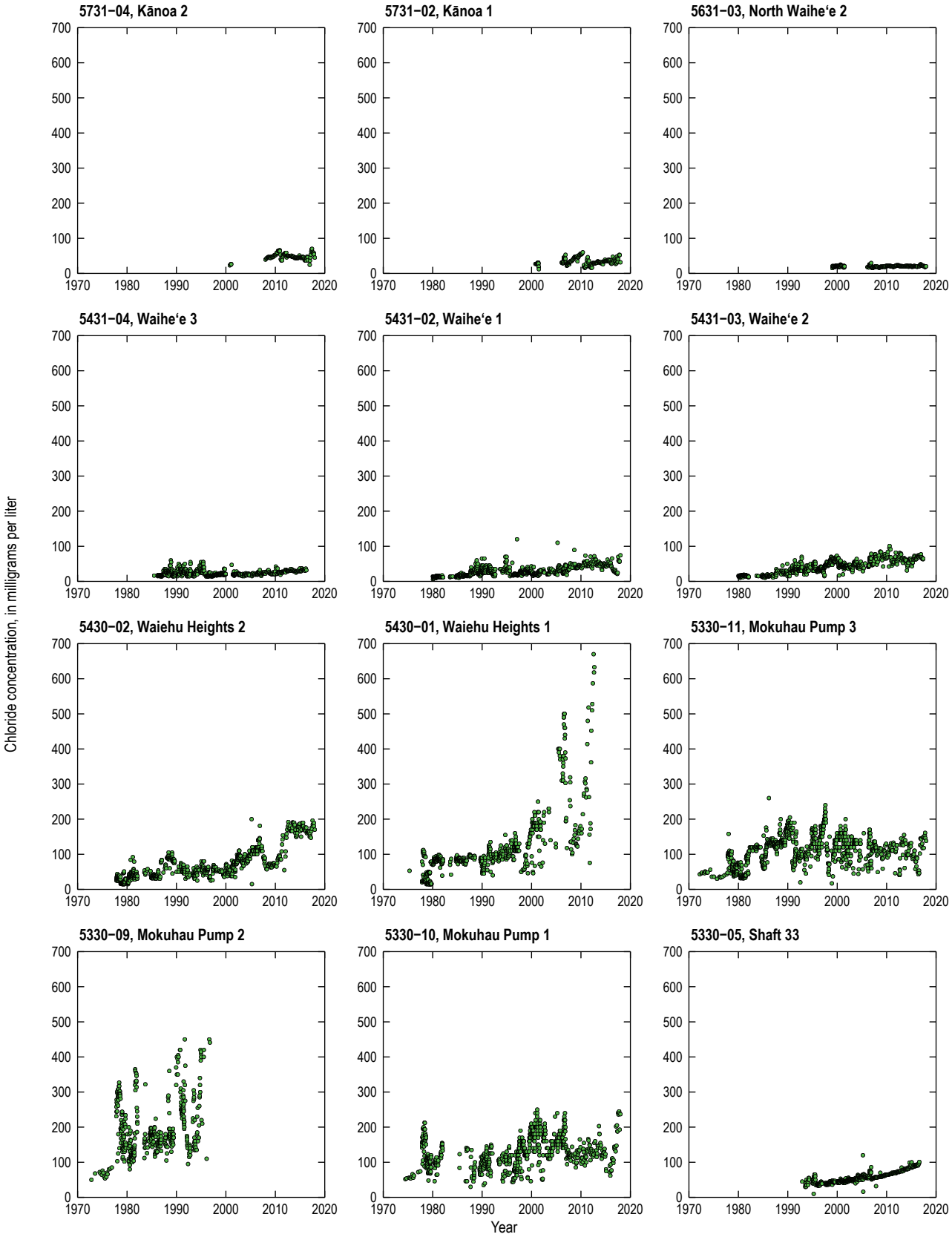

Figure 7. Chloride concentration of pumped water from selected wells during 1970–2018 in the Wailuku area, central Maui, Hawai'i. Data are from U.S. Geological Survey National Water Information System database and Maui Department of Water Supply. At the time of publication, data had not been published by the Maui Department of Water Supply.

guided by previous modeling studies for Maui (Gingerich, 2008; Gingerich and Engott, 2012; Izuka and others, 2021).

The modeled area includes the dike-free volcanic rocks of the Kahakuloa, Waihe‘e, ‘Īao, and Waikapū aquifer systems; parts of the Honokōhau aquifer system in the north; the Ukumehame aquifer system in the south; and the Kahului aquifer system in the east (fig. 1 and fig. 8). The modeled area extends beyond the Waihe‘e, ‘Īao, and Waikapū aquifer systems to avoid boundary effects that may influence the model results in the study area. The interior, dike-intruded parts of these aquifer systems are not included in the model, although groundwater inflow from these areas is included. The model extends offshore to account for freshwater discharge to the ocean and saltwater inflow to the aquifer.

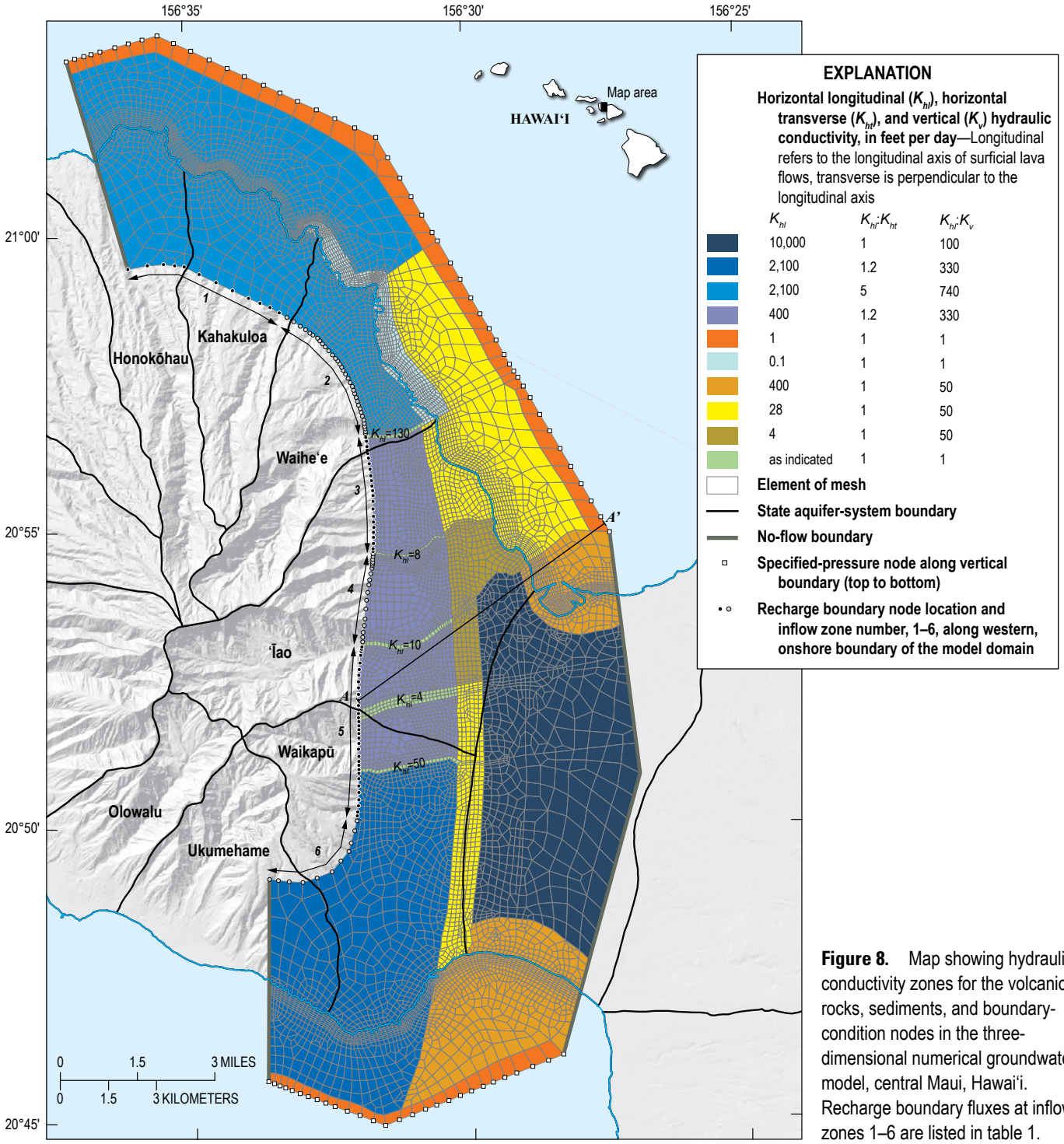

Base modified from U.S. Geological Survey National Hydrography Dataset, Scale of 1:24,000
Shaded relief from U.S. Geological Survey digital elevation model data
Universal Transverse Mercator Projection, Zone 4
North American Datum of 1983

Figure 8. Map showing hydraulic-conductivity zones for the volcanic rocks, sediments, and boundary-condition nodes in the three-dimensional numerical groundwater model, central Maui, Hawai‘i. Recharge boundary fluxes at inflow zones 1–6 are listed in table 1.

Model Mesh

The finite-element model mesh used in this study consists of 1,074,838 nodes and 1,043,685 variably sized elements (fig. 8). In the vertical direction, the mesh has 116 horizontal layers of elements where the top of the model is not truncated by the ocean. Offshore, the mesh has fewer than 116 elements in the vertical direction.

The western boundary of the model domain is formed by rift zones and by the eastern extent of the dike-intruded area of West Maui volcano. Groundwater inflow from the dike-intruded area of West Maui volcano is included in the model and is estimated from an island-wide model (Izuka and others, 2021). The eastern boundary of the model domain roughly corresponds to the surface contact between sedimentary deposits and volcanic rocks from Haleakalā Volcanics (fig. 3) and includes the entire zone where fresh groundwater is expected to occur in Wailuku Basalt. Groundwater inflow from Haleakalā westward through the isthmus is ignored. However, Gingerich (2008) found little interaction between groundwater in Honomanū Basalt/Kula Volcanics and Wailuku Basalt. The mesh extends offshore in the north and south to include the entire zone in which fresh groundwater is expected to discharge to the ocean.

Onshore, the top of the model is set at an altitude of 0 ft, consistent with the simplifying assumption of Gingerich (2008) and Gingerich and Engott (2012). Offshore, the top of the model is defined by the ocean floor altitude (University of Hawai‘i, 2011). Gaps in the bathymetry data are filled by linear interpolation. The bottom of the model domain is assumed to be a no-flow boundary at 6,000 ft below mean sea level defined by an assumed aquifer bottom (Souza and Voss, 1987) and seismic-velocity discontinuity (Furumoto and others, 1970; Kauahikaua, 1993).

Node spacing is variable in both the vertical and horizontal directions and is finest in the upper part of the aquifer and near areas of groundwater discharge or potential barriers to groundwater flow to support representation of results that have steep spatial gradients. The vertical spacing between nodes ranges from 1 ft in onshore areas at the top of the model to 765 ft near the bottom of the mesh where only saltwater is simulated (fig. 9).

Representation of the System

For modeling purposes, the model domain is divided into hydraulic-conductivity zones representing the volcanic rocks, the coastal sediments overlying the volcanic rocks, and hydrologic barriers to groundwater flow (fig. 8). Hydraulic conductivity is related to permeability, which is the parameter used by SUTRA, according to the following equation:

$$K = k\rho g/\mu \quad (1)$$

where:

K is hydraulic conductivity [LT^{-1}],
k is permeability [L^2],
ρ is fluid density [ML^{-3}],
g is gravitational acceleration [LT^{-2}], and
μ is fluid dynamic viscosity [$ML^{-1}T^{-1}$].

Because the CWRM aquifer-system boundaries do not necessarily represent subsurface hydrogeologic features, the hydraulic-conductivity zones generally are not aligned with the aquifer-system boundaries. A total of

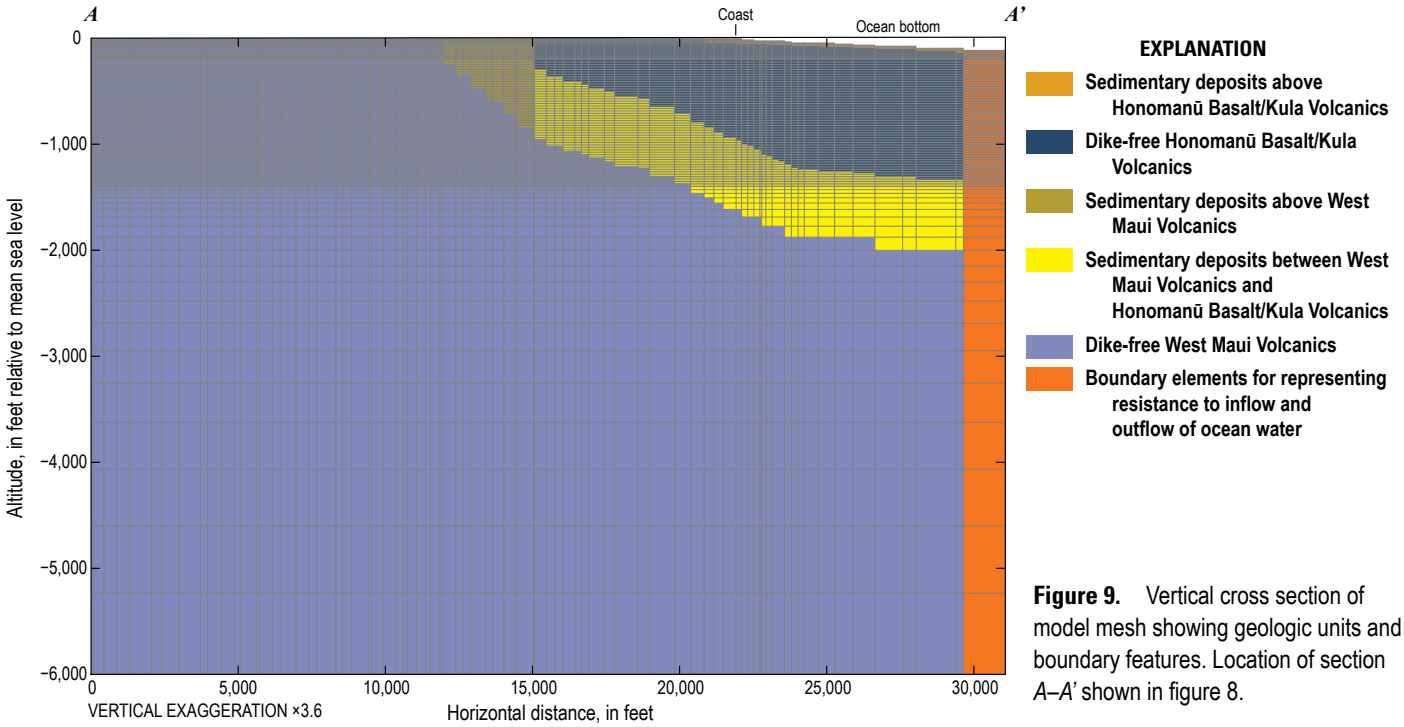

Figure 9. Vertical cross section of model mesh showing geologic units and boundary features. Location of section *A–A'* shown in figure 8.

15 hydraulic-conductivity zones were created, although some of the zones share some common hydraulic properties. Zones were created to represent shield-stage Wailuku Basalt and volcanic rocks from Haleakalā, post-shield stage Honolua Volcanics, buried groundwater barriers, and sedimentary deposits. Zones also were created along the northern and southern offshore boundaries to simulate resistance to inflow and outflow of ocean water into the modeled domain.

Several hydrogeologic features of low permeability are represented in the numerical model to cause a discontinuity in water level across adjacent areas in the simulation. These zones represent groundwater barriers to flow (for example, valley fill or other features) and are configured in the model as partially penetrating, vertical, low-permeability zones stretching from the inland inferred dike zone to the low-permeability sedimentary wedge. All modeled barriers extend to an altitude of –1,800 ft, except the barrier associated with the Waiheʻe Valley, which only penetrates to an altitude of –285 ft. A shallower barrier gave better agreement between model-calculated and observed water levels, vertical salinity profiles, and salinities of pumped water in the Waiheʻe aquifer system than were given by a deeper, more conductive barrier.

A uniform thickness of about 650 ft is applied to the sedimentary layer between West Maui volcano and Haleakalā, similar to the thickness used by Gingerich (2008). The thickness of sediments above Honomanū Basalt/Kula Volcanics was estimated using structural contours of the volcanic rocks from Haleakalā (fig. 3; modified from Gingerich, 2008; Izuka and others, 2018).

Comparison of the simulated and measured salinity profiles indicated during model calibration that the simulation results underestimate the thickness of freshwater near well 5230–02 if the hydraulic conductivity is not varied with depth. This underestimation of freshwater thickness may reflect model inaccuracy or possibly borehole flow that can occur in wells of this type with long open intervals (for example, Rotzoll, 2010; Rotzoll, 2012). The simulated freshwater thickness near well 5230–02 was increased by reducing the hydraulic conductivity in the model below an altitude of about −230 ft near well 5230–02 to 0.5 ft/d for horizontal conductivity and 0.05 ft/d for vertical conductivity.

Boundary Conditions

The lateral extent of the model domain is defined by boundaries that are either no flow, recharge, or specified pressure. The western boundaries at the northern and southern parts of the model within the Honokōhau and Ukumehame aquifer systems are formed by rift zones of West Maui volcano and are treated as no-flow boundaries in the model. The western boundary of the model formed by the eastern extent of the dike-intruded area of West Maui volcano is a recharge boundary between altitudes of −20 and −105 ft and a no-flow boundary below an altitude of −105 ft. Recharge from the dike-intruded area of West Maui volcano is allowed to enter the western boundary between altitudes of −20 and −105 ft. Recharge rates from the dike-intruded area were estimated from an island-wide model (Izuka and others, 2021) for six inflow zones (fig. 8), and the depths were selected to allow recharge to occur mainly within the freshwater part of the groundwater body. The eastern boundary of the model domain is modeled as a no-flow boundary.

The offshore, vertical boundaries of the model domain in the northern and southern parts of the model are represented with a specified-pressure (hydrostatic ocean-water) boundary condition, except where the boundary is defined by rift zones of West Maui volcano and is assumed to be a no-flow boundary. At the offshore, vertical specified-pressure boundaries of the model, pressure at each node is equal to the pressure at the bottom of a column of ocean water extending from the node up to sea level. Water may either enter or exit the flow system across the vertical specified-pressure boundaries of the model, and the flow direction may change with time depending on transient aquifer conditions within the model domain. Water entering at the vertical specified-pressure boundaries has salinity equal to that of ocean water, and water exiting at the boundary has salinity equal to that of groundwater within the adjacent aquifer.

The top of the offshore model domain is defined by the ocean-bottom bathymetry (University of Hawaiʻi, 2011) and is a specified-pressure (hydrostatic ocean-water) boundary condition. In offshore areas, ocean water may enter the model domain at its top boundary or water from the aquifer may exit at its top boundary. The top of the onshore model domain is set at an altitude of 0 ft and is treated as a recharge boundary. Rather than simulating an unsaturated zone, a simplified representation of water-table storage was implemented in SUTRA to simulate aquifer-specific yield (Gingerich, 2008; Gingerich and Engott, 2012), providing an equivalent representation of water contributed to the aquifer by drainage of the unsaturated zone.

Recharge

For this study, recharge to the onshore, top boundary of the model was estimated from a daily water budget for nine periods from 1926 to 2012 (1926–69, 1970–79, 1980–84, 1985–89, 1990–94, 1995–99, 2000–04, 2005–09, and 2010–12; appendix 1). Recharge for each onshore node at the top of the model domain was based on the area-weighted average recharge from the irregularly shaped water-budget-model subareas within a Thiessen polygon surrounding the node. Total recharge at the top of the model domain for the nine periods ranged from about 98.4 Mgal/d during 1926–69 to 30.2 Mgal/d during 2010–12. The difference in recharge between periods is largely caused by differences in rainfall and irrigation. Recharge used in the groundwater model may differ slightly from that estimated by the water budget because of discretization near the coast that causes some onshore areas to be assigned to offshore cells. The recharge water at the top of the model domain is assumed to have a salinity 0.077 percent that of ocean water, corresponding to a chloride concentration of about 15 mg/L (assuming ocean water has a chloride concentration of about 19,500 mg/L). This is

generally consistent with the lowest chloride concentrations in groundwater from wells in the study area.

Recharge in the form of groundwater inflow from the dike-intruded area of West Maui volcano was estimated from an island-wide model (Izuka and others, 2021). The inflow was also assumed to have a salinity of 0.077 percent that of ocean water. The inflow from the dike-intruded area was assumed to be steady and was estimated to be 39.6 Mgal/d based on average conditions during 1978–2007 (table 1). This assumption is based on the following considerations. Groundwater inflow from the dike-impounded system to the freshwater-lens system is controlled by the hydraulic gradient between these two groundwater systems. Existing water-level data from well 5332–04 (Kepaniwai observation well) in the dike-intruded area and well 5431–01 (Waiehu TH–B) in the freshwater-lens system tend to indicate that the gradient does not change substantially over time. Thus, although the inflow from the dike-impounded system to the modeled aquifer likely does change over time, the changes are small relative to concurrent changes in rainfall.

Table 1. Recharge input to the boundary-inflow zones shown in figure 8 of the three-dimensional model mesh, central Maui, Hawai‘i.

[Period refers to recharge period of the island-wide model by Izuka and others (2020). Recharge values given in million gallons per day (Mgal/d).]

Period	Zone						Total
	1	2	3	4	5	6	
1978–2007	7.33	5.72	4.85	5.32	11.03	5.38	39.62
2071–2100	6.91	5.24	4.39	4.78	8.31	3.03	32.66

Withdrawals

Information on groundwater withdrawals was obtained from CWRM, MDWS, and a previously published study (Gingerich, 2008). Withdrawals from the Honomanū Basalt/Kula Volcanics in the Kahului aquifer system were included in the model. The open or screened interval of each pumped well was represented in the model using one or more nodes within a vertical column of nodes in the mesh (table 2). Withdrawals from all wells in the model, except for the two Waiehu Heights wells in the ‘Īao aquifer system (5430–01 and 5430–02), were uniformly distributed with depth along the open interval. During construction of well 5430–01, low-permeability alluvium was encountered from ground surface to about −200 ft, and higher permeability rocks were encountered below that, indicating water production comes mostly from an interval from −200 feet to −350 ft. In the model, 95 percent of the withdrawals from wells 5430–01 and

Table 2. Values of top and bottom altitudes of open well interval used in the three-dimensional numerical groundwater model, central Maui, Hawai‘i.

[all values rounded to the nearest foot; --, no reliable data available]

Well no.	Top altitude of well in the model, in feet	Bottom altitude of well in the model, in feet	Land-surface altitude, in feet	Bottom altitude of solid casing, in feet	Bottom altitude of open hole, in feet
4728–08	−15	−95	5	−15	−95
4829–01	−19	−24	16	−20	−24
4829–02	−81	−140	14	−81	−140
4829–03	−81	−112	19	−82	−112
4829–04	−85	−115	15	−85	−115
4830–01	[1]−5	−32	52	−2	−32
4928–02	[1]−5	−10	50	10	−4
4930–01	[1]−5	−29	321	−9	−29
5030–01	[1]−5	−46	654	4	−46
5030–02	[1]−5	−131	466	311	−131
5128–02	[1]−5	−10	124	0	−10
5129–01	−32	−107	143	−32	−107
5129–02	−5	−31	224	−9	−31
5129–03	−29	−69	232	−29	−69
5129–04	[1]−5	−25	183	6	−25
5129–05	[1]−5	−33	184	3	−33
5129–06	[1]−5	−37	173	3	−37
5130–01	−58	−206	551	−58	−206
5130–04	[1]−5	−79	523	1	−79
5131–01	[1]−5	−106	764	−1	−106
5131–02	[1]−5	−125	780	2	−125

Table 2. Values of top and bottom altitudes of open well interval used in the three-dimensional numerical groundwater model, central Maui, Hawaiʻi—Continued

Well no.	Top altitude of well in the model, in feet	Bottom altitude of well in the model, in feet	Land-surface altitude, in feet	Bottom altitude of solid casing, in feet	Bottom altitude of open hole, in feet
5227–04	[1]−5	−10	75	0	−4
5227–05	[1]−5	−10	75	0	−3
5227–07	[1]−5	−40	40	--	−40
5227–08	[1]−5	−25	40	−5	−25
5228–07	−37	−74	116	−37	−74
5228–13	−5	−20	40	−9	−20
5228–14	[1]−10	−30	60	−10	−30
5228–17	[1]−5	−34	83	−2	−34
5228–18	[1]−5	−47	94	−2	−47
5228–20	[1]−5	−45	94	3	−45
5229–02	−11	−52	148	−12	−52
5229–03	[1]−5	−25	150	−5	−25
5229–04	[1]−5	−32	178	6	−32
5229–05	[1]−5	−37	183	8	−37
5229–06	[1]−5	−33	190	9	−33
5229–07	[1]−5	−54	244	0	−54
5230–01	−30	−50	250	−30	−50
5230–03	[1]−5	−103	506	6	−103
5230–04	[1]−5	−102	480	6	−102
5230–05	−30	−100	615	−30	−100
5327–10	−5	−10	--	--	--
5328–01	−5	−10	24	0	−4
5328–02	−120	−280	20	−120	−280
5328–27	−257	−287	30	−257	−287
5328–28	−258	−292	20	−258	−292
5328–31	[1]−5	−16	35	4	−16
5328–48	[1]−5	−36	44	9	−36
5328–49	[1]−5	−56	51	−5	−57
5328–51	[1]−5	−10	30	--	--
5329–04	[1]−5	−10	--	--	--
5329–05	[1]−5	−10	--	--	--
5329–09	[1]−5	−32	80	15	−32
5329–14	[1]−5	−10	120	14	−8
5329–15	−14	−31	37	−14	−31
5329–19	−5	−34	76	−5	−35
5329–20	−5	−40	70	−10	−40
5329–21	−13	−33	51	−14	−34
5330–02	[1]−5	−10	--	--	--
5330–05	[1]−5	−280	30	0	−280
5330–09	−58	−247	353	−58	−247
5330–10	−69	−247	353	−69	−247
5330–11	−49	−251	354	−49	−251
5331–02	[1]−5	−10	--	--	--

Table 2. Values of top and bottom altitudes of open well interval used in the three-dimensional numerical groundwater model, central Maui, Hawai'i—Continued

Well no.	Top altitude of well in the model, in feet	Bottom altitude of well in the model, in feet	Land-surface altitude, in feet	Bottom altitude of solid casing, in feet	Bottom altitude of open hole, in feet
5427–01	−166	−216	9	−166	−216
5427–02	−111	−191	9	−111	−191
5427–03	−101	−228	9	−101	−228
5427–04	−101	−236	9	−101	−236
5427–05	−111	−248	9	−111	−248
5427–06	−92	−241	9	−92	−241
5427–07	−90	−246	9	−90	−246
5427–09	−96	−188	12	−96	−188
5427–10	−96	−188	12	−96	−188
5427–11	−96	−188	12	−96	−188
5429–02	[1]−5	−55	85	5	−55
5429–03	[1]−5	−60	80	10	−60
5430–01	[1]−5	−338	337	0	−338
5430–02	[1]−5	−206	337	0	−206
5431–02	−29	−182	498	−29	−182
5431–03	[1]−5	−150	500	5	−150
5431–04	[1]−5	−156	494	−1	−156
5529–02	−35	−70	10	−35	−70
5530–04	−5	−76	74	−6	−76
5531–01	−5	−25	404	−5	−25
5631–02	−5	−106	281	−9	−106
5631–03	−19	−106	281	−19	−106
5631–05	−38	−58	142	−38	−58
5631–06	[1]−5	−50	151	51	−49
5631–07	[1]−5	−24	241	−4	−24
5631–08	[1]−5	−14	171	6	−14
5731–01	[1]−5	−50	480	450	−50
5731–02	[1]−5	−51	308	3	−51
5731–03	[1]−5	−50	637	5	−50
5731–04	[1]−5	−52	280	3	−52
5731–09	−17	−36	355	−17	–
5731–10	[1]−5	−10	--	--	--
5731–11	[1]−5	−10	--	--	--
5832–02	[1]−5	−62	608	8	−62
5832–03	[1]−5	−25	610	10	−25
P1	[1]−5	[1]−23	--	--	--
P2	[1]−5	[1]−23	--	--	--
P3	[1]−5	[1]−25	--	--	--
P4	[1]−5	[1]−164	--	--	--
P5	[1]−5	[1]−148	--	--	--
P6	[1]−5	[1]−180	--	--	--

[1]Estimate or reassignment to −5 feet if top altitude is above an altitude of −5 feet relative to sea level.

5430–02 were equally distributed to the vertical column of nodes representing each well below −200 ft, and the remaining 5 percent of the withdrawals were assigned to the shallower nodes representing each well. This nonuniform distribution was adjusted during model calibration to match the salinity of pumped water from these wells.

Simulated chloride concentrations from withdrawal wells were determined using a withdrawal-weighted average concentration of the nodes representing the well. That is, for well discharge represented by multiple nodes in the model, the simulated overall salinity from the well was determined by weighting the salinity at each node by the withdrawal at the node and then determining the overall withdrawal-weighted average. As an example, suppose a well covers two nodes in the model, that the upper node represents withdrawal from the upper 5 ft of the well and the bottom node represents withdrawal from the lower 15 ft of the well, and that the well was pumped uniformly. If the simulated salinity was 20 mg/L at the top node and 60 mg/L at the bottom node, then the simulated overall salinity from the well would be: 20 mg/L × 5 ft / 20 ft + 60 mg/L × 15 ft / 20 ft = 5 mg/L + 45 mg/L = 50 mg/L.

Other Model Properties

For all model simulations, water is assigned a single fluid-compressibility value of 2.14×10^{-8} square feet per pound (ft^2/lb) (4.47×10^{-10} Pa^{-1}) and a dynamic-viscosity value of 2.1×10^{-5} slug per foot per second (slug/[ft×s]) [0.001 kilograms per meters per second (kg/[m×s])]. Viscosity is a property of a fluid that measures its resistance to deformation (flow). Dynamic viscosity is the ratio of shear stress (shear force per unit area) to velocity gradient. Molecular diffusion of a solute is driven by concentration gradients in the fluid and may take place in the absence of groundwater flow. Molecular diffusion of a solute in a fluid is characterized by the molecular diffusivity. In the model, molecular diffusivity is assigned a value of 1.1×10^{-8} square feet per second (ft^2/s) (1.0×10^{-9} square meters per second [m^2/s]).

Solute concentrations in the model are expressed as a mass fraction: mass of total dissolved solids (TDS) per unit mass of fluid. Pure freshwater is assigned a TDS concentration of zero, and 100 percent ocean water is assigned a TDS concentration of 0.0357 kilograms per kilogram (kg/kg). For this study, the simulated chloride concentration of water is calculated from the TDS concentration using the following equation:

$$Cl = TDS \times 19{,}500 / 0.0357 \quad (2)$$

where:

Cl is chloride concentration, in mg/L, and

TDS is simulated total dissolved solids concentration, in kg/kg.

The density of water is assumed to increase linearly with salinity from 62.43 pounds per cubic foot (lb/ft^3; 1,000 kilograms per cubic meter [kg/m^3]) for freshwater to 63.99 lb/ft^3 (1,024.99 kg/m^3) for saltwater. In the model, compressibility of the porous-rock matrix is assigned a value of 1.2×10^{-7} ft^2/lb (2.5×10^{-9} Pa^{-1}) and density of the solid rock grain is assigned a value of 162 lb/ft^3 (2,600 kg/m^3). Acceleration due to gravity was assigned a value of 32.2 ft/s^2 (9.81 m/s^2).

Initial Conditions and Time Step

A simulation using 1926–69 recharge and zero withdrawals was run for sufficient time until the saltwater and freshwater distributions reached steady-state conditions, which were the initial conditions for the 1926–2012 transient simulation. A 1-day time step was used for the transient simulation.

Estimation of Hydraulic Properties

Hydraulic-conductivity, effective-porosity, and dispersivity values were estimated by trial and error. The hydraulic properties were varied in the model to obtain reasonable agreement between model-calculated and observed values. Water-level data were available since 1940, vertical salinity profiles were available since 1985, and salinity data of pumped water were available since 1970. The estimated hydraulic-property values generally are consistent with previous estimates (Gingerich, 2008; Izuka and others, 2021), although values differ from previous estimates because of differences in estimated recharge and available observation data.

Effective porosity of 0.15 for all zones was found to allow reasonable calibration to observed data. Horizontal hydraulic-conductivity values were estimated to be: 400, 2,100, or 10,000 ft/d for the mainly dike-free volcanic rocks; 0.1 ft/d for Honolua Volcanics; ranging from 4 to 130 ft/d for the zones representing groundwater barriers to flow (valley fill or other features); and ranging from 4 to 400 ft/d for coastal sedimentary deposits overlying volcanic rocks (fig. 8). Horizontal anisotropy (ratio of longitudinal-to-transverse horizontal hydraulic conductivity) was only included in the model for zones representing Wailuku Basalt. Longitudinal refers to the assumed longitudinal axis of the surficial lava flows, which is approximately perpendicular to the topographic contours. Horizontal anisotropy for Wailuku Basalt was estimated to be 5:1 in the Waiheʻe and Kahakuloa and 1.2:1 in the ʻĪao, Waikapū, and Ukumehame aquifer systems. All other units were estimated to be horizontally isotropic (1:1). Vertical anisotropy (ratio of longitudinal-horizontal-to-vertical hydraulic conductivity) was estimated to be 100:1, 330:1, or 740:1 for the mainly dike-free volcanic rocks; 1:1 for Honolua Volcanics and for the zones representing groundwater barriers to flow (valley fills or other features); and 50:1 for sedimentary deposits.

SUTRA allows specification of three longitudinal-dispersivity values and three transverse-dispersivity values. Longitudinal-dispersivity values estimated are 213, 213, and 2.1 ft in directions of maximum (horizontal longitudinal) hydraulic conductivity, middle (horizontal transverse) hydraulic conductivity, and minimum (vertical) hydraulic

conductivity, respectively. Transverse-dispersivity values estimated were 0.066 ft in all three directions (maximum hydraulic conductivity, middle hydraulic conductivity, and minimum hydraulic conductivity).

Simulated Historical Conditions 1926–2012 (Calibration)

Simulated groundwater levels in 2012 (at the end of the historical simulation) range from about 20 ft inland in the southern part of the ʻĪao aquifer system to less than 2 ft in the coastal area of the Waiheʻe aquifer system (fig. 10). Simulated water levels of less than 4 ft that occur near the Waiheʻe 1–3 wells (5431–02 to –04) in the central part of the ʻĪao aquifer system may be related to withdrawals during 1985–2000 above the water-use permit rate. The simulated 50-percent ocean-water salinity surface is deepest in the northern part of the Waikapū aquifer system and ranges in altitude from –1,000 ft to greater than –200 ft in the coastal area of the Waiheʻe aquifer system (fig. 10).

Simulated groundwater levels declined most in the ʻĪao aquifer system during 1926–2012, due to increased withdrawal and decreased recharge. Relative to 1926 water levels, simulated water levels were more than 24 ft lower near the Waiheʻe 1–3 wells (5431–02 to –04) and 21 ft lower near Shaft 33 (5330–05) in 2012. Simulated water levels declined

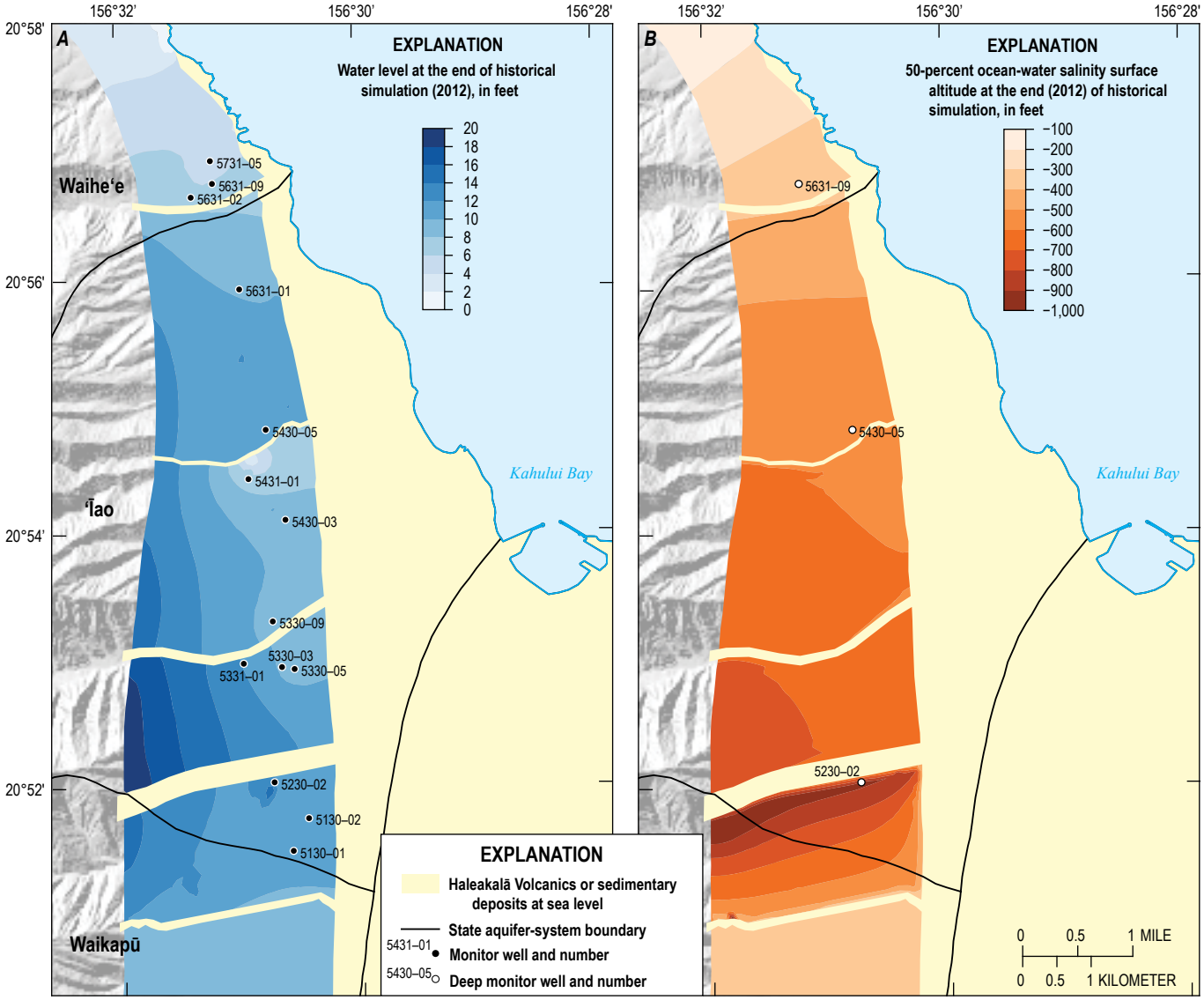

Base modified from U.S. Geological Survey National Hydrography Dataset, Scale of 1:24,000
Shaded relief from U.S. Geological Survey digital elevation model data
Universal Transverse Mercator Projection, Zone 4
North American Datum of 1983

Figure 10. Simulated (*A*) water level and (*B*) 50-percent ocean-water salinity surface altitude in the study area at the end of the historical simulation (2012), central Maui, Hawaiʻi.

about 10 ft during 1926–2012 in the southern Waiheʻe aquifer system and less than 9 ft in the Waikapū aquifer system. The freshwater lens thinned during this period, with the simulated 50-percent ocean-water salinity surface up to 500 ft higher in the ʻĪao aquifer system in 2012 relative to 1926. Similarly, the simulated 50-percent ocean-water salinity surface was more than 300 ft higher in the southern Waiheʻe aquifer system. In the Waikapū aquifer system, the 50-percent ocean-water salinity surface was less than 200 ft higher in 2012 relative to 1926 (fig. 11) because groundwater withdrawals there did not start until 2015.

Simulated transient groundwater levels are in reasonable agreement with observed water levels in the Waiheʻe, ʻĪao, and Waikapū aquifer systems (fig. 12). At some sites, available water levels (U.S. Geological Survey, 2019) are uncertain because of uncertainty in the reference measuring-point altitude used at the site. Water levels measured prior to 2003 were updated based on recent survey results. Although these survey results reflect the best available information, determining the accuracy of the earlier surveys may not be possible given potential site changes over time and irretrievable starting reference marks used for the early surveys.

Simulated water levels in observation wells in the Waiheʻe aquifer system (5631–02 and 5631–09) declined from about 17 ft in 1930 to about 5 ft in 2012, with a steeper decline occurring since 1980. In the northern part of the ʻĪao aquifer system,

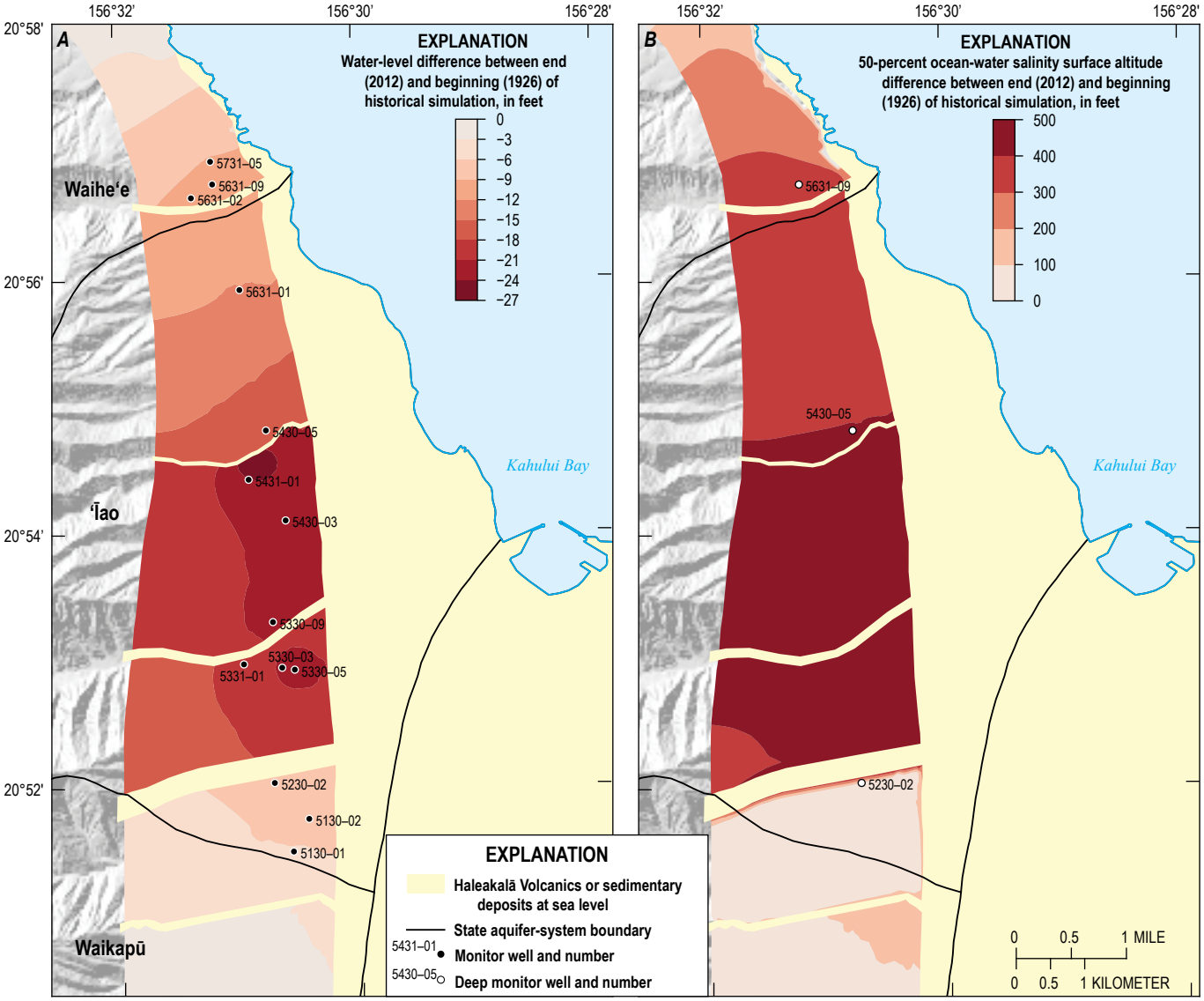

Base modified from U.S. Geological Survey National Hydrography Dataset, Scale of 1:24,000
Shaded relief from U.S. Geological Survey digital elevation model data
Universal Transverse Mercator Projection, Zone 4
North American Datum of 1983

Figure 11. Simulated changes in (*A*) water level and (*B*) 50-percent ocean-water salinity surface altitude in the study area between 1926 and 2012, central Maui, Hawaiʻi.

simulated water levels in observation wells declined from about 22 ft (5631–01) and 26 ft (5430–05) in 1930 to 10 ft in both wells in 2012. In the southern part of the ʻĪao aquifer system, simulated water levels in observation wells declined from about 31 ft in 1930 to about 10 ft (5430–03 and 5330–09) and to 6 ft (5431–01) in 2012. Simulated water levels in observation wells in the southern part of the Waikapū aquifer system declined from about 7 ft in 1930 to about 4 ft in 2012 (4831–01), with a steeper decline occurring since 1980 (fig. 12).

Simulated and measured salinity profiles are generally in agreement, although the simulated profiles indicate that the model underestimates the thickness of freshwater near well 5430–05 for the two later simulated dates shown (January 2005 and December 2012; fig. 13). This underestimation of freshwater thickness may reflect model inaccuracy or possibly may be due to borehole flow that can occur in wells of this type with long open or screened intervals (for example, Rotzoll, 2010; Rotzoll, 2012). A larger porosity value would provide a

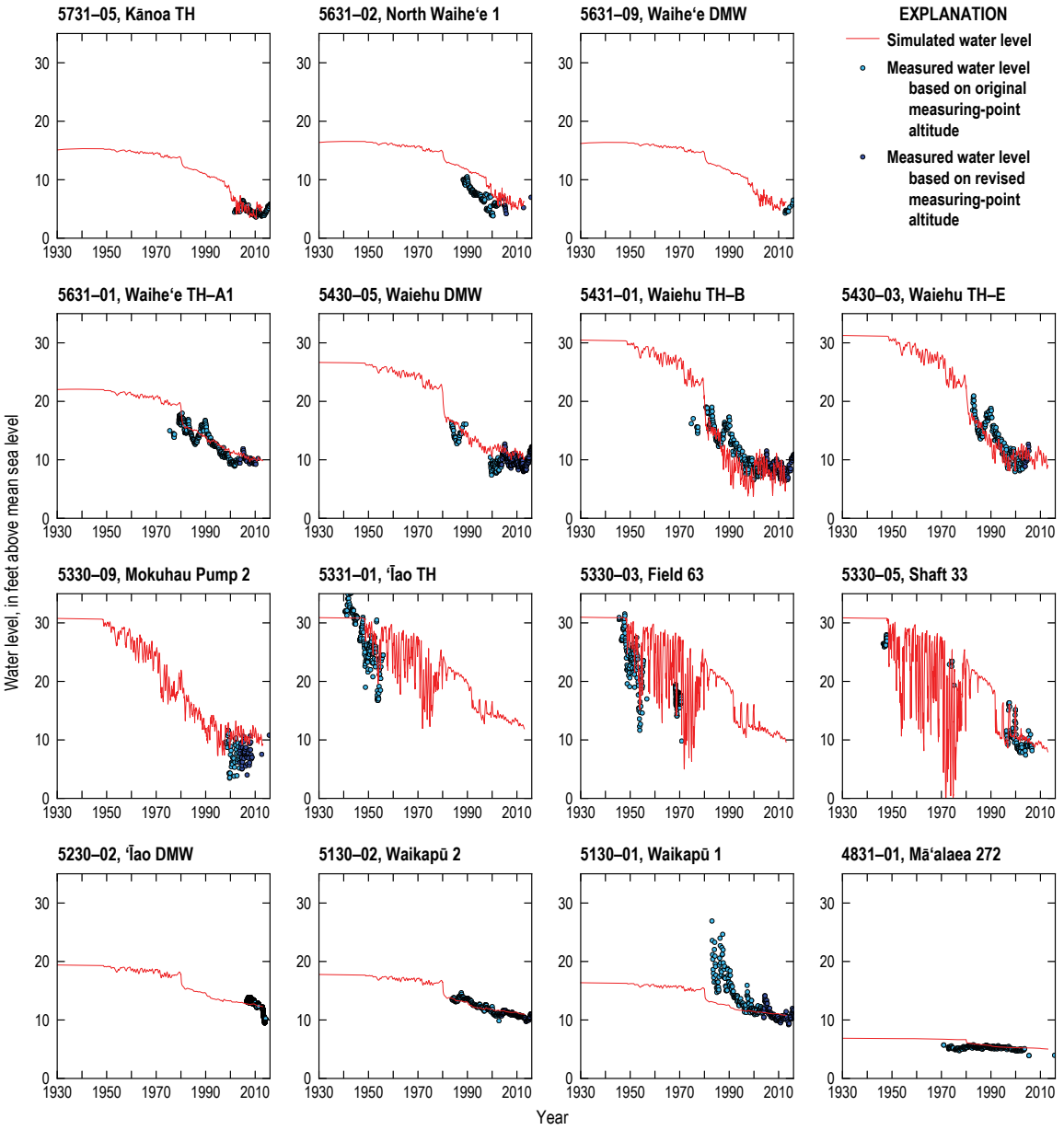

Figure 12. Graphs showing measured and simulated groundwater levels at selected wells during 1930–2016 in the Wailuku area, central Maui, Hawaiʻi. Well locations are shown in figure 1. Data from U.S. Geological Survey (2019), Gingerich (2008; well 5330–03), and Hawaiʻi Commission on Water Resource Management (5631–09 and 5230–02). DMW, deep monitor well; TH, test hole. At the time of publication, data had not been published by the Hawaiʻi Commission on Water Resource Management.

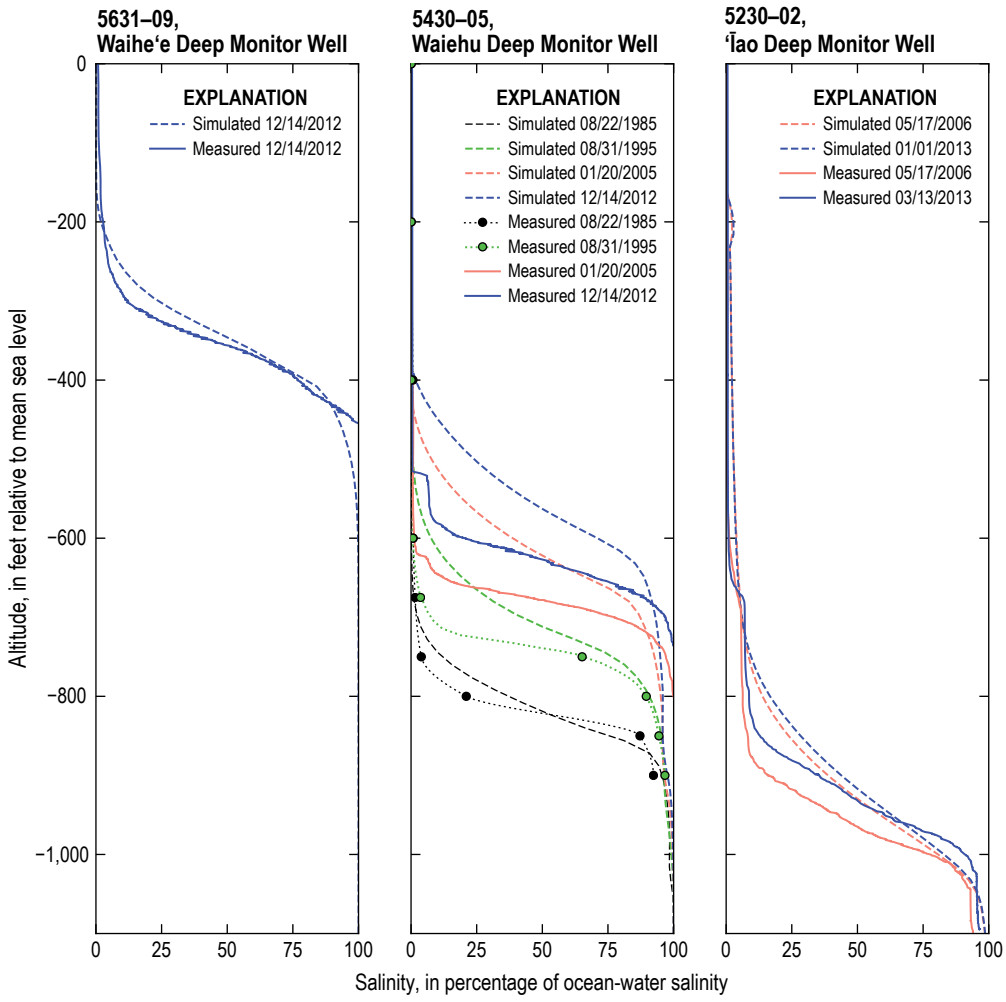

Figure 13. Measured and simulated salinity profiles in selected wells in the Wailuku area, central Maui, Hawaiʻi. Well locations shown in figure 1. Specific conductance of 50,000 microsiemens per centimeter at 25 degrees Celsius and chloride concentration of 19,500 milligrams per liter correspond to 100 percent salinity; dotted lines are from a piecewise cubic hermite interpolating polynomial. Data from U.S. Geological Survey (2019; well 5430–05) and Hawaiʻi Commission on Water Resource Management (5230–02, 5430–05, and 5631–09). At the time of publication, data had not been published by the Hawaiʻi Commission on Water Resource Management.

better match between simulated and measured salinity profiles for all dates in well 5430–05. However, the better match between simulated and measured salinity profiles in well 5430–05 would also be associated with a poorer match between simulated and measured chloride concentrations of pumped water in nearby wells. Overall, in all simulated wells and dates (fig. 13), the model is conservative from the standpoint of freshwater thickness observed in deep open boreholes.

Simulated chloride concentrations of water withdrawn by wells are in general agreement with observed chloride concentrations (fig. 14). Simulated chloride concentrations from wells 5431–02, 5430–02, 5330–09, and 5330-05 are exceptions; these wells all have simulated chloride concentrations lower than observed concentrations. Because of large uncertainties in local-scale aquifer heterogeneity that can affect the quality of water withdrawn by a well and mesh discretization limitations (for example, wells 5330–09 to –11 occupy the same vertical column of nodes), the model cannot be expected to produce an exact match between simulated and observed chloride concentrations at all locations. However, the model does appear to generally capture the overall quality of water withdrawn by wells in the study area.

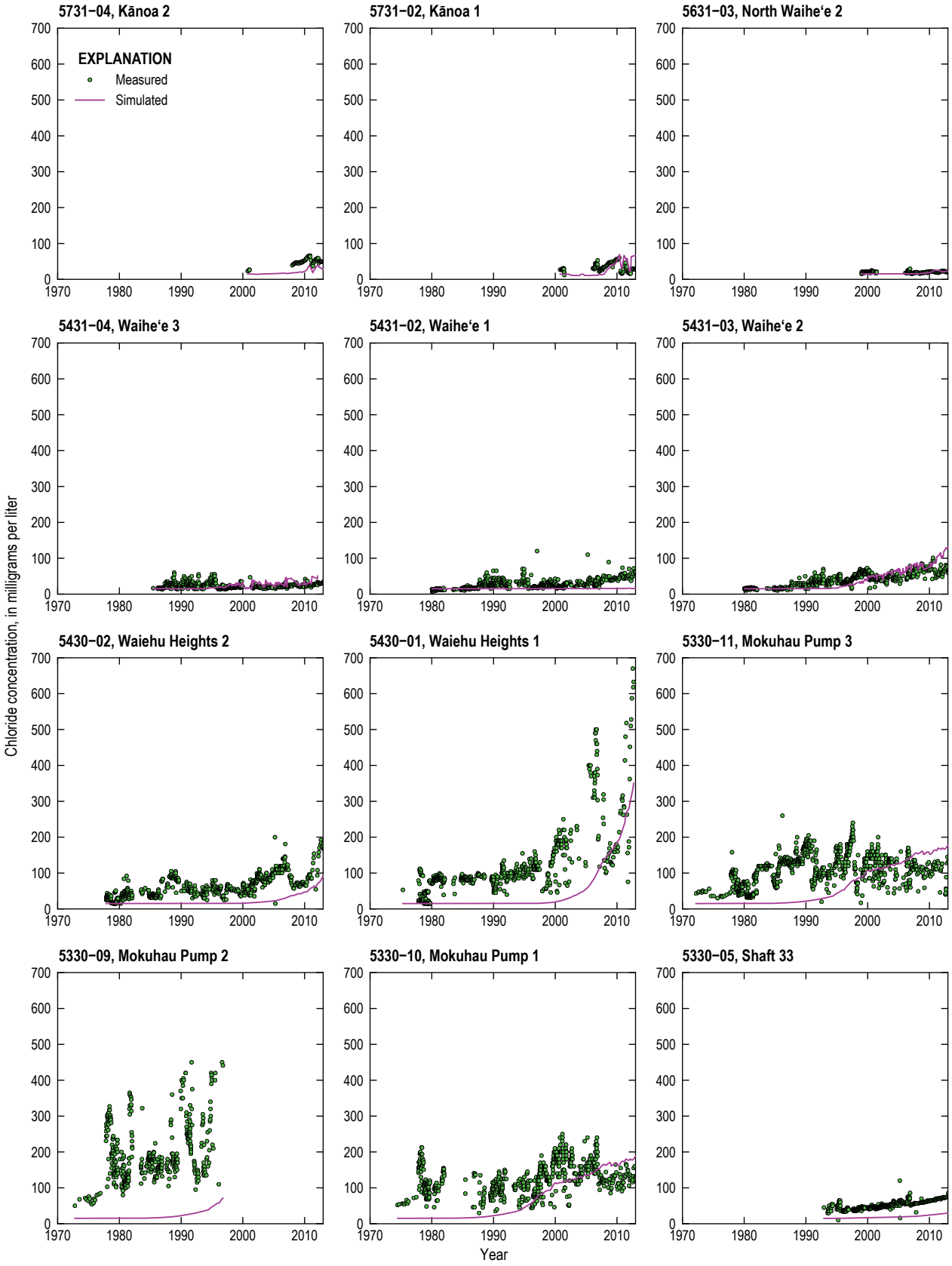

Figure 14. Graphs showing measured and simulated chloride concentration of pumped water from selected wells during 1970–2012 in the Wailuku area, central Maui, Hawai‘i. Data are from U.S. Geological Survey (2019), National Water Information System database and Maui Department of Water Supply. At the time of publication, data had not been published by the Maui Department of Water Supply.

Simulated Future Scenarios

The long-term hydrologic effects of withdrawal and recharge on the quality of water pumped from wells were simulated with the model (Rotzoll, 2022) for a variety of possible future conditions, which are here termed "scenarios." The following simulated withdrawal and recharge scenarios were selected in consultation with representatives of the MDWS: (1) a baseline scenario using average recharge (1980−2010 rainfall and 2017 land cover) and average 2017−18 withdrawals; (2) a scenario using average recharge and withdrawals from existing wells withdrawing at water-use permit rates (as of 2019); (3) four scenarios using average recharge and selected withdrawals from existing and proposed new wells; and (4) a scenario using reduced recharge based on rainfall projections for a RCP8.5 warming scenario during 2071–99 and 2017 land cover (Mair and others, 2019) and one selected withdrawal scenario from item (3). All simulations were run for sufficient time to reach steady-state conditions, providing an estimate of the long-term effects of each scenario on groundwater resources.

For each scenario, the simulated long-term chloride concentration (derived from the simulated TDS concentration; see equation 2 above) of groundwater withdrawn by each production well in the Waiheʻe, ʻĪao, and Waikapū aquifer systems was generalized into one of four categories: (1) less than 100 mg/L; (2) greater than or equal to 100 mg/L and less than or equal to 200 mg/L; (3) greater than 200 mg/L and less than or equal to 250 mg/L; and (4) greater than 250 mg/L. Although the EPA secondary standard for chloride concentration in drinking water is 250 mg/L, maintaining the chloride concentration of produced water less than 200 mg/L helps provide a buffer to avoid concentrations greater than 250 mg/L. Because water withdrawn from wells 5431–02 to –04 can be blended in a tank before entering the water distribution system, a weighted chloride concentration was additionally calculated for this well field. That is, for chloride concentrations of groundwater withdrawn from wells in the well field, the weighted chloride concentration was determined by weighting chloride concentrations of groundwater withdrawn from each well by the withdrawal amount at the well and then determining the overall withdrawal-weighted average.

Scenario 1—Baseline

A baseline scenario was developed to provide a basis for evaluating the long-term effects of existing withdrawal rates in the Waiheʻe, ʻĪao, and Waikapū aquifer systems, in terms of salinity of groundwater from the production wells. The baseline scenario used average recharge conditions—estimated using 1980–2010 rainfall and 2017 land-cover condition—and average withdrawals during 2017–18. Recharge values from the baseline scenario were 39.6 Mgal/d from the inland boundary; 21.1 Mgal/d from the top, onshore boundary within the modeled area; and 12.5 Mgal/d from restored streamflow in the Waiheʻe River (1.5 Mgal/d), Waiehu Stream (2.5 Mgal/d), Wailuku River (5.6 Mgal/d), and Waikapū Stream (2.9 Mgal/d). Total simulated withdrawal represented in the model from wells was 69.9 Mgal/d. Simulated withdrawal from the Honomanū Basalt/Kula Volcanics in the Kahului aquifer system was 49.7 Mgal/d, which included 45.9 Mgal/d of withdrawals of brackish water from wells 5427–01 to –11. Simulated withdrawal rates from the Kahului aquifer system remained unchanged in all scenarios. For the purpose of this report, the wells in the ʻĪao aquifer system are separated into northern and southern parts: the northern part contains production wells north of and including well P4 and the southern part contains production wells south of and including Mokuhau 3 well (5330−11; fig. 1). In the model, production wells in the Waiheʻe, ʻĪao, and Waikapū aquifer systems were pumped at 4.8, 15.4 (about 7.3 in the northern part and 8.2 in the southern part), and less than 0.1 Mgal/d, respectively (table 3).

Regional changes of simulated water levels in the baseline scenario, relative to conditions at the end of the historical simulation (2012), are greatest in the ʻĪao aquifer system with a water-level rise of 6−8 ft (fig. 15). Water levels are higher for the baseline scenario due to greater recharge relative to the 2010−12 recharge at the end of the historical simulation. The average rainfall during 1980−2010 in the Waiheʻe, ʻĪao, and Waikapū aquifer systems was similar to average rainfall during 1920−2012, and was much lower during 2010−12 (see inset graph in fig. 2), and the estimated recharge from restored streamflow represents about 20 percent of additional recharge in scenario 1. The simulated 50-percent ocean-water salinity surface is up to 100 ft lower in areas where the water level increases 4−8 ft (fig. 15). The simulated 50-percent ocean-water salinity surface is up to 400 ft higher near the ʻĪao Deep Monitor Well (5230–02) in the baseline scenario, relative to conditions at the end of the historical simulation. The thinning of the freshwater lens most likely reflects the long-term response to historical withdrawals. The change in the 50-percent ocean-water salinity surface is not expected to follow the Ghyben-Herzberg principle (that is, for each foot of water-level rise, the 50-percent ocean-water salinity surface would be 40 ft lower) because the system was not at steady state at the end of the historical simulation.

For the baseline scenario, the simulated chloride concentrations of groundwater withdrawn from wells in the Waiheʻe, ʻĪao, and Waikapū aquifer systems are less than 100 mg/L (fig. 16). The weighted chloride concentration of groundwater withdrawn from wells 5431–02 to –04 is less than 100 mg/L (table 3). Model results from the Wailuku area indicate that withdrawals under the baseline condition will ultimately produce water with chloride concentrations below the EPA secondary standard for drinking water, although the model likely does not represent the exact salinity of withdrawn water from an individual well for several reasons (see Limitations section below).

Table 3. Withdrawal rates used in the modeled scenarios for selected production wells in the Waiheʻe, ʻĪao, and Waikapū aquifer systems, central Maui, Hawaiʻi.

[Withdrawal values without footnote references indicate simulated chloride concentration of pumped water is less than 100 milligrams per liter (mg/L). Withdrawals are from production wells. Mgal/d, million gallons per day; --, no simulated withdrawal rate.]

Well	Withdrawal rate in Mgal/d						
	Scenario 1, baseline with 2017–18 withdrawals	Scenario 2, permitted withdrawal rates	Scenario 3, 28.3 Mgal/d withdrawals	Scenario 4, 26.9 Mgal/d withdrawals	Scenario 5, 27.5 Mgal/d withdrawals	Scenario 6, 28.2 Mgal/d withdrawals	Scenario 7, scenario 4 withdrawals (reduced recharge)
Waiheʻe aquifer system							
P1	--	--	--	--	[6]1.122	--	--
5731–03	1.231	[1]1.231	[1]1.684	1.000	[1]1.122	[6]1.000	1.000
P2	--	--	--	1.000	1.122	[1,6]1.122	1.000
5731–02	0.828	0.850	1.764	1.000	1.175	1.764	1.000
5731–04	1.071	1.071	--	--	--	--	--
5631–03	0.753	0.753	--	--	--	--	--
5631–02	0.871	0.871	1.591	1.000	1.060	[4]1.591	1.000
ʻĪao aquifer system, northern part							
P3	--	--	0.500	--	1.080	1.080	--
5431–04	2.325	[1]2.267	3.400	3.400	[1]3.078	[1]3.078	[1]3.400
5431–02	2.521	[1]2.267	[4]1.900	[1,4]1.900	--	--	[1,5]1.900
5431–03	1.313	[5]2.267	[5]1.500	[6]1.500	[5]3.722	[5]3.722	[5]1.500
[3]5431–02–04	6.158	[4]6.800	[4]6.800	[4]6.800	[4]6.800	[4]6.800	[4]6.800
5430–02	1.094	[2,6]1.000	[1]0.500	[2,6]1.000	[1]1.000	[1,4]1.000	[2,6]1.000
P4	--	--	--	1.080	1.080	1.080	1.080
ʻĪao aquifer system, southern part							
5330–11	2.481	[2,4]2.353	[1]3.853	[2,4]2.750	[2]1.100	[2]2.000	[2,5]2.750
5330–10	1.169	[2,5]1.500	--	--	[2,4]0.500	--	--
5230–03	0.951	[1,4]2.083	1.852	2.083	2.083	1.300	[1,4]2.083
5230–04	0.839	2.190	1.852	2.190	2.190	2.190	2.190
5230–05	1.710	1.852	1.852	1.852	1.852	2.300	1.852
5131–01	[2]1.045	1.285	1.852	1.285	1.285	1.285	1.285
Waikapū aquifer system							
5030–02	--	0.374	0.480	0.480	0.480	--	0.480
P5	--	[4]0.419	[2,6]0.537	[5]0.537	[4]0.537	[4]0.900	[6]0.537
P6	--	0.561	--	0.719	--	--	0.719
5131–02	0.001	0.561	1.000	0.719	0.719	0.900	0.719
5030–01	0.001	0.561	0.720	0.719	0.720	0.900	0.719
5130–04	0.001	0.524	[4]1.440	0.671	0.480	--	[4]0.671
Recharge, in Mgal/d							
	73.1	73.1	73.1	73.1	73.1	73.1	57.8

[1] Negative chloride concentration in the freshwater zone simulated at one of the nodes representing the well was assigned a value of 195 mg/L.

[2] Negative chloride concentration in the freshwater zone simulated at two to ten of the nodes representing the well was assigned a value of 195 mg/L.

[3] Represents the combined withdrawal of the three wells and simulated withdrawal-weighted chloride concentration from the three wells.

[4] Simulated chloride concentration of pumped water is between 100 and 200 mg/L.

[5] Simulated chloride concentration of pumped water is greater than 200 and less than or equal to 250 mg/L.

[6] Simulated chloride concentration of pumped water exceeds 250 mg/L.

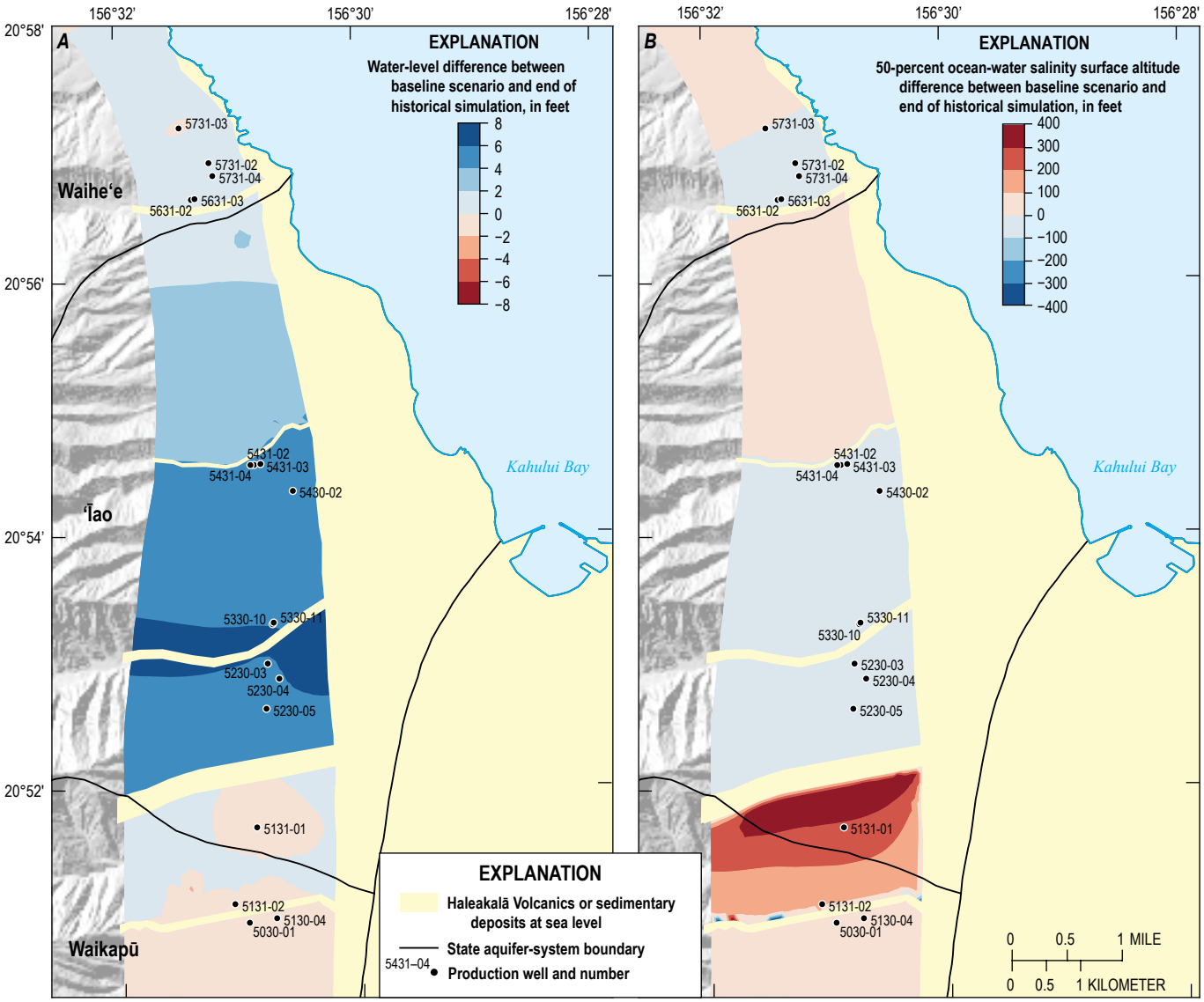

Base modified from U.S. Geological Survey National Hydrography Dataset, Scale of 1:24,000
Shaded relief from U.S. Geological Survey digital elevation model data
Universal Transverse Mercator Projection, Zone 4
North American Datum of 1983

Figure 15. Simulated change in (*A*) water level and (*B*) 50-percent ocean-water salinity surface altitude in the study area for scenario 1 (baseline conditions with 2017–18 average withdrawals: 20.2 million gallons per day in the Waiheʻe, ʻĪao, and Waikapū aquifer systems) relative to the end of the historical simulation, central Maui, Hawaiʻi.

Scenario 2—Water-Use Permit Rates in ʻĪao Aquifer System, Prorated Pump Capacity in Waiheʻe and Waikapū Aquifer Systems

Scenario 2 includes the same recharge and withdrawals as the baseline scenario, except simulated withdrawals from production wells in the ʻĪao aquifer system were changed to the CWRM water-use permit rates (as of 2019). In the absence of water-use permit rates, withdrawal rates from production wells in the Waiheʻe and Waikapū aquifer systems were changed to rates corresponding to the prorated pump capacities of the wells. The prorated pump capacity is the pump capacity for each well divided by the sum of pump capacities from all wells considered in the aquifer system multiplied by 4 Mgal/d (the CWRM-recommended total) in the Waiheʻe and multiplied by 3 Mgal/d (the CWRM-estimated sustainable yield) in the Waikapū aquifer system, respectively. If the 2017–18 average pumping rate for a well was higher than the prorated pump capacity, the 2017–18 average pumping rate was used instead. Total simulated withdrawal represented in the model from wells was 76.6 Mgal/d, including 49.7 Mgal/d withdrawals from the Honomanū Basalt/Kula Volcanics in the Kahului aquifer system. Simulated withdrawals from production wells in the Waiheʻe, ʻĪao, and Waikapū aquifer systems were 4.8, 19.1 (about 7.8 in the northern part and 11.3 in the southern part), and 3.0 Mgal/d, respectively (table 3).

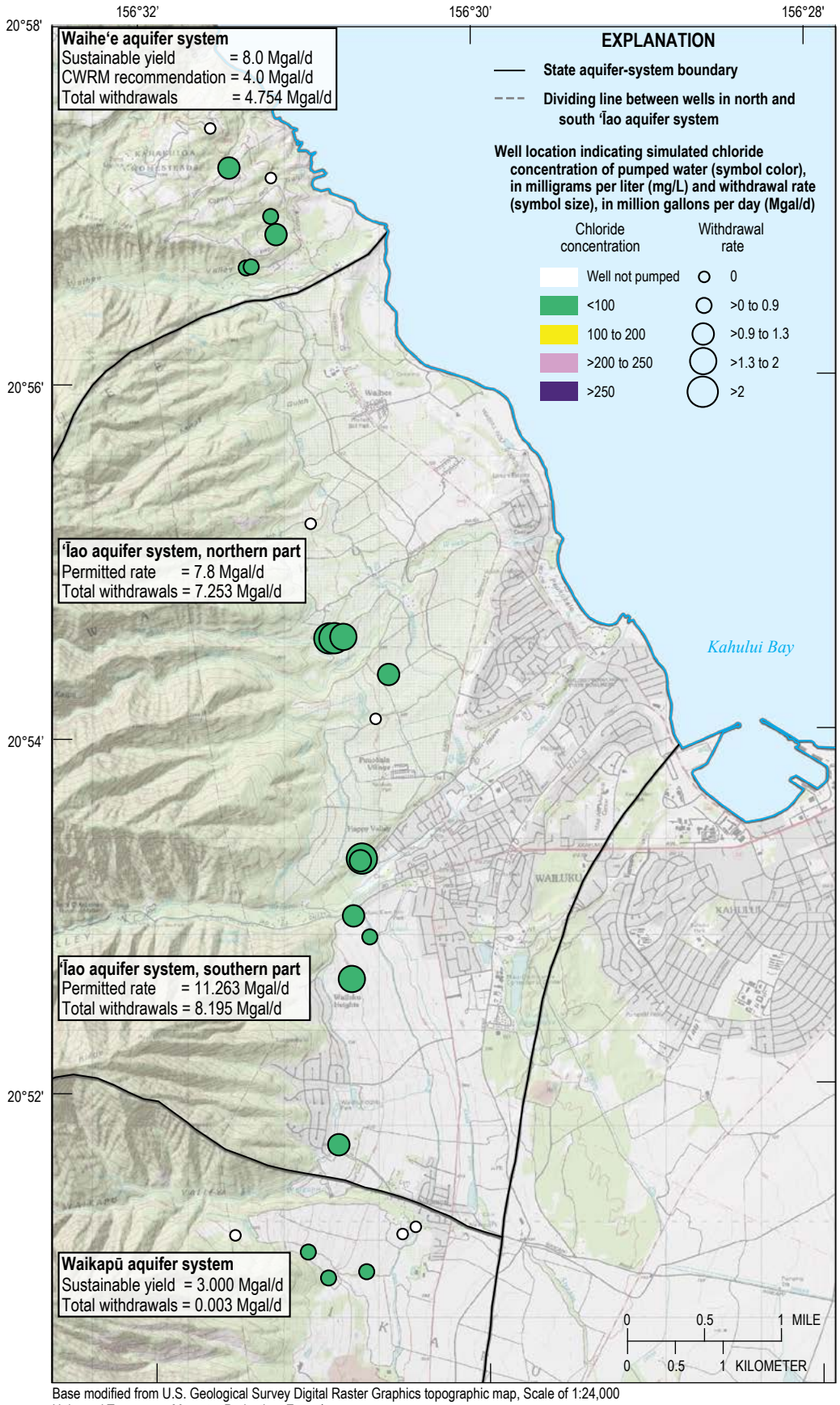

Base modified from U.S. Geological Survey Digital Raster Graphics topographic map, Scale of 1:24,000
Universal Transverse Mercator Projection, Zone 4
North American Datum of 1983

Figure 16. Withdrawal rates and simulated chloride concentrations of pumped water from wells included in scenario 1 (baseline conditions with 2017–18 average withdrawals: 20.2 million gallons per day in the Waihe'e, 'Īao, and Waikapū aquifer systems), central Maui, Hawai'i. CWRM, State of Hawai'i Commission on Water Resource Management.

Regional changes of simulated water levels in scenario 2, relative to the baseline scenario, are greatest in the southern part of the ʻĪao aquifer system with a water-level decline of greater than 8 ft near wells 5230–03 and 5230–04. The water-level decline is related to the increase in withdrawals. Accordingly, the simulated 50-percent ocean-water salinity surface ultimately rises between 150 and 250 ft in the southern part of the ʻĪao aquifer system (fig. 17).

For scenario 2, the simulated chloride concentrations of groundwater withdrawn from wells in Waiheʻe and Waikapū aquifer systems are less than 100 mg/L, except for well P5 in the Waikapū aquifer system, where the simulated chloride concentration of groundwater withdrawn is in the 100–200 mg/L category. In the ʻĪao aquifer system, the simulated chloride concentrations of groundwater withdrawn from wells 5230–03, 5330–11, and 5431–02 are in the 100–200 mg/L category, whereas the simulated chloride concentrations of groundwater withdrawn from wells 5330–10 and 5431–03 are in the 200–250 mg/L category, and the simulated chloride concentration of groundwater withdrawn from well 5430–02 is in the greater than 250 mg/L category (fig. 18). The weighted chloride concentration of groundwater withdrawn from wells 5431–02 to –04 is in the 100–200 mg/L category (table 3). The simulated chloride concentrations from production wells indicate that chloride concentrations of pumped water from the wells in the Wailuku area for scenario 2 remain below the EPA secondary standard, except withdrawals at well 5430–02.

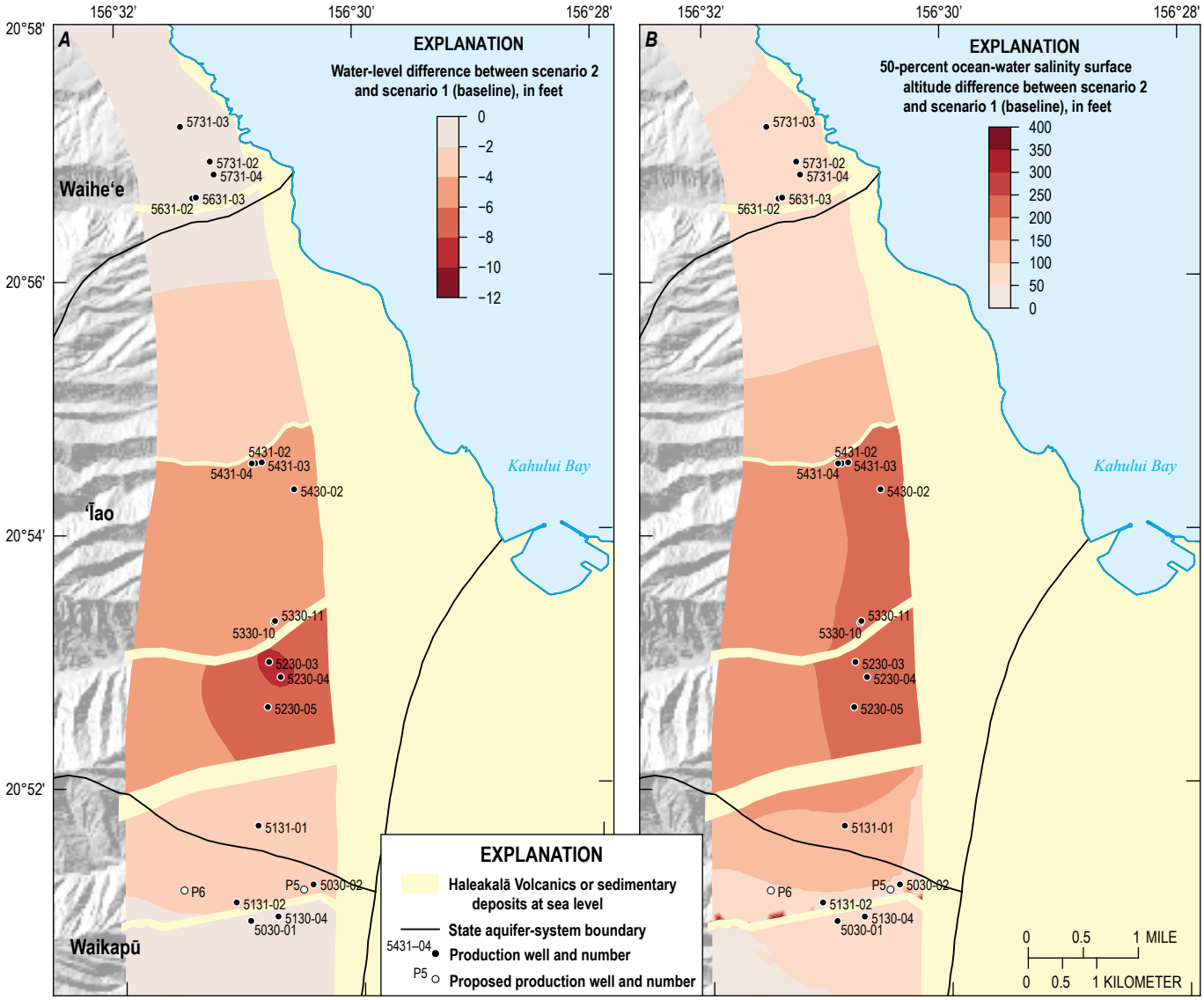

Base modified from U.S. Geological Survey National Hydrography Dataset, Scale of 1:24,000
Shaded relief from U.S. Geological Survey digital elevation model data
Universal Transverse Mercator Projection, Zone 4
North American Datum of 1983

Figure 17. Simulated change in (*A*) water level and (*B*) 50-percent ocean-water salinity surface altitude in the study area for scenario 2 (permitted rates from production wells: 26.8 million gallons per day in the Waiheʻe, ʻĪao, and Waikapū aquifer systems) relative to scenario 1 (baseline), central Maui, Hawaiʻi.

Scenario 3—28.3 Mgal/d Withdrawals from Waiheʻe, ʻĪao, and Waikapū Aquifer System Production Wells

Scenario 3 includes the same recharge and withdrawals as the baseline scenario, except simulated withdrawals from production wells in the Waiheʻe, ʻĪao, and Waikapū aquifer systems were changed. In the Waiheʻe aquifer system, wells 5731–03, 5731–02, and 5631–02 were pumped at the pump-capacity rate. The Waiheʻe aquifer system total withdrawal rate of 5 Mgal/d is above the CWRM-recommended value of 4 Mgal/d for the southern part of the aquifer system, although the withdrawal rate falls below the CWRM-estimated sustainable-yield of 8 Mgal/d for the entire aquifer system. In the northern part of the ʻĪao aquifer system, wells 5431–02, 5431–03, and 5431–04 were pumped at the water-use permit rate, and the water-use permit rate for well 5430–02 was equally distributed among 5430–02 and P3. In the southern part of the ʻĪao aquifer system, well 5330–10 was not pumped, and the pumping rate at well 5330–11 was consistent with the combined water-use permit rate for 5330–10 and 5330–11. A

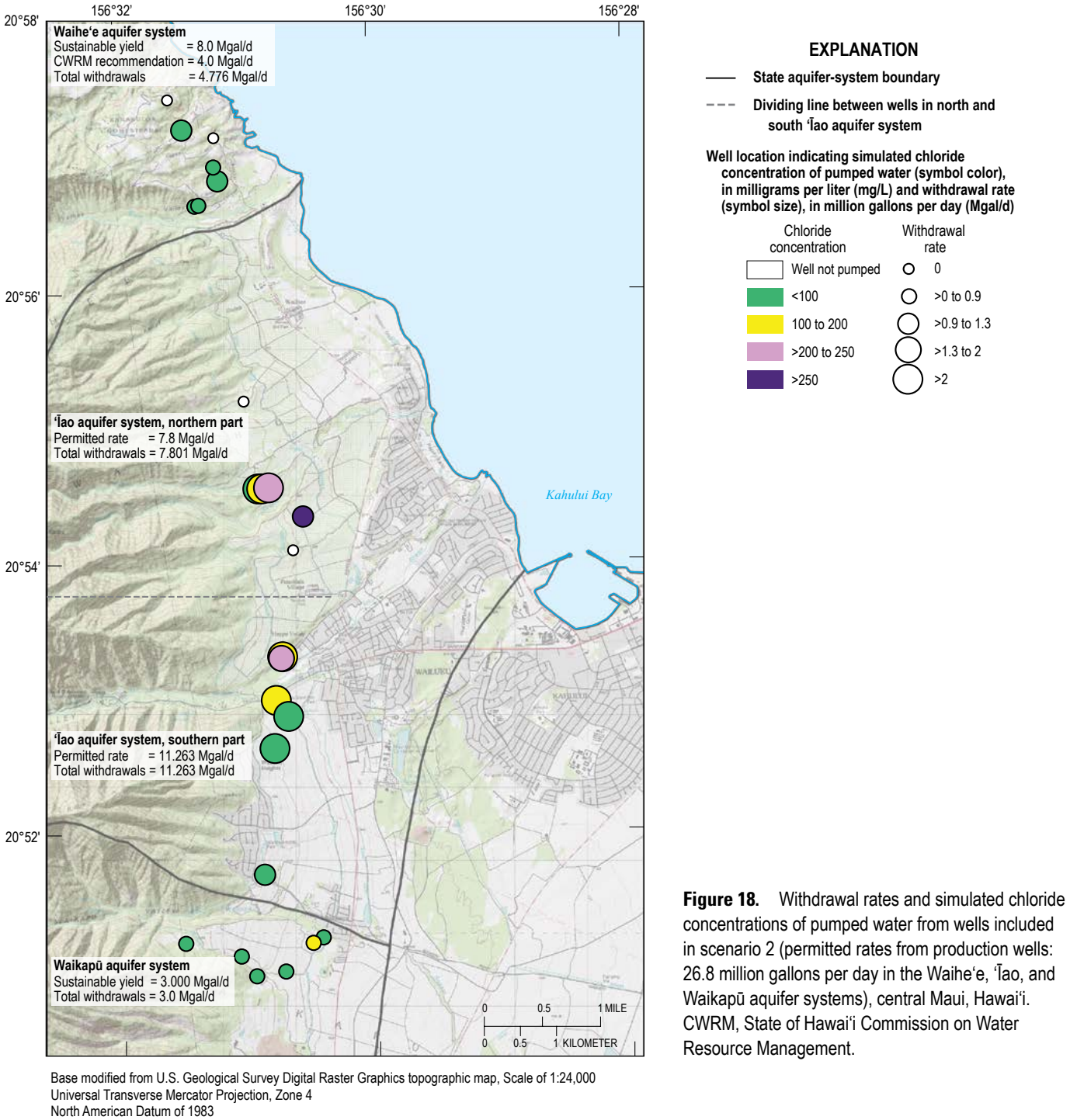

Base modified from U.S. Geological Survey Digital Raster Graphics topographic map, Scale of 1:24,000
Universal Transverse Mercator Projection, Zone 4
North American Datum of 1983

Figure 18. Withdrawal rates and simulated chloride concentrations of pumped water from wells included in scenario 2 (permitted rates from production wells: 26.8 million gallons per day in the Waiheʻe, ʻĪao, and Waikapū aquifer systems), central Maui, Hawaiʻi. CWRM, State of Hawaiʻi Commission on Water Resource Management.

typical withdrawal rate of 7.4 Mgal/d that occurred at Shaft 33 (5330–05) in the 1970s was equally distributed among four wells (5230–03, 5230–04, 5230–05, and 5131–01). In the Waikapū aquifer system, withdrawals were distributed according to proposed rates by Planning Consultants Hawaii, LLC (2016), which excluded withdrawals from well P6. The total simulated withdrawal represented in the model from wells was 78.0 Mgal/d, including 49.7 Mgal/d withdrawals from the Honomanū Basalt/Kula Volcanics in the Kahului aquifer system. Simulated withdrawals from production wells in the Waiheʻe, ʻĪao, and Waikapū aquifer systems were 5, 19.1 (about 7.8 in the northern part and 11.3 in the southern part), and 4.2 Mgal/d, respectively (table 3).

Regional changes of simulated water levels in scenario 3, relative to the baseline scenario, are greatest in the southern part of the ʻĪao aquifer system due to the increase in withdrawals in this area. Water levels decline 6–8 ft near wells 5230–03 and 5230–04. The simulated 50-percent ocean-water salinity surface ultimately rises between 100 and 200 ft in the southern part of the ʻĪao aquifer system (fig. 19), less than the simulated 50-percent ocean-water salinity surface rise in scenario 2.

For scenario 3, the simulated chloride concentrations of groundwater withdrawn from wells in Waiheʻe and southern part of the ʻĪao aquifer systems are less than 100 mg/L. The simulated chloride concentrations of groundwater withdrawn from wells 5431–02 and 5130–04 are in the 100–200 mg/L category, whereas the simulated chloride concentration of groundwater withdrawn from well 5431–03 is in the 200–250 mg/L category, and the simulated chloride concentration of groundwater withdrawn from well P5 is in the greater than 250 mg/L category (fig. 20). The weighted

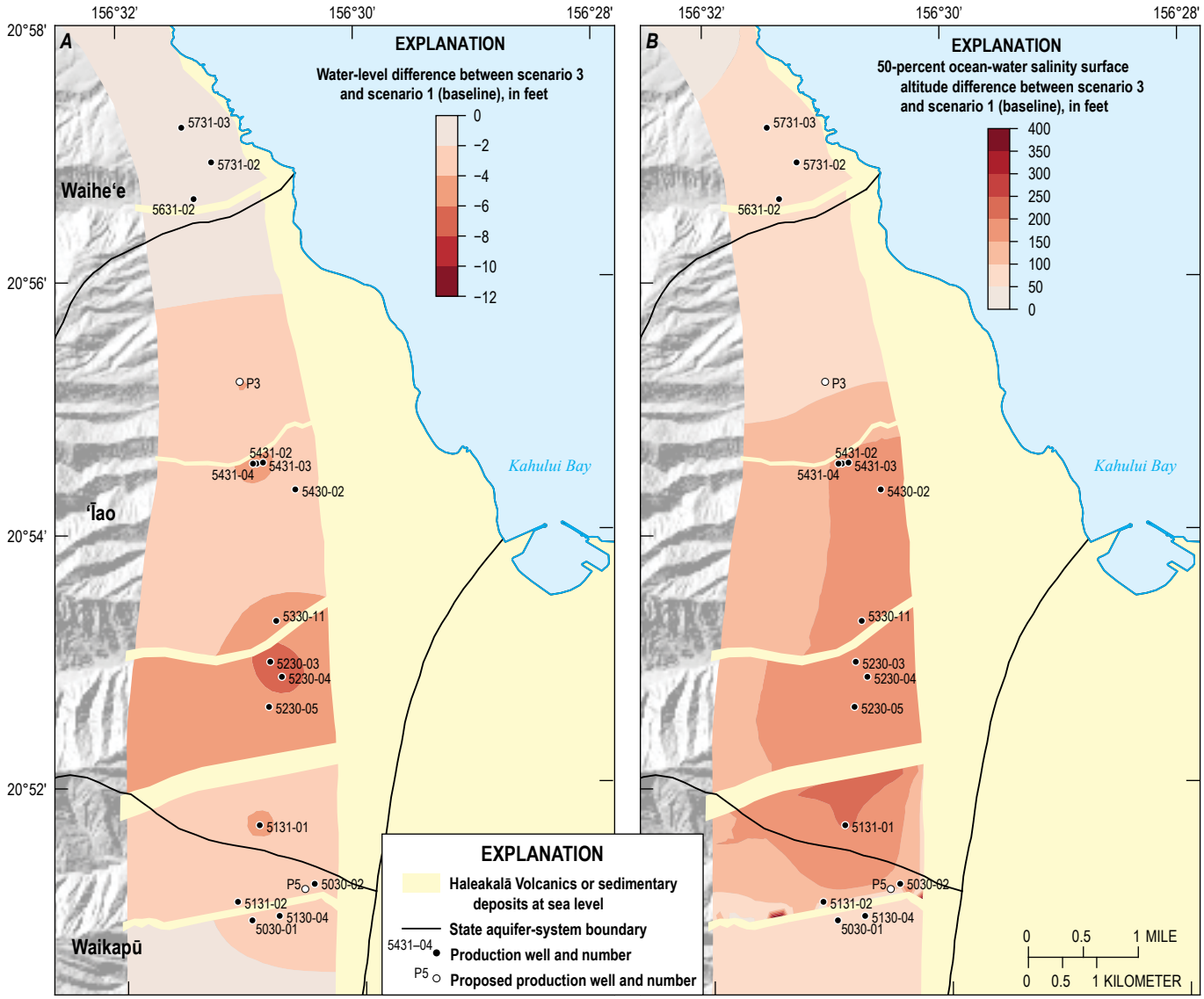

Base modified from U.S. Geological Survey National Hydrography Dataset, Scale of 1:24,000
Shaded relief from U.S. Geological Survey digital elevation model data
Universal Transverse Mercator Projection, Zone 4
North American Datum of 1983

Figure 19. Simulated change in (*A*) water level and (*B*) 50-percent ocean-water salinity surface altitude in the study area for scenario 3 (28.3 million gallons per day withdrawals from production wells in the Waiheʻe, ʻĪao, and Waikapū aquifer systems) relative to scenario 1 (baseline), central Maui, Hawaiʻi.

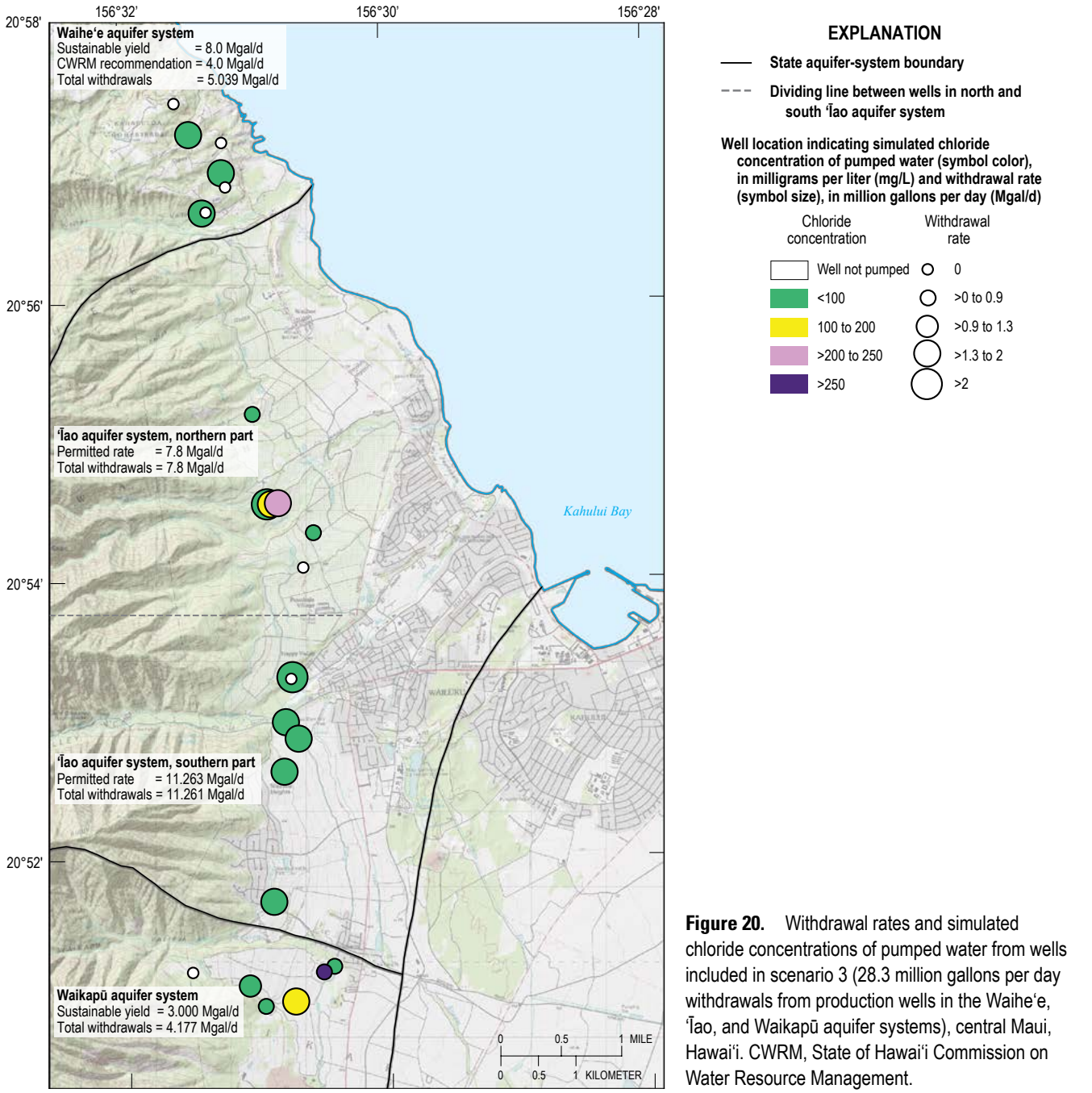

Base modified from U.S. Geological Survey Digital Raster Graphics topographic map, Scale of 1:24,000
Universal Transverse Mercator Projection, Zone 4
North American Datum of 1983

Figure 20. Withdrawal rates and simulated chloride concentrations of pumped water from wells included in scenario 3 (28.3 million gallons per day withdrawals from production wells in the Waiheʻe, ʻĪao, and Waikapū aquifer systems), central Maui, Hawaiʻi. CWRM, State of Hawaiʻi Commission on Water Resource Management.

chloride concentration of groundwater withdrawn from wells 5431–02 to –04 is in the 100–200 mg/L category (table 3). The simulated chloride concentrations from production wells indicate that chloride concentrations of pumped water from the wells in the Wailuku area for scenario 3 remain below the EPA secondary standard except at well P5.

Scenario 4—26.9 Mgal/d Withdrawals from Waiheʻe, ʻĪao, and Waikapū Aquifer System Production Wells

Scenario 4 includes the same recharge and withdrawals as the baseline scenario, except simulated withdrawals from production wells in the Waiheʻe, ʻĪao, and Waikapū aquifer systems were changed. In the Waiheʻe aquifer system, withdrawal from wells 5731–03, 5731–02, 5631–02, and P2 was 1 Mgal/d, resulting in a total withdrawal consistent with the CWRM-recommended value of 4 Mgal/d for the southern part of the aquifer system. In the ʻĪao aquifer system, withdrawals were redistributed from the south to the north relative to scenario 3. In the northern part of the ʻĪao aquifer system, the withdrawals at wells 5431–02, 5431–03, 5431–04, and 5430–02 were at the water-use permit rate and 1.1 Mgal/d was pumped at well P4. In the southern part of the ʻĪao aquifer system, withdrawal from well 5330–11 was decreased to 2.8 Mgal/d from 3.9 Mgal/d in scenario 3. A typical withdrawal rate of 7.4 Mgal/d that occurred at Shaft 33

(5330–05) in the 1970s was distributed among wells 5230–03, 5230–04, 5230–05, and 5131–01 according to their water-use permit rates. In the Waikapū aquifer system, withdrawals were distributed according to proposed rates by Planning Consultants Hawaii, LLC (2016), revised based on input from MDWS. Total simulated withdrawal represented in the model from wells was 76.6 Mgal/d, including 49.7 Mgal/d withdrawals from the Honomanū Basalt/Kula Volcanics in the Kahului aquifer system. Simulated withdrawals from production wells in the Waiheʻe, ʻĪao, and Waikapū aquifer systems were 4, 19.0 (about 8.9 in the northern part and 10.2 in the southern part), and 3.8 Mgal/d, respectively (table 3).

Regional changes of simulated water levels in scenario 4, relative to the baseline scenario, are greatest in the southern part of the ʻĪao aquifer system with a water-level decline of 8–10 ft near wells 5230–03 and 5230–04. The water-level decline is related to the increase in withdrawals in this area. Similarly, the simulated 50-percent ocean-water salinity surface in scenario 4 rises 150–250 ft near well 5430–02 and near well 5230–04 and in the southern part of the ʻĪao aquifer system (fig. 21).

For scenario 4, the simulated chloride concentrations of groundwater withdrawn from wells in the Waiheʻe aquifer system are less than 100 mg/L. The simulated chloride

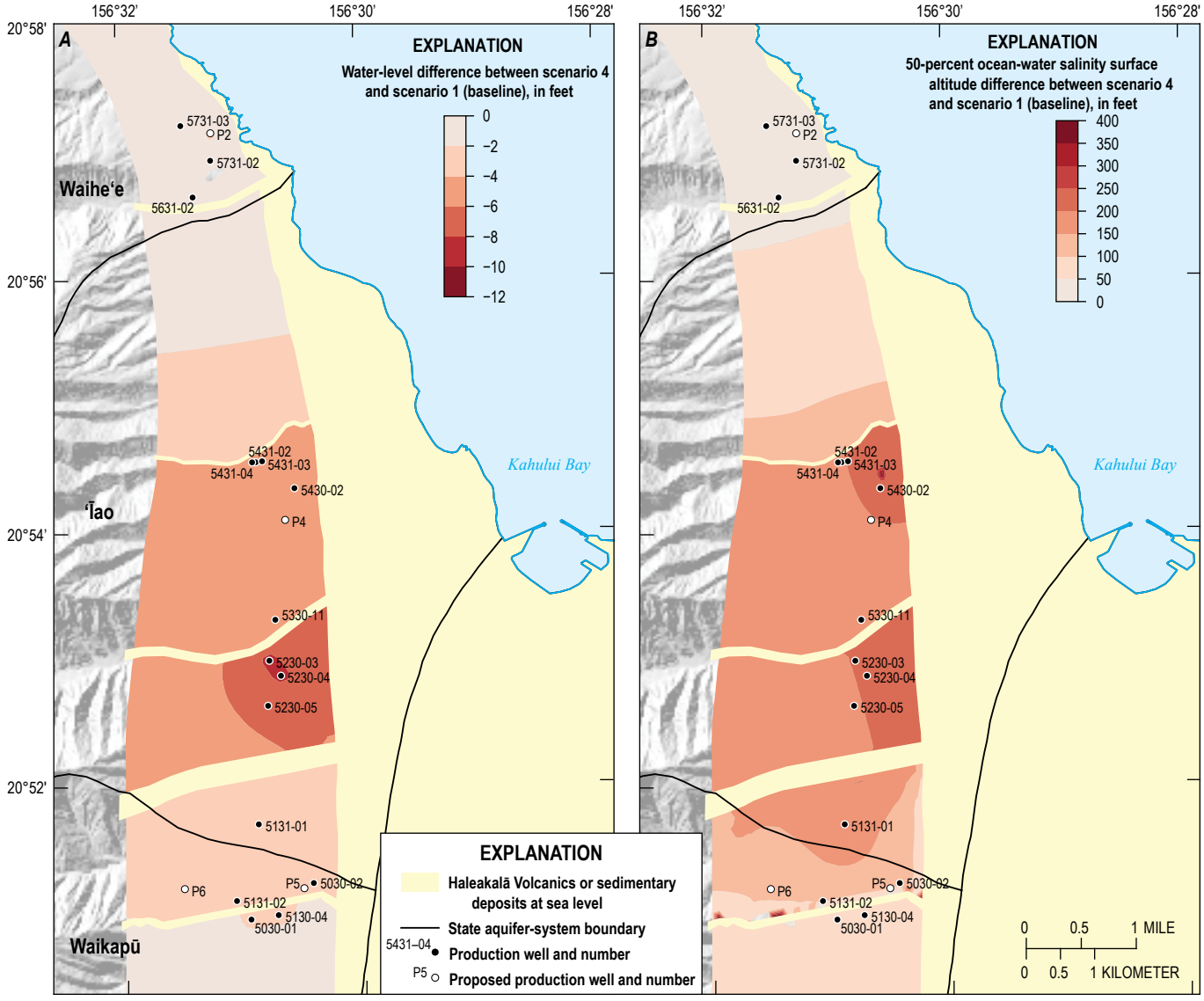

Base modified from U.S. Geological Survey National Hydrography Dataset, Scale of 1:24,000
Shaded relief from U.S. Geological Survey digital elevation model data
Universal Transverse Mercator Projection, Zone 4
North American Datum of 1983

Figure 21. Simulated change in (*A*) water level and (*B*) 50-percent ocean-water salinity surface altitude in the study area for scenario 4 (26.9 million gallons per day withdrawals from production wells in the Waiheʻe, ʻĪao, and Waikapū aquifer systems) relative to scenario 1 (baseline), central Maui, Hawaiʻi.

concentrations of groundwater withdrawn from wells 5330–11 and 5431–02 are in the 100–200 mg/L category, the simulated chloride concentration of groundwater withdrawn from well P5 is in the 200–250 mg/L category, and the simulated chloride concentrations of groundwater withdrawn from wells 5431–03 and 5430–02 are in the greater than 250 mg/L category (fig. 22). The weighted chloride concentration of groundwater withdrawn from wells 5431–02 to –04 is in the 100–200 mg/L category (table 3). The simulated chloride concentrations from production wells indicate that chloride concentrations of pumped water from the wells in the Wailuku area for scenario 4 remain below the EPA secondary standard, except at wells 5431–03 and 5430–02.

Scenario 5—27.5 Mgal/d Withdrawals from Waiheʻe, ʻĪao, and Waikapū Aquifer System Production Wells

Scenario 5 includes the same recharge and withdrawals as the baseline scenario, except simulated withdrawals from production wells in the Waiheʻe, ʻĪao, and Waikapū aquifer systems were changed. In the Waiheʻe aquifer system, pumping was expanded to two proposed wells and total withdrawals were increased to 5.6 Mgal/d. Withdrawals from wells 5731–03, 5731–02, 5631–02, P1, and P2 composed 66.7 percent of the pump capacity. In the ʻĪao aquifer system, withdrawals were redistributed from the south to the north relative to scenario 4. The withdrawals from wells 5431–03 and 5431–04

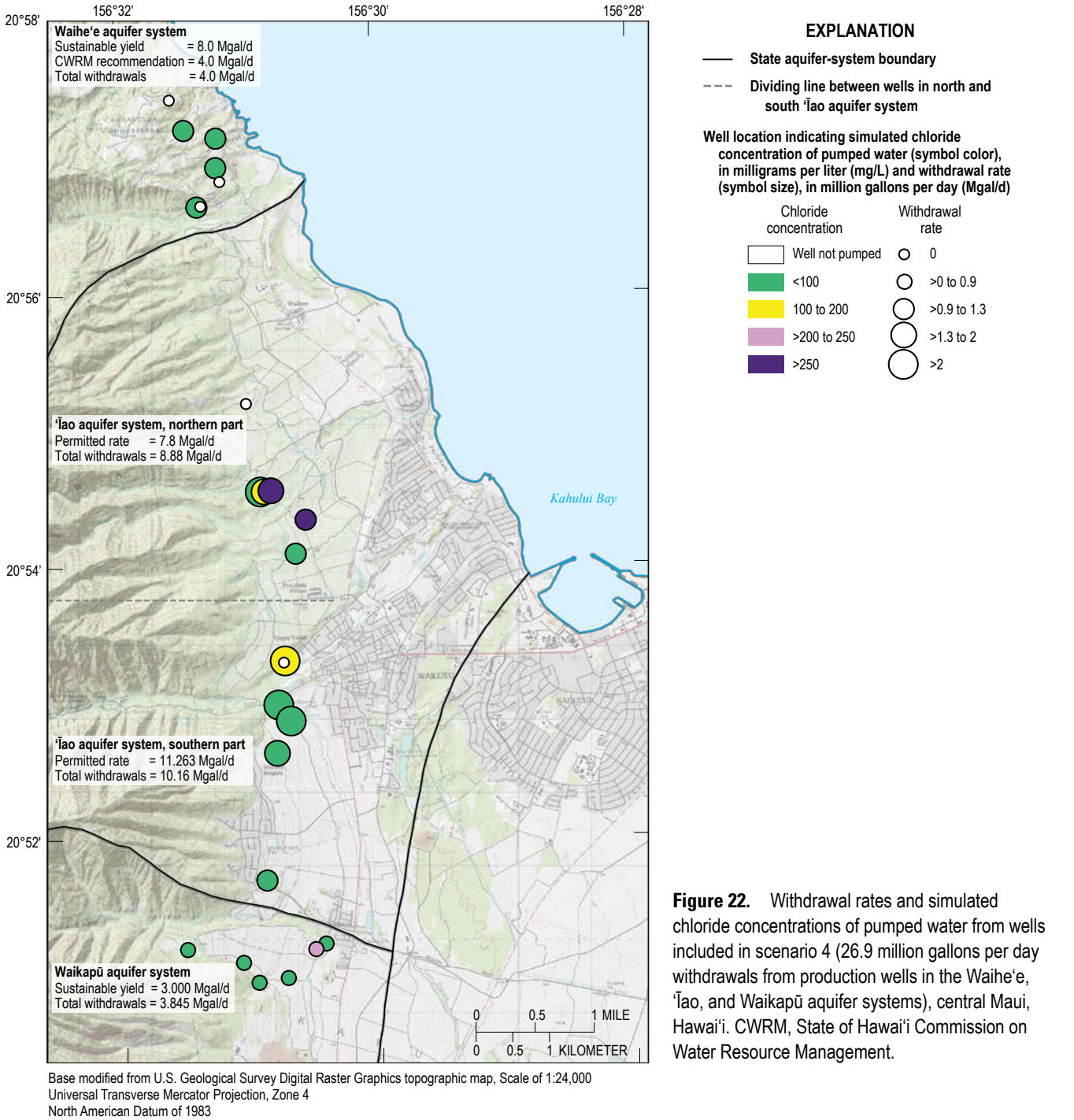

Base modified from U.S. Geological Survey Digital Raster Graphics topographic map, Scale of 1:24,000
Universal Transverse Mercator Projection, Zone 4
North American Datum of 1983

Figure 22. Withdrawal rates and simulated chloride concentrations of pumped water from wells included in scenario 4 (26.9 million gallons per day withdrawals from production wells in the Waiheʻe, ʻĪao, and Waikapū aquifer systems), central Maui, Hawaiʻi. CWRM, State of Hawaiʻi Commission on Water Resource Management.

were consistent with the combined water-use permit rate for wells 5431–02, 5431–03, and 5431–04. Withdrawals from wells 5430–02 and P4 were as in scenario 4, and 1 Mgal/d was redistributed from wells 5330–10 and 5330–11 to P4. In the southern part of the ʻĪao aquifer system, combined withdrawals from wells 5330–10 and 5330–11 were substantially decreased compared to all previous scenarios to 1.6 Mgal/d. A typical withdrawal rate of 7.4 Mgal/d that occurred at Shaft 33 (5330–05) in the 1970s was redistributed among wells 5230–03, 5230–04, 5230–05, and 5131–01 according to their water-use permit rate, as in scenario 4. In the Waikapū aquifer system, withdrawals were adjusted to the CWRM-estimated sustainable yield of 3 Mgal/d. Total simulated withdrawal represented in the model from wells was 77.2 Mgal/d, including 49.7 Mgal/d withdrawals from the Honomanū Basalt/Kula Volcanics in the Kahului aquifer system. Simulated withdrawals from production wells in the Waiheʻe, ʻĪao, and Waikapū aquifer systems were 5.6, 19.0 (about 10.0 in the northern part and 9.0 in the southern part), and 2.9 Mgal/d, respectively (table 3).

Regional changes of simulated water levels in scenario 5, relative to the baseline scenario, are greatest in the southern part of the ʻĪao aquifer system with a water-level decline of 6–8 ft near wells 5230–03 and 5230–04, due to the increase in withdrawals in this area. The simulated 50-percent ocean-water salinity surface in the southern part of the ʻĪao aquifer system is 100–200 ft higher, relative to the baseline scenario. Compared to previous scenarios, simulated water levels in the Waiheʻe aquifer system also decline 2–4 ft in scenario 5, accompanied by a rise of the simulated 50-percent ocean-water salinity surface that is related to increased withdrawals (fig. 23).

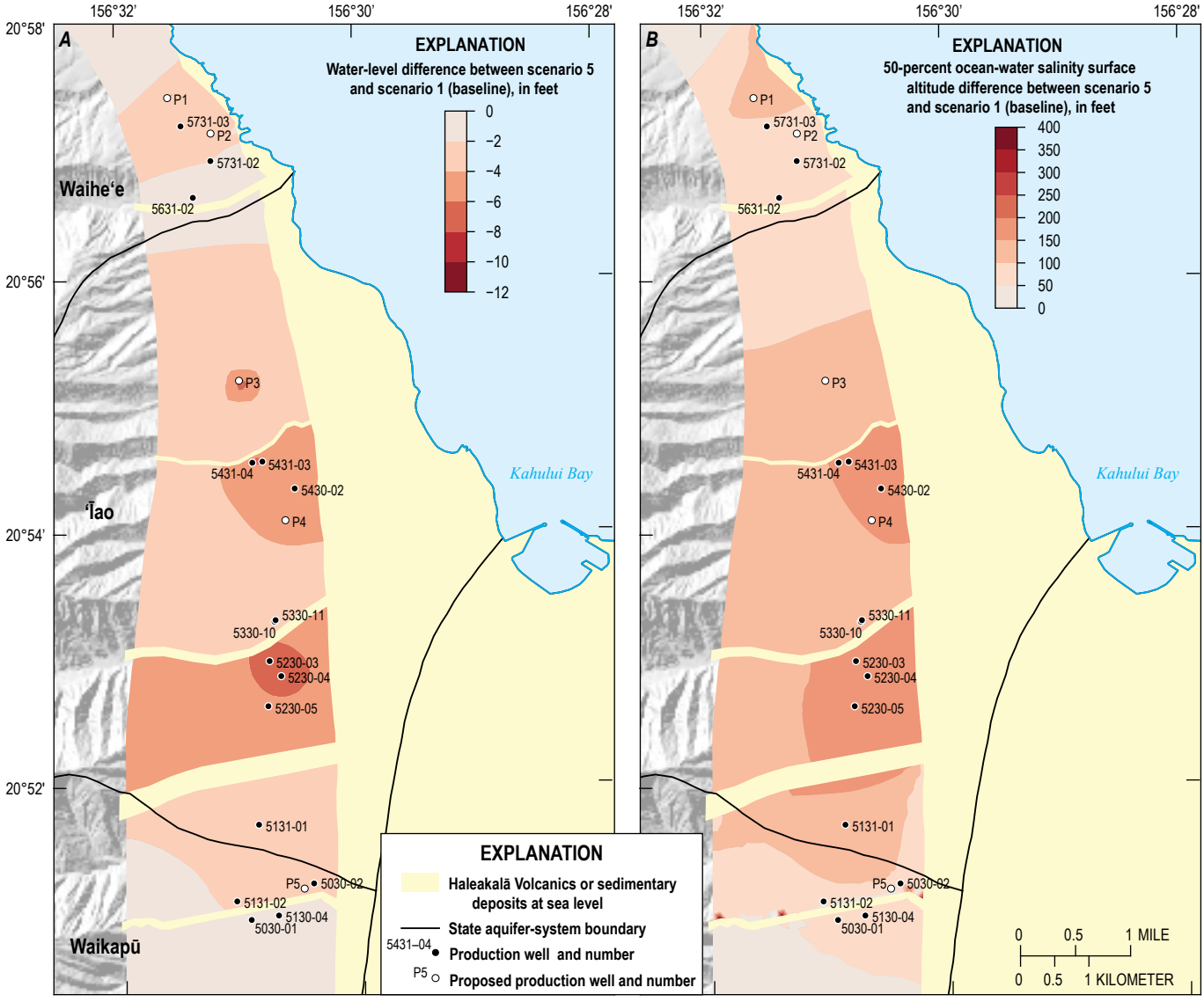

Base modified from U.S. Geological Survey National Hydrography Dataset, Scale of 1:24,000
Shaded relief from U.S. Geological Survey digital elevation model data
Universal Transverse Mercator Projection, Zone 4
North American Datum of 1983

Figure 23. Simulated change in (*A*) water level and (*B*) 50-percent ocean-water salinity surface altitude in the study area for scenario 5 (27.5 million gallons per day withdrawals from production wells in the Waiheʻe, ʻĪao, and Waikapū aquifer systems) relative to scenario 1 (baseline), central Maui, Hawaiʻi.

For scenario 5, the simulated chloride concentrations of groundwater withdrawn from wells P5 and 5330–10 are in the 100–200 mg/L category, the simulated chloride concentration of groundwater withdrawn from well 5431–03 is in the 200–250 mg/L category, and the simulated chloride concentration of groundwater withdrawn from well P1 is in the greater than 250 mg/L category (fig. 24). The weighted chloride concentration of groundwater withdrawn from wells 5431–02 to –04 is in the 100–200 mg/L category (table 3). The simulated chloride concentrations from production wells indicate that chloride concentrations of pumped water from the wells in the Wailuku area for scenario 5 remain below the EPA secondary standard, except for withdrawals at well P1.

Scenario 6—27.2 Mgal/d Withdrawals from Waiheʻe, ʻĪao, and Waikapū Aquifer System Production Wells

Scenario 6 includes the same recharge and withdrawals as the baseline scenario, except simulated withdrawals from production wells in the Waiheʻe, ʻĪao, and Waikapū aquifer systems were changed and represent a modification of scenario 5. In the Waiheʻe aquifer system, withdrawals were as in scenario 5, although P1 was not pumped, withdrawal from well 5731–03 was decreased to 1 Mgal/d, and withdrawals from wells 5731–02 and 5631–02 were increased to 1.8 and 1.6 Mgal/d, respectively. Withdrawals in the northern part of the ʻĪao aquifer system were equal to those in scenario 5.

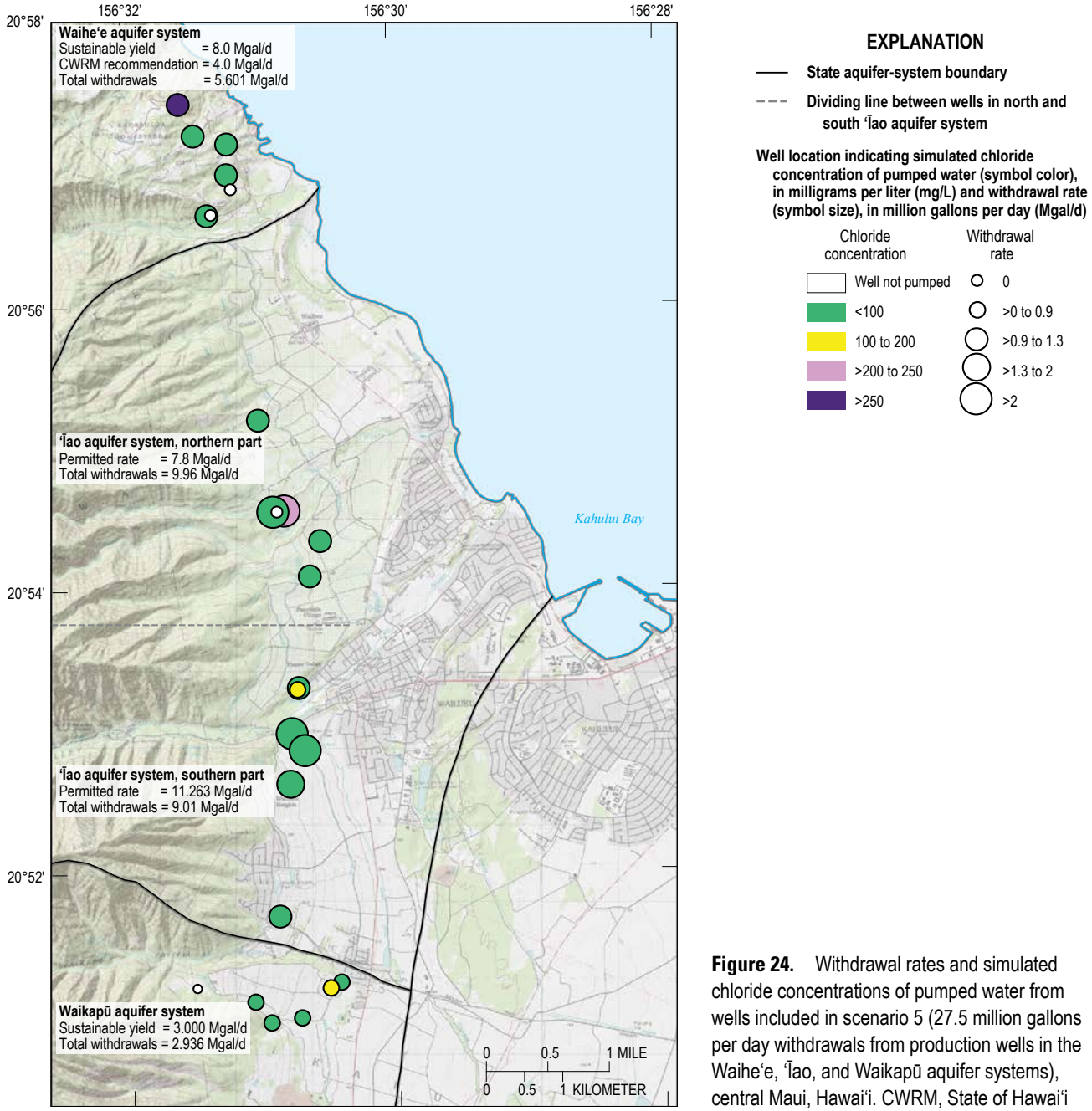

Base modified from U.S. Geological Survey Digital Raster Graphics topographic map, Scale of 1:24,000
Universal Transverse Mercator Projection, Zone 4
North American Datum of 1983

Figure 24. Withdrawal rates and simulated chloride concentrations of pumped water from wells included in scenario 5 (27.5 million gallons per day withdrawals from production wells in the Waiheʻe, ʻĪao, and Waikapū aquifer systems), central Maui, Hawaiʻi. CWRM, State of Hawaiʻi Commission on Water Resource Management.

In the southern part of the ʻĪao aquifer system, withdrawal from well 5330–11 was increased to 2 Mgal/d relative to scenario 5, and well 5330–10 was not pumped. Withdrawals from wells 5230–03, 5230–04, 5230–05, and 5131–01 were redistributed from scenario 5 with a decrease at well 5230–03 and an increase at well 5230–05. In the Waikapū aquifer system, withdrawals were adjusted to total 90 percent of the CWRM-estimated sustainable yield of 3 Mgal/d with no pumping from wells 5030–02, 5130–04, and P6. Total simulated withdrawal represented in the model from wells was 76.9 Mgal/d, including 49.7 Mgal/d withdrawals from the Honomanū Basalt/Kula Volcanics in the Kahului aquifer system. Simulated withdrawals from production wells in the Waiheʻe, ʻĪao, and Waikapū aquifer systems were 5.5, 19.0 (about 10.0 in the northern part and 9.1 in the southern part), and 2.7 Mgal/d, respectively (table 3).

Regional changes of simulated water levels in scenario 6, relative to the baseline scenario, are greatest with a water-level decline of 6–8 ft in the northern part of the ʻĪao aquifer system near wells P3, 5431–03, and 5431–04 and in the southern part of the ʻĪao aquifer system near wells 5230–03 and 5230–04. The simulated 50-percent ocean-water salinity surface rises more than 200 ft near well 5431–03. As in scenario 5, simulated water levels in the Waiheʻe aquifer system decline due to increased withdrawals. Water levels decline 4–6 ft near well P2, accompanied by a rise of the simulated 50-percent ocean-water salinity surface of more than 100 ft (fig. 25).

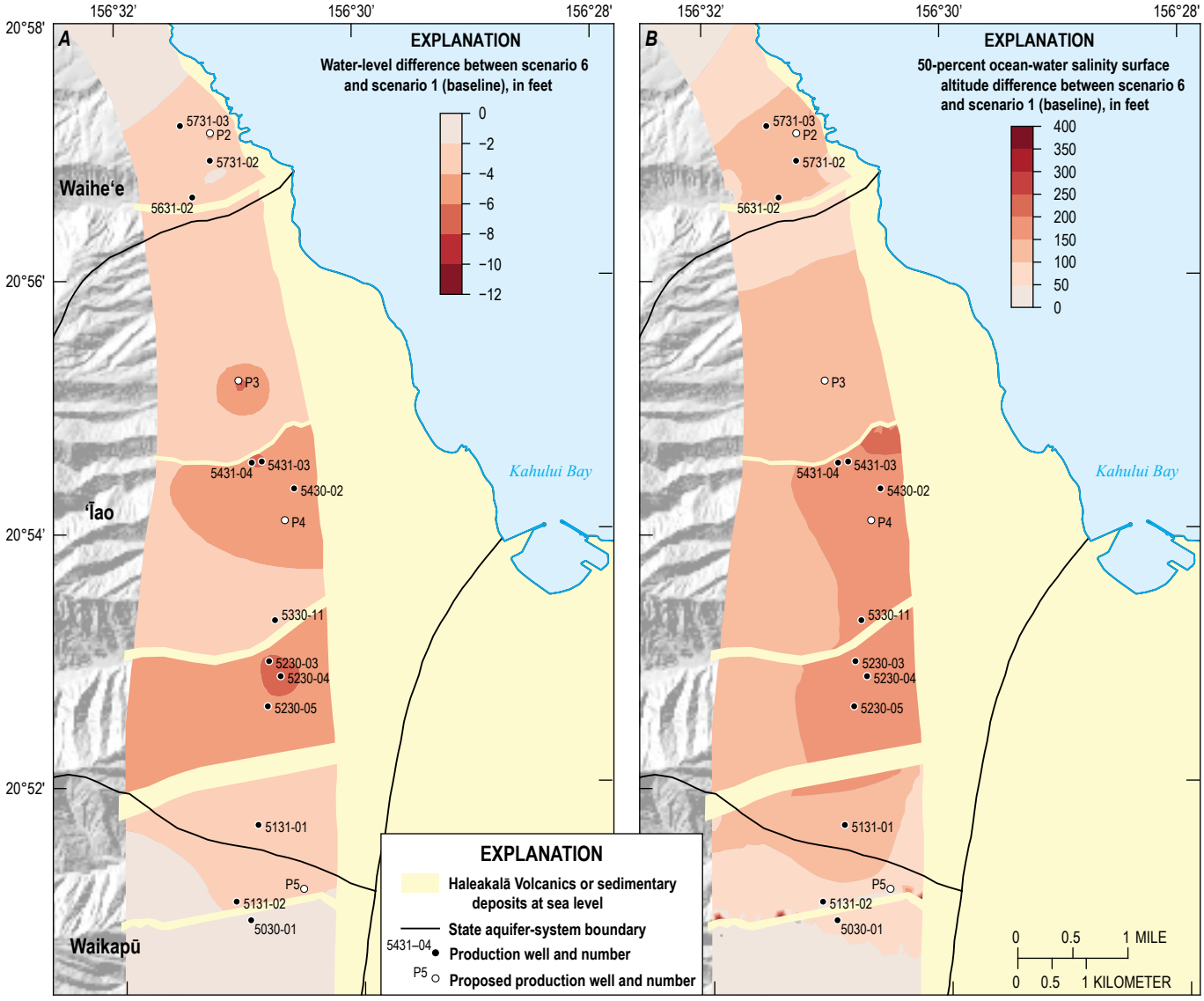

Base modified from U.S. Geological Survey National Hydrography Dataset, Scale of 1:24,000
Shaded relief from U.S. Geological Survey digital elevation model data
Universal Transverse Mercator Projection, Zone 4
North American Datum of 1983

Figure 25. Simulated change in (*A*) water level and (*B*) 50-percent ocean-water salinity surface altitude in the study area for scenario 6 (27.2 million gallons per day withdrawals from production wells in the Waiheʻe, ʻĪao, and Waikapū aquifer systems) relative to scenario 1 (baseline), central Maui, Hawaiʻi.

For scenario 6, the simulated chloride concentrations of groundwater withdrawn from wells in southern part of the ʻĪao aquifer system are less than 100 mg/L. The simulated chloride concentrations of groundwater withdrawn from wells 5631–02, 5430–02, and P5 are in the 100–200 mg/L category, the simulated chloride concentration of groundwater withdrawn from well 5431–03 is in the 200–250 mg/L category, and the simulated chloride concentrations of groundwater withdrawn from wells 5731–03 and P2 are in the greater than 250 mg/L category (fig. 26). The weighted chloride concentration of groundwater withdrawn from wells 5431–02 to –04 is in the 100–200 mg/L category (table 3). The simulated chloride concentrations from MDWS production wells indicate that, for scenario 6, chloride concentrations of pumped water from most wells in the Wailuku area remain below the EPA secondary standard. However, chloride concentrations of groundwater withdrawn from two wells (5731–03 and P2) are above the EPA secondary standard in the Waiheʻe aquifer system.

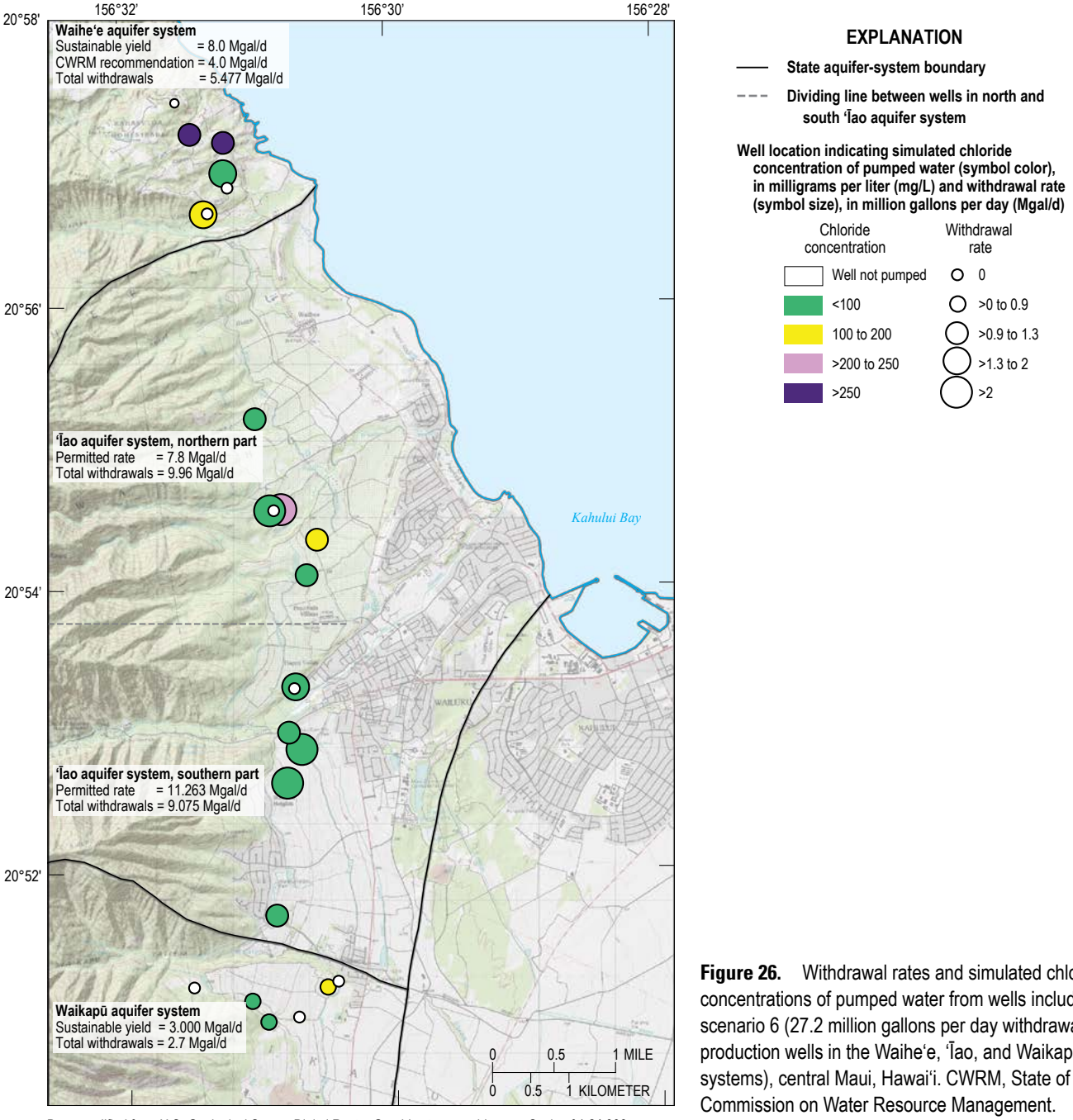

Base modified from U.S. Geological Survey Digital Raster Graphics topographic map, Scale of 1:24,000
Universal Transverse Mercator Projection, Zone 4
North American Datum of 1983

Figure 26. Withdrawal rates and simulated chloride concentrations of pumped water from wells included in scenario 6 (27.2 million gallons per day withdrawals from production wells in the Waiheʻe, ʻĪao, and Waikapū aquifer systems), central Maui, Hawaiʻi. CWRM, State of Hawaiʻi Commission on Water Resource Management.

Scenario 7—Withdrawals as Scenario 4 and Future Recharge

Scenario 7 represents a drier future recharge scenario. Recharge values for future conditions, using a rainfall projection for a RCP8.5 warming scenario and 2017 land cover, were estimated in the Waiheʻe, ʻĪao, and Waikapū aquifer systems to be about 20.3, 33.8, and 8.4 Mgal/d, respectively (Mair and others, 2019). Recharge in the form of steady inflow of groundwater from the dike-intruded area of West Maui volcano was estimated using an island-wide groundwater-flow model (Izuka and others, 2021), applying the future recharge (2071–99 rainfall using RCP8.5 and 2017 land cover) estimated by Mair and others (2019). Recharge values from scenario 7 were 32.7 Mgal/d from the inland boundary (table 1); 14.2 Mgal/d from the top, onshore boundary within the modeled area; and 10.9 Mgal/d from restored streamflow in the Waiheʻe River (1.5 Mgal/d), Waiehu Stream (2.5 Mgal/d), Wailuku River (5.6 Mgal/d), and Waikapū Stream (1.3 Mgal/d). The total future recharge is about 21 percent less than the total recharge in scenarios 1–6. Simulated withdrawals in scenario 7 were identical to those in scenario 4.

Relative to the baseline scenario, regional changes of simulated water levels in scenario 7 are greatest in the southern part of the ʻĪao aquifer system with a water-level decline of more than 10 ft near wells 5230–03 and 5230–04. The water-level decline is related to the reduction in recharge and increase in withdrawals relative to the baseline scenario in this area. The simulated 50-percent ocean-water salinity

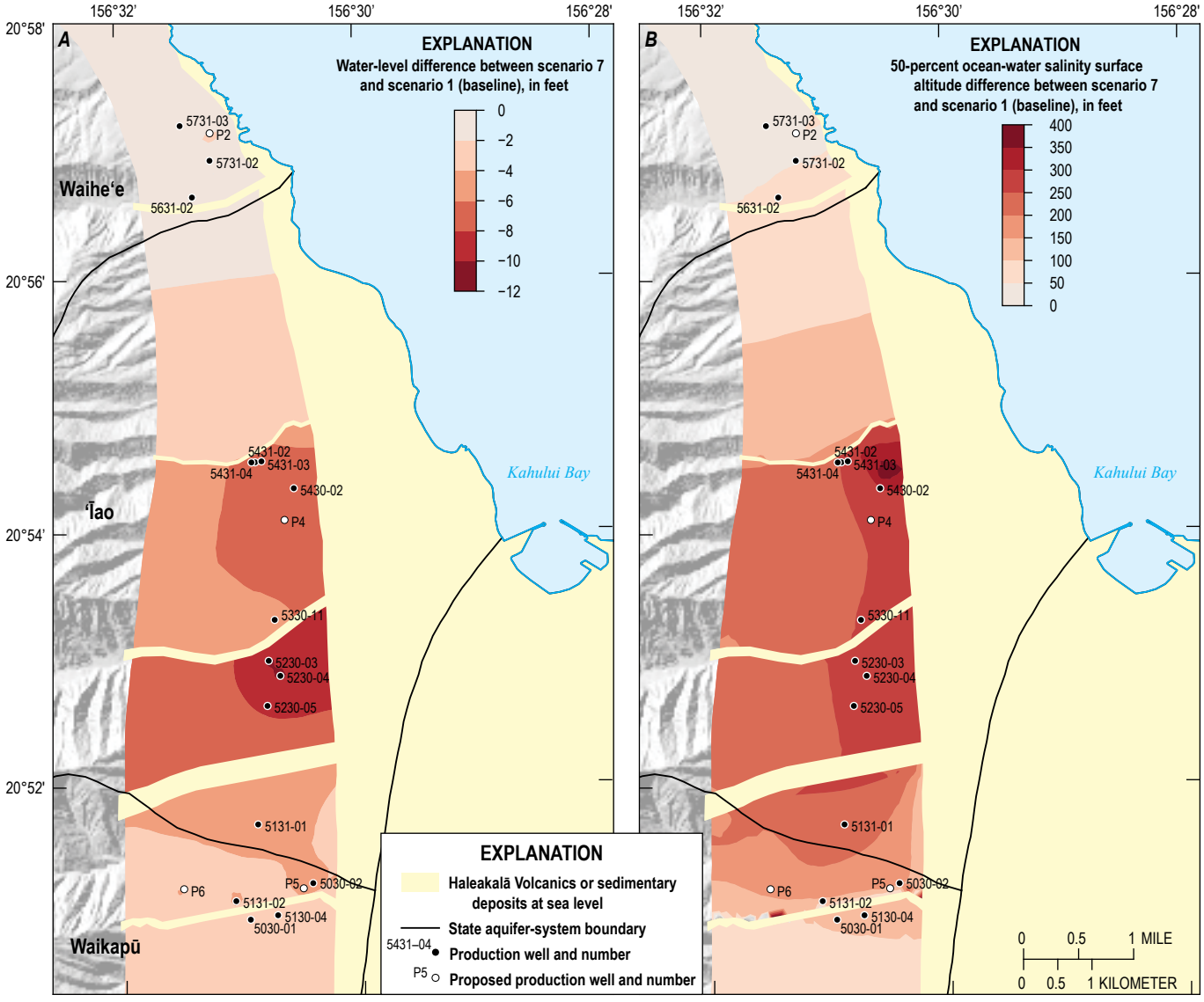

Base modified from U.S. Geological Survey National Hydrography Dataset, Scale of 1:24,000
Shaded relief from U.S. Geological Survey digital elevation model data
Universal Transverse Mercator Projection, Zone 4
North American Datum of 1983

Figure 27. Simulated change in (*A*) water level and (*B*) 50-percent ocean-water salinity surface altitude in the study area for scenario 7 (same withdrawal as scenario 4 but reduced recharge) relative to scenario 1 (baseline), central Maui, Hawaiʻi.

surface rises more than 350 ft near well 5430–02 (fig. 27). Relative to scenario 4, simulated water levels are lower and the simulated 50-percent ocean-water salinity surface is higher in the southern part of the ʻĪao and Waikapū aquifer systems. These simulated results are consistent with the decreased recharge in the southern part of the of the study area.

For scenario 7, the simulated chloride concentrations of groundwater withdrawn from wells in the Waiheʻe aquifer system were less than 100 mg/L. The simulated chloride concentrations of groundwater withdrawn from wells 5230–03 and 5130–04 are in the 100–200 mg/L category, the simulated chloride concentrations of groundwater withdrawn from wells 5330–11, 5431–02, and 5431–03 are in the 200–250 mg/L category, and the simulated chloride concentrations of groundwater withdrawn from wells 5430–02 and P5 are in the greater than 250 mg/L category (fig. 28). In the ʻĪao and Waikapū aquifer systems, where recharge reductions were greatest, the salinity of water withdrawn from production wells increased compared to scenario 4, except for well 5431–03. The weighted chloride concentration of groundwater withdrawn from wells 5431–02 to –04 is in the 100–200 mg/L category (table 3). The simulated chloride concentrations from production wells indicate that chloride concentrations of pumped water from the wells in the Wailuku area for scenario 7 remain below the EPA secondary standard, except at wells 5430–02 and P5.

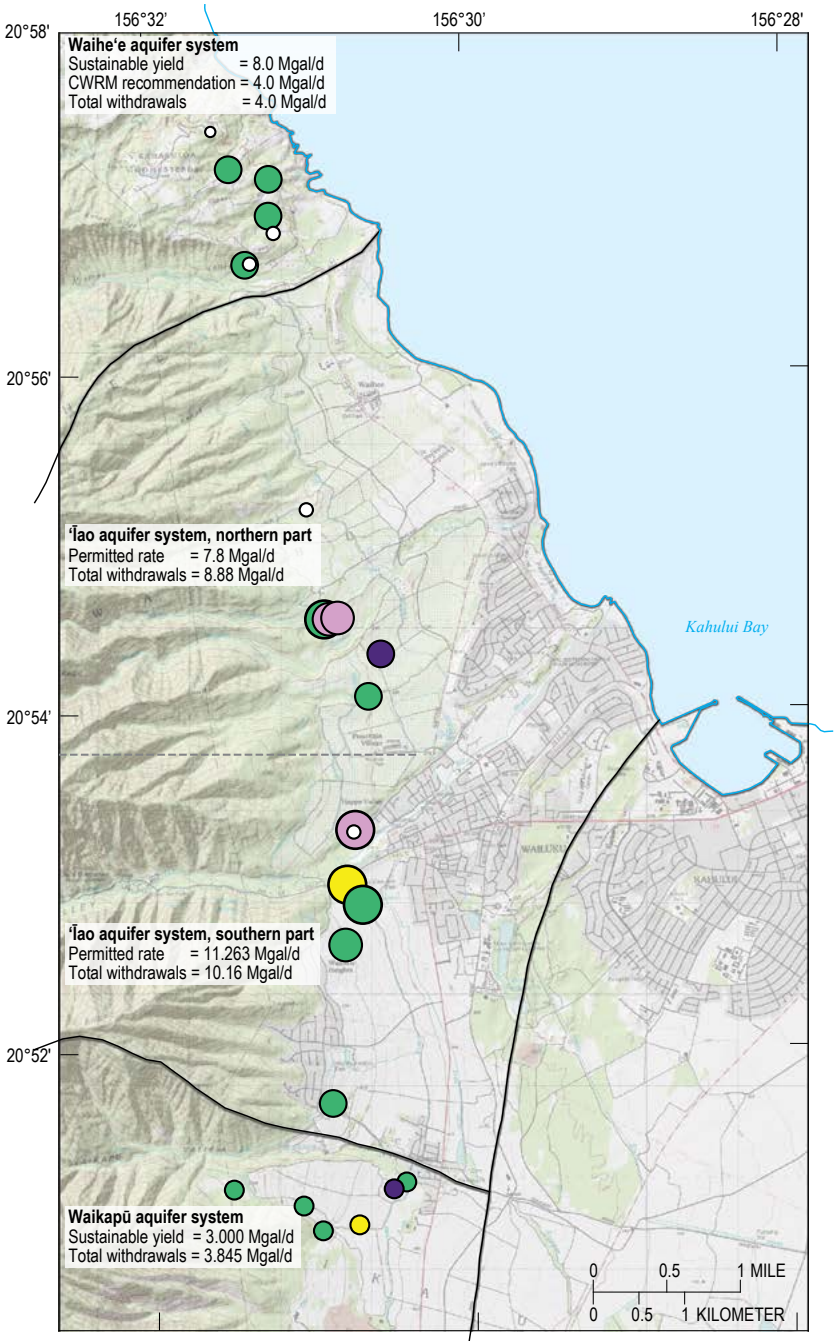

Base modified from U.S. Geological Survey Digital Raster Graphics topographic map, Scale of 1:24,000
Universal Transverse Mercator Projection, Zone 4
North American Datum of 1983

Figure 28. Withdrawal rates and simulated chloride concentrations of pumped water from wells included in scenario 7 (same withdrawal as scenario 4 but reduced recharge), central Maui, Hawaiʻi. CWRM, State of Hawaiʻi Commission on Water Resource Management.

Implications of Scenarios

Results of the simulated withdrawal and recharge scenarios indicate that increased withdrawals, relative to 2017–18 rates, will lead to long-term lower water levels and a shallower 50-percent ocean-water salinity surface and may ultimately produce groundwater with chloride concentrations above the EPA secondary standard of 250 mg/L. However, the amount of drawdown near production wells and the quality of water withdrawn from production wells is dependent on the rate and distribution of the withdrawals. High rates of withdrawal from closely spaced wells (for example, wells 5431–02 to 04) tend to enhance the potential for water-level decline, rise of the 50-percent ocean-water salinity surface, and increased salinity of the water withdrawn from production wells in the Waiheʻe, ʻĪao, and Waikapū aquifer systems. Spatially spreading out withdrawals may help to produce water of acceptable quality. Model results also indicate that the rate of groundwater recharge is a controlling factor for water levels, the 50-percent ocean-water salinity surface, and the quality of water withdrawn from production wells in the Wailuku area. A reduction in groundwater recharge in the future with all other factors remaining equal would cause lower water levels, a shallower 50-percent ocean-water salinity surface, and increased salinity of water withdrawn from production wells.

Limitations

The numerical groundwater model developed for this study has several limitations, including its non-uniqueness and inability to account for local-scale heterogeneities. Different distributions of hydraulic properties and recharge may result in comparable model results, although recharge estimates were based on the best available information. Data from a limited number of wells are available to constrain the model. For example, limited historical information from wells that were recently drilled are available in the Waikapū aquifer system to understand hydrogeologic conditions and groundwater quality there. Also, information about the effectiveness of hydrologic barriers in impeding groundwater flow in the study area is limited.

The numerical model developed for this study also simulates conditions on a regional scale and may not accurately predict either the water level at an individual well or the salinity of water withdrawn from that well. Withdrawals represented in the model were based on available information. Unreported withdrawals and uncertainties in reported withdrawals that cannot be quantified also affect the accuracy of model results. Salinity of water pumped from a well may be controlled by local heterogeneities in the aquifer that are not represented in the model. Also, the level of model discretization affects the numerical accuracy of the simulated transport mechanisms. The model has several other limitations for predictive purposes because of the various assumptions used and possible uncertainties in input data. These limitations are discussed below.

Differences between measured and simulated water levels are greater in some areas than others, which may reflect uncertainties in recharge or withdrawal, boundary conditions, assigned parameter values in the model, or representations of the different hydrogeological features in the model. Recharge estimates in Hawaiʻi generally are based on water-budget computations that could be improved with a better understanding of the spatial distributions of rainfall, evapotranspiration, runoff, and land-cover characteristics. Additional climate stations and continuous-record stream-gaging stations on Maui would lead to improved recharge estimates. Other studies that could enhance understanding of recharge include (1) quantifying rates of evapotranspiration of native and non-native forest species, (2) directly measuring recharge using field lysimeters, (3) measuring changes in soil moisture below the plant-root zone, (4) quantifying increases in the chloride concentration of infiltrating water caused by evapotranspiration, (5) measuring groundwater discharge with offshore seepage meters, and (6) developing an integrated surface-water/groundwater model. Improved recharge estimates in the study area will lead to improved estimates for parameter values in the numerical groundwater model and will result in greater confidence in model results.

Heterogeneity in the groundwater system likely exists but is currently poorly understood. Values assigned to model hydraulic parameters were generally based on existing estimates and were controlled by observed hydrogeologic conditions. However, some of these parameter values may be poorly known. Simulated water levels are typically controlled by the hydraulic-conductivity values assigned in the model. Simulated salinity can be controlled by various hydraulic parameters, such as effective porosity, dispersivity, and vertical anisotropy of the aquifer.

Additional wells or geophysical studies in areas with limited information would improve the understanding of hydrogeologic conditions, presence and geometry of barriers to flow, thickness of coastal sedimentary deposits, and distribution of hydraulic characteristics. Running controlled aquifer tests that monitor withdrawal and water-level conditions throughout the aquifer can improve estimates of the distribution of hydraulic characteristics in the study area. Accurate water-level and withdrawal data can be used for calibration of numerical groundwater models, particularly during periods when recharge does not vary. Confidence in model results can be improved by addressing the limitations described in this section. In particular, improved estimates of recharge and the distribution of model parameters will lead to an increase of model reliability.

Summary

In the Wailuku area of central Maui, Hawaiʻi, groundwater levels have declined since the 1940s, mainly in response to increased groundwater withdrawals. Available groundwater data since the 1980s also indicate a thinning of the freshwater lens and an increase in chloride concentrations of pumped water from production wells. These trends, combined with

projected increases in demand for groundwater in central Maui, have led to concerns over groundwater availability and created a need to improve understanding of the hydrologic effects of proposed groundwater withdrawals in the Waiheʻe, ʻĪao, and Waikapū aquifer systems of central Maui. Recent changes that affect hydrologic conditions in the study area include: (1) restoration of streamflow, which results in additional recharge; (2) the 2016 shutdown of Shaft 33 (5330–05); (3) cessation of sugarcane cultivation in central Maui at the end of 2016, which resulted in reduced recharge from irrigation and reduced groundwater withdrawals; and (4) groundwater withdrawal from new and planned wells. An accurate understanding of how much fresh groundwater in the Wailuku area can be developed under current conditions and for future needs is critically important from economic, cultural, and resource standpoints.

To ensure effective management of the groundwater resources and to plan for possible growth in the Wailuku area, the U.S. Geological Survey developed a numerical groundwater model capable of simulating water-level and salinity change in central Maui, updating and refining a previously developed numerical groundwater flow and transport model of the Wailuku area (Gingerich, 2008). Mean annual recharge from the soil root zone was estimated using a daily water-budget model for the study area for nine historical periods between 1926 and 2012: 1926–69, 1970–79, 1980–84, 1985–89, 1990–94, 1995–99, 2000–04, 2005–09, and 2010–12. For these nine periods, estimated recharge from infiltration and direct recharge within the area of the groundwater model ranged from 30.4 million gallons per day (Mgal/d) during 2010–12 to 98.7 Mgal/d during 1926–69. Average groundwater inflow of about 39.6 Mgal/d from inland, dike-intruded areas to the main area of interest was estimated from an existing island-wide numerical groundwater-flow model.

Aquifer hydraulic properties for the three-dimensional numerical groundwater model were estimated using available water-level and salinity information from representative wells in the modeled area during 1926−2012. Simulated withdrawal and recharge scenarios were selected in consultation with the Maui Department of Water Supply and include: (1) a baseline scenario using average recharge (1980−2010 rainfall and 2017 land cover) and average 2017−18 withdrawals; (2) a scenario using average recharge and withdrawals from existing wells (as of 2019) consistent with water-use permit rates; (3) four scenarios using average recharge and selected withdrawals from existing and proposed new wells; and (4) a scenario using reduced recharge and one of the withdrawal scenarios from item (3). The reduced recharge incorporates rainfall projections for a Representative Concentration Pathway warming scenario during 2071–99 with total radiative forcing of 8.5 Watts per square meter by the year 2100 and 2017 land cover. The effects of all scenarios on groundwater levels and salinity of pumped water were evaluated for long-term, future steady-state conditions.

For the baseline scenario, simulation results indicate that water levels in the ʻĪao aquifer system ultimately rise by 6–8 feet (ft) and the 50-percent ocean-water salinity surface lowers by as much as 100 ft, relative to conditions at the end of the historical simulation (2012) due to greater recharge. Consistent with the water-level recovery, the simulated chloride concentrations of groundwater withdrawn from wells in the Waiheʻe, ʻĪao, and Waikapū aquifer systems are less than 100 milligrams per liter (mg/L).

Simulation results from the scenario using average recharge and withdrawals from existing wells consistent with water-use permit rates are compared to the baseline scenario and indicate that water levels decline in the ʻĪao aquifer system by 4–10 ft and the 50-percent ocean-water salinity surface rises as much as 200 ft. The simulated chloride concentrations from production wells in the Wailuku area remain below the U.S. Environmental Protection Agency (EPA) secondary standard, except at well 5430–02.

Simulation results from the four scenarios using average recharge and selected withdrawals from existing and proposed new wells indicate that water levels decline in the ʻĪao aquifer system by up to 10 ft and that the 50-percent ocean-water salinity surface rises as much as 400 ft relative to the baseline scenario. The simulated chloride concentrations from production wells in the Wailuku area remain below the EPA secondary standard. However, at least one well in each scenario has a simulated chloride concentration of more than 250 mg/L.

Simulation results from the scenario using reduced recharge and selected withdrawals from existing and proposed new wells indicate that water levels in the ʻĪao aquifer system decline more than 10 ft and that the 50-percent ocean-water salinity surface rises as much as 400 ft. The simulated chloride concentrations from production wells in the Wailuku area remain below the EPA secondary standard, except at wells 5430–02 and P5.

Overall, results of the simulated withdrawal scenarios indicate that increased withdrawals relative to 2017–18 rates ultimately lead to lower water levels and a higher 50-percent ocean-water salinity surface and produce some groundwater with chloride concentrations above 250 mg/L. However, the amount of drawdown near production wells and the quality of water withdrawn from production wells is dependent on the rate and distribution of the withdrawals. Results of the reduced recharge scenario indicate that the rate of groundwater recharge is a controlling factor for future water levels, the 50-percent ocean-water salinity surface, and the future quality of water withdrawn from production wells in the Wailuku area. A reduction in groundwater recharge (all other factors remaining equal) would tend to cause lower future water levels, a higher 50-percent ocean-water salinity surface, and increased future salinity of water withdrawn from production wells.

The three-dimensional numerical groundwater model developed for this study has several limitations, including its non-uniqueness and inability to account for local-scale heterogeneities. Data from a limited number of wells are available to constrain the model. The numerical model developed for this study may not accurately predict the salinity of water withdrawn from a production well because salinity of water pumped from a well may be controlled by local

heterogeneities in the aquifer that are not represented in the model. The model has several other limitations for predictive purposes because of the various assumptions used and possible uncertainties in input data. Nevertheless, the three-dimensional numerical groundwater model developed for this study uses the latest available hydrologic and geologic information, and it is considered a useful tool for understanding the long-term hydrologic effects of additional groundwater withdrawals in the Waiheʻe, ʻĪao, and Waikapū areas of central Maui, Hawaiʻi.

Future work based on this model could include an evaluation of the timing of saltwater intrusion and the timing of salinity changes in wells. For example, the evaluation could examine how long increased withdrawals can be allowed during a drought before salinity of pumped water exceeds a threshold value. Additional future work could include a determination of maximum amounts of withdrawal (using a simulation-optimization technique) and the most effective spatial distribution of withdrawal at existing or new wells without causing excessive drawdown in wells and unacceptable increases in salinity of pumped water. Potential other scenarios could include other future recharge scenarios based on different climate models.

References Cited

Blumenstock, D.I., and Price, S., 1967, Climate of Hawaii, *in* Climatography of the United States: Washington, D.C., U.S. Department of Commerce, p. 27.

County of Maui, 2012, Maui island plan, General Plan 2030: County of Maui Department of Planning, variously paginated, accessed October 14, 2019, at https://www.mauicounty.gov/1503/Maui-Island-Plan.

Domenico, P.A., and Schwartz, F.W., 1990, Physical and chemical hydrogeology: New York, John Wiley, 824 p.

Engott, J.A., and Vana, T.T., 2007, Effects of agricultural land-use changes and rainfall on ground-water recharge in central and west Maui, Hawaii, 1926–2004: U.S. Geological Survey Scientific Investigations Report 2007–5103, 56 p., accessed October 2, 2007, at https://pubs.usgs.gov/sir/2007/5103/.

Flinders, A.F., Ito, G., Garcia, M.O., Sinton, J.M., Kauahikaua, J., and Taylor, B., 2013, Intrusive dike complexes, cumulate cores, and the extrusive growth of Hawaiian volcanoes: Geophysical Research Letters, v. 40, p. 3367–3373, accessed November 26, 2013, at https://doi.org/10.1002/grl.50633.

Fontaine, R.A., 1996, Evaluation of the surface-water quantity, surface-water quality, and rainfall data-collection programs in Hawaii, 1994: U.S. Geological Survey Water-Resources Investigations Report 95–4212, 125 p., accessed July 10, 2020, at https://doi.org/10.3133/wri954212.

Frazier, A.G., Giambelluca, T.W., Diaz, H.D., and Needham, H.L., 2016, Comparison of geostatistical approaches to spatially interpolate month-year rainfall for the Hawaiian Islands: International Journal of Climatology, v. 36, no. 3, p. 1459–1470, accessed November 21, 2016, at https://doi.org/10.1002/joc.4437.

Furumoto, A.S., Campbell, J.F., and Hussong, D.M., 1970, Seismic studies of subsurface structure in the Ewa coastal plain, Oahu, Hawaii: Pacific Science, v. 24, no. 4, p. 529–542., accessed January 4, 2015, at http://hdl.handle.net/10125/6267.

Giambelluca, T.W., Chen, Q., Frazier, A.G., Price, J.P., Chen, Y., Chu, P., Eischeid, J.K., and Delparte, D.M.,, 2013, Online rainfall atlas of Hawaiʻi: Bulletin of the American Meteorological Society, v. 94, p. 313–316, accessed September 10, 2014, at https://doi.org/10.1175/BAMS-D-11-00228.1.

Giambelluca, T.W., Shuai, X., Barnes, M.L., Alliss, R.J., Longman, R.J., Miura, T., Chen, Q., Frazier, A.G., Mudd, R.G., Cuo, L., and Businger, A.D., 2014, Evapotranspiration of Hawaiʻi —Final report: The Hawaiʻi Transpiration Project, Department of Geography, University of Hawaiʻi at Mānoa, 168 p., accessed April 26, 2020, at http://evapotranspiration.geography.hawaii.edu/assets/files/PDF/ET%20Project%20Final%20Report.pdf. [Submitted to the U.S. Army Corps of Engineers–Honolulu District and the Commission on Water Resource Management, State of Hawaiʻi.]

Gingerich, S.B., 2008, Ground-water availability in the Wailuku area, Maui, Hawaiʻi: U.S. Geological Survey Scientific Investigations Report 2008–5236, 95 p., accessed April 22, 2009, at http://pubs.usgs.gov/sir/2008/5236/.

Gingerich, S.B., and Engott, J.A., 2012, Groundwater availability in the Lahaina District, west Maui, Hawaiʻi: U.S. Geological Survey Scientific Investigations Report 2012–5010, 90 p., accessed June 14, 2012, at https://pubs.usgs.gov/sir/2012/5010/.

Izuka, S.K., Engott, J.A., Rotzoll, K., Bassiouni, M., Johnson, A.G., Miller, L., and Mair, A., 2018, Volcanic aquifers of Hawaiʻi—Hydrogeology, water budgets, and conceptual models (ver 2.0, March 2018): U.S. Geological Survey Scientific Investigations Report 2015–5164, 158 p., accessed April 6, 2018, at https://doi.org/10.3133/sir20155164.

Izuka, S.K., Rotzoll, K., and Nishikawa, T., 2021, Volcanic aquifers of Hawaiʻi—Construction and calibration of numerical models for assessing groundwater availability on Kauaʻi, Oʻahu, and Maui: U.S. Geological Survey Scientific Investigations Report 2020–5126, 63 p., accessed May 13, 2021, at https://doi.org/10.3133/sir20205126.

Johnson, A.G., Engott, J.A., Bassiouni, M., and Rotzoll, K., 2018, Spatially distributed groundwater recharge estimated using a water-budget model for the Island of Maui, Hawai‘i, 1978–2007 (ver. 2.0, February 2018): U.S. Geological Survey Scientific Investigations Report 2014–5168, 53 p., accessed April 3, 2018, at https://doi.org/10.3133/sir20145168.

Juvik, S.P., and Juvik, J.O., eds., 1998, Atlas of Hawai‘i: University of Hawai‘i Press, Honolulu, Hawai‘i, 333 p.

Kauahikaua, J., 1993, Geophysical characteristics of the hydrothermal systems of Kilauea Volcano, Hawai‘i: Geothermics, v. 22, no. 4, p. 271–299, accessed October 18, 2012, at https://doi.org/10.1016/0375-6505(93)90004-7.

Kinoshita, W.T., and Okamura, R.T., 1965, A gravity survey of the island of Maui, Hawaii: Pacific Science, v. 19, no. 3, p. 341–342, accessed April 15, 2019, at http://hdl.handle.net/10125/10755.

Langenheim, V.M., and Clague, D.A., 1987, The Hawaiian-Emperor volcanic chain—Part II, Stratigraphic framework of volcanic rocks of the Hawaiian Islands, chap. 1 *of* Decker, R.W., Wright, T.L., and Stauffer, P.H., eds., Volcanism in Hawaii: Reston, Va., U.S. Geological Survey Professional Paper 1350, v. 1, p. 55–84, accessed June 21, 2007, at https://pubs.usgs.gov/pp/1987/1350/.

Lockwood, J.P., and Lipman, P.W., 1987, Holocene eruptive history of Mauna Loa Volcano, Hawaii, chap. 18 *of* Decker, R.W., Wright, T.L., and Stauffer, P.H., eds., Volcanism in Hawaii: Reston, Va., U.S. Geological Survey Professional Paper 1350, v. 1, p. 509–535, accessed June 21, 2007, at https://pubs.usgs.gov/pp/1987/1350/.

Macdonald, G.A., Abbott, A.T., and Peterson, F.L., 1983, Volcanoes in the sea—The geology of Hawaii: Honolulu, Hawai‘i, University of Hawai‘i Press, 517 p.

Mair, A., Johnson, A.G., Rotzoll, K., and Oki, D.S., 2019, Estimated groundwater recharge from a water-budget model incorporating selected climate projections, Island of Maui, Hawai‘i: U.S. Geological Survey Scientific Investigations Report 2019–5064, 46 p., accessed August 15, 2019, at https://doi.org/10.3133/sir20195064.

Maui County Department of Water Supply, 2019, Maui Island water use and development plan: County of Maui Department of Water Supply, 1,035 p., accessed April 29, 2020, at https://waterresources.mauicounty.gov/162/Maui-Island-Water-Use-Development-Plan.

Meyer, W., and Presley, T.K., 2001, The response of the Iao aquifer to ground-water development, rainfall, and land-use practices between 1940 and 1998, island of Maui, Hawaii: U.S. Geological Survey Water-Resources Investigations Report 2000–4223, 60 p., accessed May 2, 2004, at https://doi.org/10.3133/wri20004223.

Mink, J.F., and Lau, L.S., 1990, Aquifer identification and classification for Maui—Groundwater protection strategy for Hawaii: University of Hawai‘i, Water Resources Research Center Technical Report 185, 47 p., accessed December 14, 2009, at http://hdl.handle.net/10125/1980.

Oki, D.S., 2005, Numerical simulation of the effects of low-permeability valley-fill barriers and the redistribution of ground-water withdrawals in the Pearl Harbor area, Oahu, Hawaii: U.S. Geological Survey Scientific Investigations Report 2005–5253, 111 p., accessed April 5, 2006, at https://pubs.usgs.gov/sir/2005/5253/.

Oki, D.S., Wolff, R.H., and Perreault, J.A., 2010, Effects of surface-water diversion on streamflow, recharge, physical habitat, and temperature, Na Wai ‘Eha, Maui, Hawai‘i: U.S. Geological Survey Scientific Investigations Report 2010–5011, 154 p., accessed July 9, 2010, at https://pubs.usgs.gov/sir/2010/5011/.

Palmer, H.S., 1927, The geology of the Honolulu artesian system: Honolulu Sewer and Water Commission, 68 p., accessed March 27, 2014, at http://hdl.handle.net/10524/12099.

Palmer, H.S., 1946, The geology of the Honolulu ground water supply: Honolulu Board of Water Supply, 55 p., accessed March 27, 2014, at http://hdl.handle.net/10524/12100.

Planning Consultants Hawaii, LLC, 2016, Final environmental impact statement: Waikapu Country Town, Prepared for Waikapu Properties, LLC, 2,373 p., accessed May 29, 2020, at https://www.waikapu.com/feis.

Rotzoll, K., 2010, Effects of groundwater withdrawal on borehole flow and salinity measured in deep monitor wells in Hawai‘i—Implications for groundwater management: U.S. Geological Survey Scientific Investigations Report 2010–5058, 42 p., accessed March 2, 2011, at https://pubs.usgs.gov/sir/2010/5058/.

Rotzoll, K., 2012, Numerical simulation of flow in deep open boreholes in a coastal freshwater lens, Pearl Harbor Aquifer, O‘ahu, Hawai‘i: U.S. Geological Survey Scientific Investigations Report 2012–5009, 39 p., accessed April 7, 2012, at http://pubs.usgs.gov/sir/2012/5009.

Rotzoll, K., 2022, SUTRA model used to evaluate long-term groundwater availability in the Waihe‘e, ‘Īao, and Waikapū aquifer systems, Maui, Hawai‘i: U.S. Geological Survey data release, https://doi.org/10.5066/P959B45F.

Rotzoll, K., and El-Kadi, A.I., 2008, Estimating hydraulic conductivity from specific capacity for Hawaii aquifers, USA: Hydrogeology Journal, v. 16, no. 5, p. 969–979, accessed April 9, 2008, at https://doi.org/10.1007/s10040-007-0271-0.

Rotzoll, K., El-Kadi, A.I., and Gingerich, S.B., 2007, Estimating hydraulic properties of volcanic aquifers using constant-rate and variable-rate aquifer tests: Journal of the American Water Resources Association, v. 43, no. 2, p. 334–345, accessed March 26, 2007, at https://doi.org/10.1111/j.1752-1688.2007.00026.x.

Sanderson, M., 1993, Prevailing trade winds—Weather and climate in Hawaiʻi: Honolulu, Hawaiʻi, University of Hawaiʻi Press, 126 p.

Sherrod, D.R., Sinton, J.M., Watkins, S.E., and Brunt, K.M., 2007, Geologic map of the State of Hawai'i: U.S. Geological Survey Open-File Report 2007–1089, 83 p., accessed January 13, 2011, at https://pubs.usgs.gov/of/2007/1089/.

Souza, W.R., and Voss, C.I., 1987, Analysis of an anisotropic coastal aquifer system using variable-density flow and solute transport simulation: Journal of Hydrology, v. 92, no. 1, p. 17–41, accessed August 29, 2019, at https://doi.org/10.1016/0022-1694(87)90087-4.

Stearns, H.T., and Macdonald, G.A., 1942, Geology and ground-water resources of the island of Maui, Hawaii: Hawaiʻi Division of Hydrography Bulletin 7, 334 p., accessed January 31, 2012, at http://hdl.handle.net/10125/50779.

Swain, L.A., 1973, Chemical quality of ground water in Hawaii: Hawaiʻi Division of Water and Land Development Report R48, 54 p.

Takasaki, K.J., and Mink, J.F., 1985, Evaluation of major dike-impounded ground-water reservoirs, island of Oahu: U.S. Geological Survey Water-Supply Paper 2217, 77 p., accessed January 14, 2014, at https://pubs.usgs.gov/wsp/2217/report.pdf.

University of Hawaiʻi, 2011, Main Hawaiian Islands multibeam bathymetry and backscatter synthesis—50 meter bathymetry and topography grids: The University of Hawaiʻi at Manoa, Hawaiʻi Mapping Research Group, School of Ocean and Earth Science and Technology, accessed March 22, 2013, at http://www.soest.hawaii.edu/hmrg/multibeam/grids.php.

U.S. Environmental Protection Agency, 2020, Secondary drinking water regulations—Guidance for nuisance chemicals: U.S. Environmental Protection Agency, accessed June 9, 2020, at https://www.epa.gov/sdwa/secondary-drinking-water-standards-guidance-nuisance-chemicals.

U.S. Geological Survey, 2019, National water information system—USGS groundwater data for Hawaii: U.S. Geological Survey web interface, http://dx.doi.org/10.5066/F7P55KJN, accessed January 15, 2019, at https://nwis.waterdata.usgs.gov/hi/nwis/gw. [Data available on the World Wide Web via USGS Water Data for the Nation]

Voss, C.I., and Provost, A.M., 2010, SUTRA—A model for saturated-unsaturated, variable-density ground-water flow with solute or energy transport (ver. 2.2, September 2010): U.S. Geological Survey Water-Resources Investigations Report 2002–4231, 250 p., accessed September 23, 2010, at https://doi.org/10.3133/wri024231.

Wentworth, C.K., 1939, The specific gravity of seawater and Ghyben-Herzberg ratio at Honolulu: University of Hawaiʻi Bulletin, v. 18, no. 8, p. 24, accessed March 27, 2014, at https://doi.org/10.1029/TR020i004p00690.

Wentworth, C.K., and Macdonald, G.A., 1953, Structures and forms of basaltic rocks in Hawaii: U.S. Geological Survey Bulletin 994, 98 p., accessed November 15, 2018, at https://doi.org/10.3133/b994.

Western Regional Climate Center, 2019, Kahului AP, Hawaii—Period of record monthly climate summary: Western Regional Climate Center, accessed January 4, 2020, at https://wrcc.dri.edu/cgi-bin/cliMAIN.pl?hi2572.

Wilcox, C., 1996, Sugar water—Hawaii's plantation ditches: Honolulu, Hawaiʻi, University of Hawaiʻi Press, 191 p.

Yamanaga, G., and Huxel, C.J., 1970, Preliminary report in the water resources of the Wailuku area, Maui: Hawaiʻi Division of Water and Land Development Circular C61, 43 p.

Appendix 1. Estimation of Recharge with a Water Budget

Introduction

For this study, spatially distributed groundwater recharge for part of Maui, Hawai‘i was estimated using a water-budget computation. The water budget is designed to simulate daily hydrological processes and physical conditions that affect groundwater recharge on Maui. Hydrological processes and conditions simulated by the water budget include rainfall, fog interception, irrigation, runoff, and evapotranspiration (ET). The water-budget method used in this study is a variation of the Thornthwaite and Mather (1955) mass-balance procedure and is similar to the methods used in previous U.S. Geological Survey (USGS) recharge studies of various parts of Hawai‘i (Oki, 2002; Izuka and others, 2005; Engott and Vana, 2007; Engott, 2011; Engott and others, 2017; Izuka and others, 2018; Johnson and others, 2018; Oki and others, 2020). The two generalized flow diagrams of the water budget—one for non-forest land covers and one for forest land covers—are shown in figure 1.1. See Izuka and others (2018) for details on the water-budget equations used in this study.

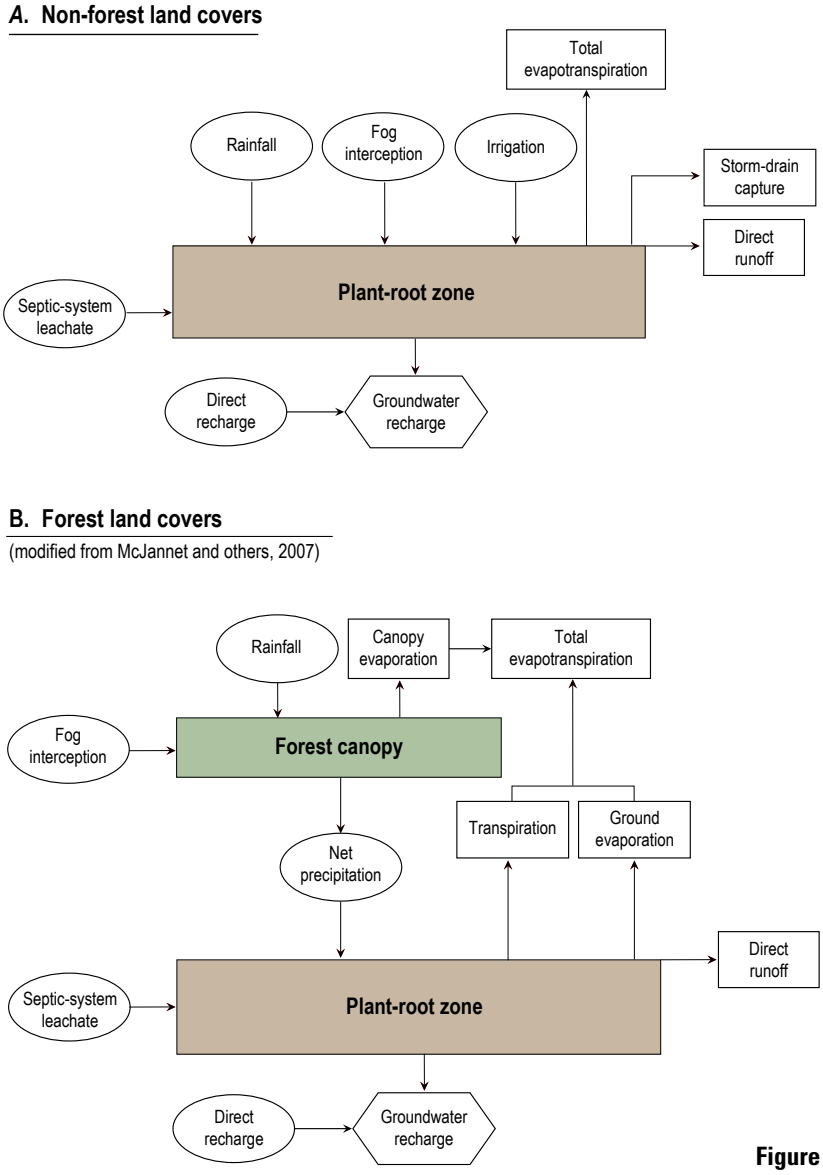

Figure 1.1. Generalized water-budget flow diagrams for (*A*) non-forest and (*B*) forest land covers.

The 444-square-mile water-budget study area comprises 16 aquifers systems (State of Hawaiʻi, 2010a) in the west, central, and upcountry parts of Maui (fig. 1.2). The water budget was used to compute mean annual recharge and water-budget components for the water-budget study area for nine historical scenarios with time periods 1926–69, 1970–79, 1980–84, 1985–89, 1990–94, 1995–99, 2000–04, 2005–09, and 2010–12.

Recharge was also computed for the water-budget study area for a hypothetical scenario that used 1980–2010 rainfall and 2017 land-cover conditions in which all plantation sugarcane on Maui, as of 2015, was replaced by non-irrigated grassland. The hypothetical scenario was included because Hawaiian Commercial and Sugar Company (HC&S) completed its last haul of sugarcane in December 2016 ("The History of Hawaiian Commercial & Sugar Co.," The Maui News,

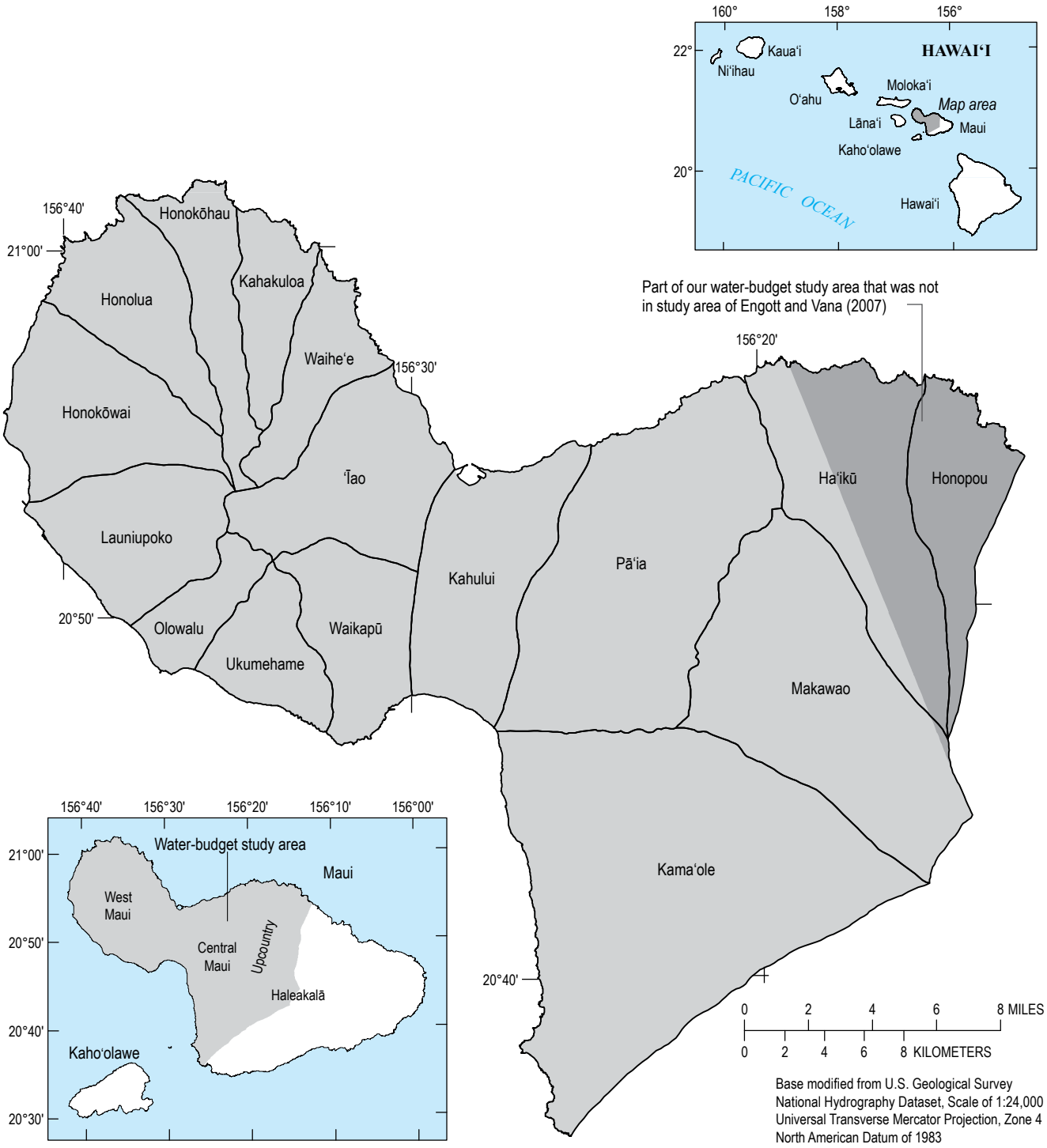

Figure 1.2. Map of water-budget study area for the water-budget calculations and boundaries of sixteen aquifer systems on Maui, Hawaiʻi (modified from Engott and Vana, 2007; State of Hawaiʻi, 2010a).

December 13, 2016). Sugarcane was an irrigated crop that had been grown by plantations on Maui since 1850, and HC&S was the last plantation on Maui to grow sugarcane (Dorrance and Morgan, 2000). The absence of HC&S sugarcane and associated reductions in applied irrigation water reduces recharge in central Maui, relative to recharge during historical periods when sugarcane was widespread and irrigated.

Water-Budget Subareas

The water-budget study area was subdivided into sections with homogeneous properties, termed subareas, for the water-budget calculations. Two subarea maps were created for this study: one map for the historical scenarios and a second map for the hypothetical scenario. Both subarea maps were generated using Esri ArcGIS software (www.esri.com) by intersecting (merging) spatial datasets that characterize the distribution of rainfall, fog, irrigation, septic effluent, reference ET, runoff, soil type, and land cover. The subarea map for the historical scenarios contained 432,199 subareas with an average area of 0.66 acres. The subarea map for the hypothetical scenario contained 450,556 subareas with an average area of 0.63 acres. Daily recharge estimates from the water-budget calculations were used to compute annual and mean annual recharge for each subarea and scenario. Mean annual recharge for the subareas also was summed over larger areas of interest, including 16 aquifer systems within the water-budget study area.

Input Data

Required input consisted of data that quantify the spatial and temporal distributions of land cover, rainfall, fog interception, irrigation, septic effluent, runoff, ET, and soil properties.

Land Cover, 1926–2012

Seven land-cover maps that are generally representative of conditions during 1926–79, 1980–84, 1985–89, 1990–94, 1995–99, 2000–04, 2005–12 were developed for this study. These maps identify 21 classes of land cover (fig. 1.3) and were merged with other spatial datasets when creating the map of subareas for the water budget. The periods for the seven maps were chosen because Engott and Vana (2007) mapped the locations and general types of agriculture in most of the water-budget study area for the six map periods between 1926 and 2004. The 1926–79 map was used in the water-budget calculations for the 1926–69 and 1970–79 scenarios and the 2005–12 map was used in the calculations for the 2005–09 and 2010–12 scenarios. Each of the five remaining maps was used in the water-budget calculations for the historical scenario with the corresponding time period.

A 2010 map of land cover for Maui (Johnson, 2014) was cropped to the water-budget study area and used as the 2005–12 map. The 2010 map, which is a modified version of the USGS (2010) existing vegetation-type map, was also used to define land cover for the recharge analysis in Johnson and others (2018). Land cover in each of the pre-2005 land-cover maps developed for this study was assumed to be the same as that in the 2010 map except in areas where changes in agriculture and development were identified and defined. Hence, the land-cover maps developed for this study account for land-cover changes in areas with identifiable changes in agriculture or development only. The spatial extents of agricultural and developed areas in each of the pre-2005 land-cover maps developed for this study were defined mainly from existing land-cover maps.

The spatial extents of agriculture in the 1926–79, 1980–84, 1985–89, 1990–94, 1995–99, and 2000–04 land-cover maps developed for this study were defined mainly from six land-cover maps developed by Engott and Vana (2007) for the same periods. Agricultural classes defined by Engott and Vana (2007) consisted of sugarcane, pineapple, macadamia nuts, and diversified agriculture. Areas defined as "orchards, groves, vineyards, nurseries, and ornamental horticulture areas" were included in the diversified-agriculture class in the maps developed for this study. Areas that changed from an agricultural class to "cropland and pasture" were assigned as grassland in the corresponding maps developed for this study.

Further analysis was needed to estimate the spatial extent of agriculture in an additional area on northern Haleakalā (figs. 1–2) that was not included in the maps developed by Engott and Vana (2007). Agriculture in the additional area during 1926–2004 was assumed to consist of diversified agriculture and pineapple; the spatial extents of these two land-cover classes in the six pre-2005 land-cover maps developed for this study were defined as follows. Areas classified as "orchards, groves, vineyards, nurseries, and ornamental horticulture areas" in a 1976 map (State of Hawai‘i, 1976) were mapped as diversified agriculture in the 1926–79 and 1980–84 maps. Areas with pineapple in a general land-use map for 1937 (Territorial Planning Board, 1939) were mapped as pineapple in the 1926–79 map. Areas classified as cultivated land in a 1992 map (National Oceanic and Atmospheric Administration, 2009a) were assigned as pineapple in the 1980–84, 1985–89, and 1990–94 maps. Pineapple fields between 1995 and 1999 were assumed to be the same as those in the 1990–94 map, except in selected areas that were not classified as cultivated land in a 2001 land-cover map (National Oceanic and Atmospheric Administration, 2009b). These selected areas were assigned as grassland in the 1995–99 map. Aerial images in Google Earth (https://www.google.com/earth/) taken between 2000 and 2004 were examined and used to assign areas that had pineapple in the 1995–99 map as either pineapple or grassland in the 2000–04 map. At the time of the analysis, pre-2000 images of the additional area were not available in Google Earth.

The spatial extents of developed classes for the 1926–79, 1980–84, 1985–89, 1990–94, 1995–99, 2000–04 land-cover maps developed for this study were defined using existing land-cover maps. The golf land-use class in the 1926–79, 1980–84, 1985–89, 1990–94, 1995–99, and 2000–04 land-cover maps developed by Engott and Vana (2007)

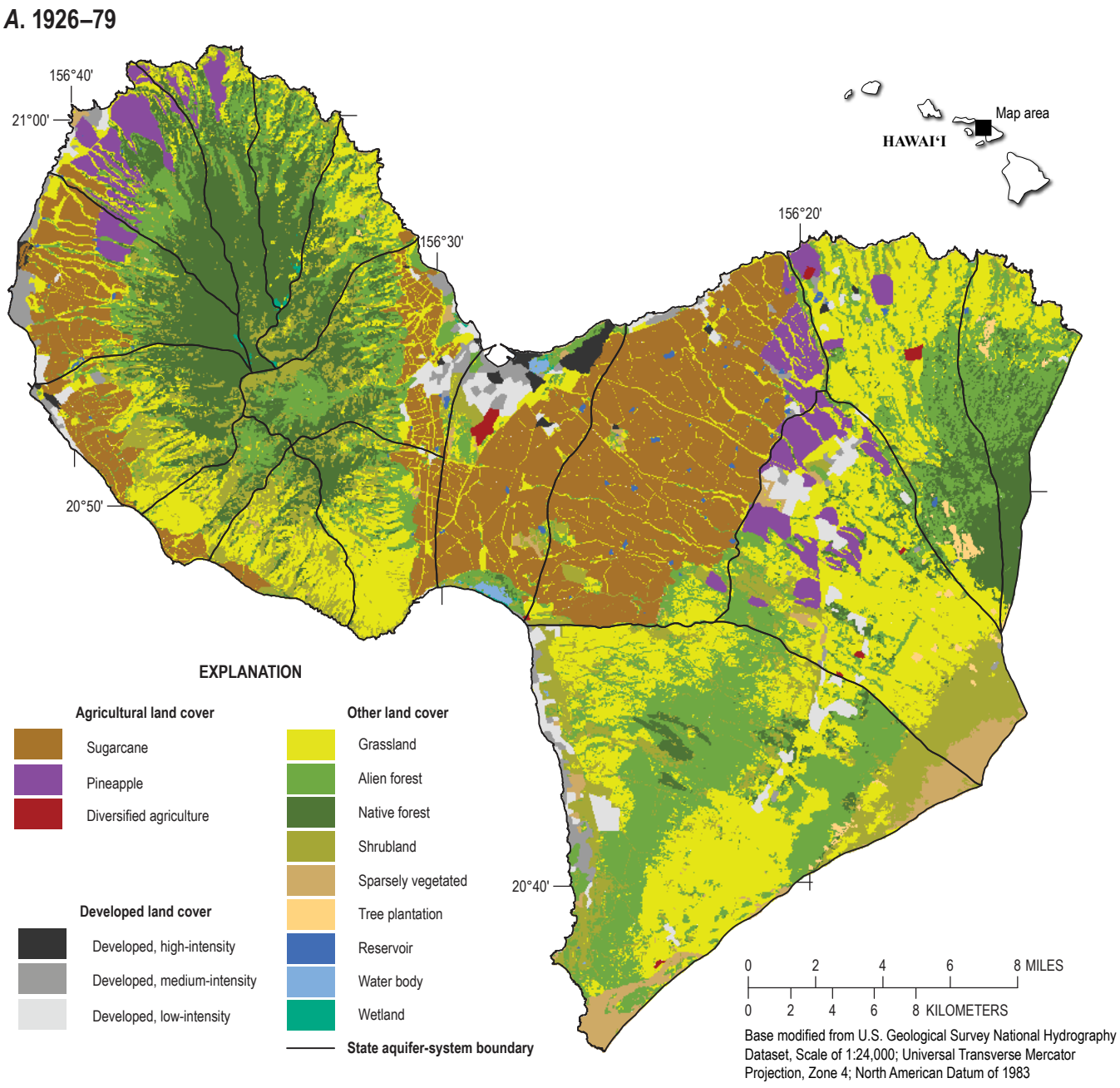

Figure 1.3. Maps of generalized land cover for water-budget study area on Maui, Hawaiʻi, for (*A*) 1926–79, (*B*) 1980–84, (*C*) 1985–89, (*D*) 1990–94, (*E*) 1995–99, (*F*) 2000–04, (*G*), 2005–12, and (*H*) 2017.

was assigned to the golf-course class in the corresponding land-cover maps developed for this study. Seven land-use categories in a 1976 map (State of Hawaiʻi, 1976) were reclassified and used to define the spatial extent of developed classes in the 1926–79 and 1980–84 maps developed for this study. The seven land-use categories in the 1976 land-cover map were reclassified as follows: the residential category was reclassified as low-intensity developed, two categories ([1]

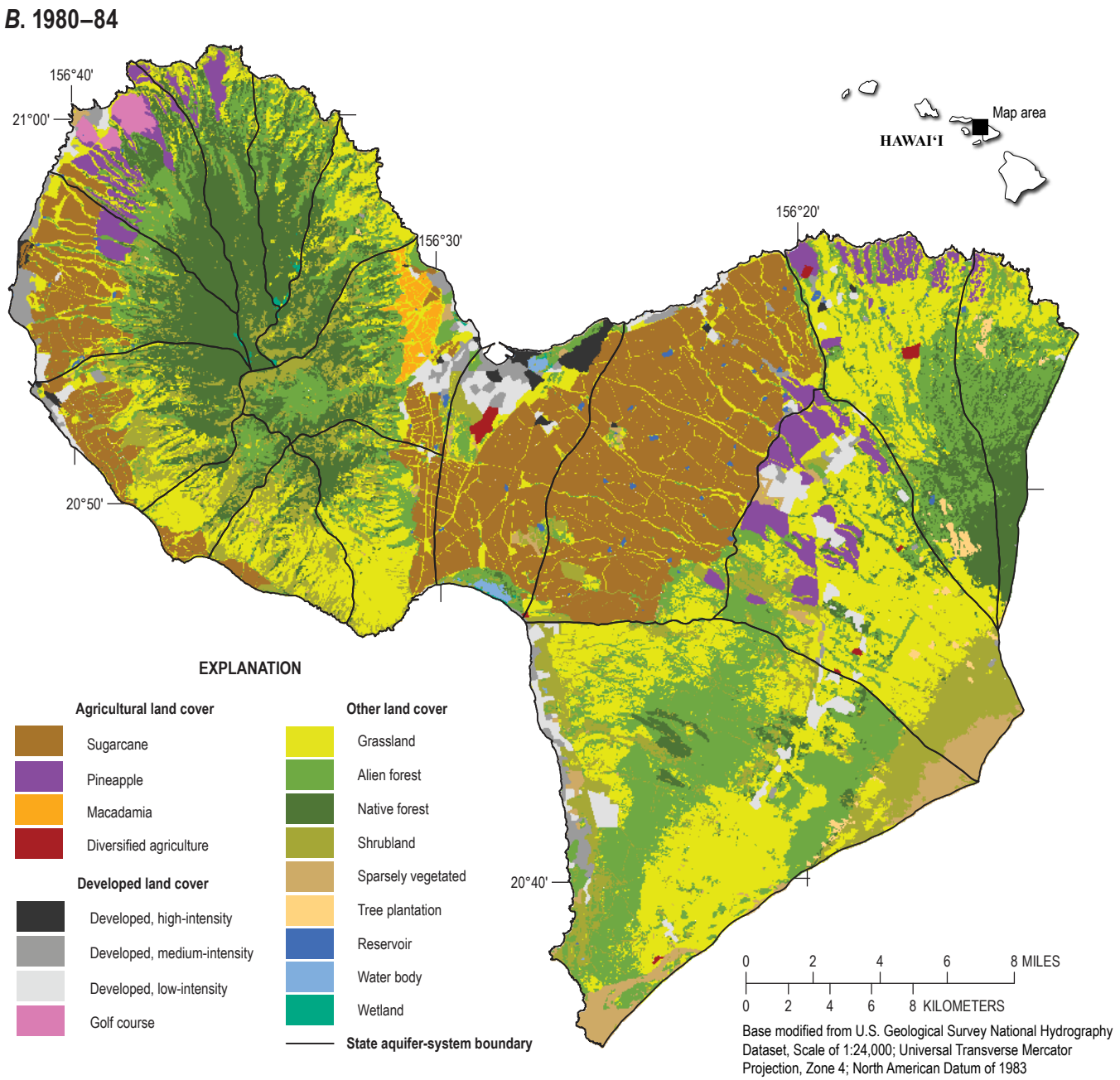

Figure 1.3. —Continued

commercial and services and [2] mixed urban or built-up land) were reclassified as medium-intensity developed, and three categories ([1] industrial; [2] transportation, communications, and utilities; and [3] industrial and commercial complexes) were reclassified as high-intensity developed. Developed classes in a 1992 map (National Oceanic and Atmospheric Administration, 2009a) were used in the 1985–89 and 1990–94 maps developed for this study. Developed land-cover

classes in a 2001 land-cover map (National Oceanic and Atmospheric Administration, 2009b) were used in the 1995–99 and 2000–04 maps developed for this study.

Land cover in all remaining areas—those that were neither agriculture nor developed—was considered an "other" type of land cover (fig. 1.3) and was defined using the 2010 map (Johnson, 2014). The 2010 map was used to define land cover in the non-agriculture and non-developed areas because this map differentiated alien forest from native forests, and this differentiation was relevant for the water-budget calculations.

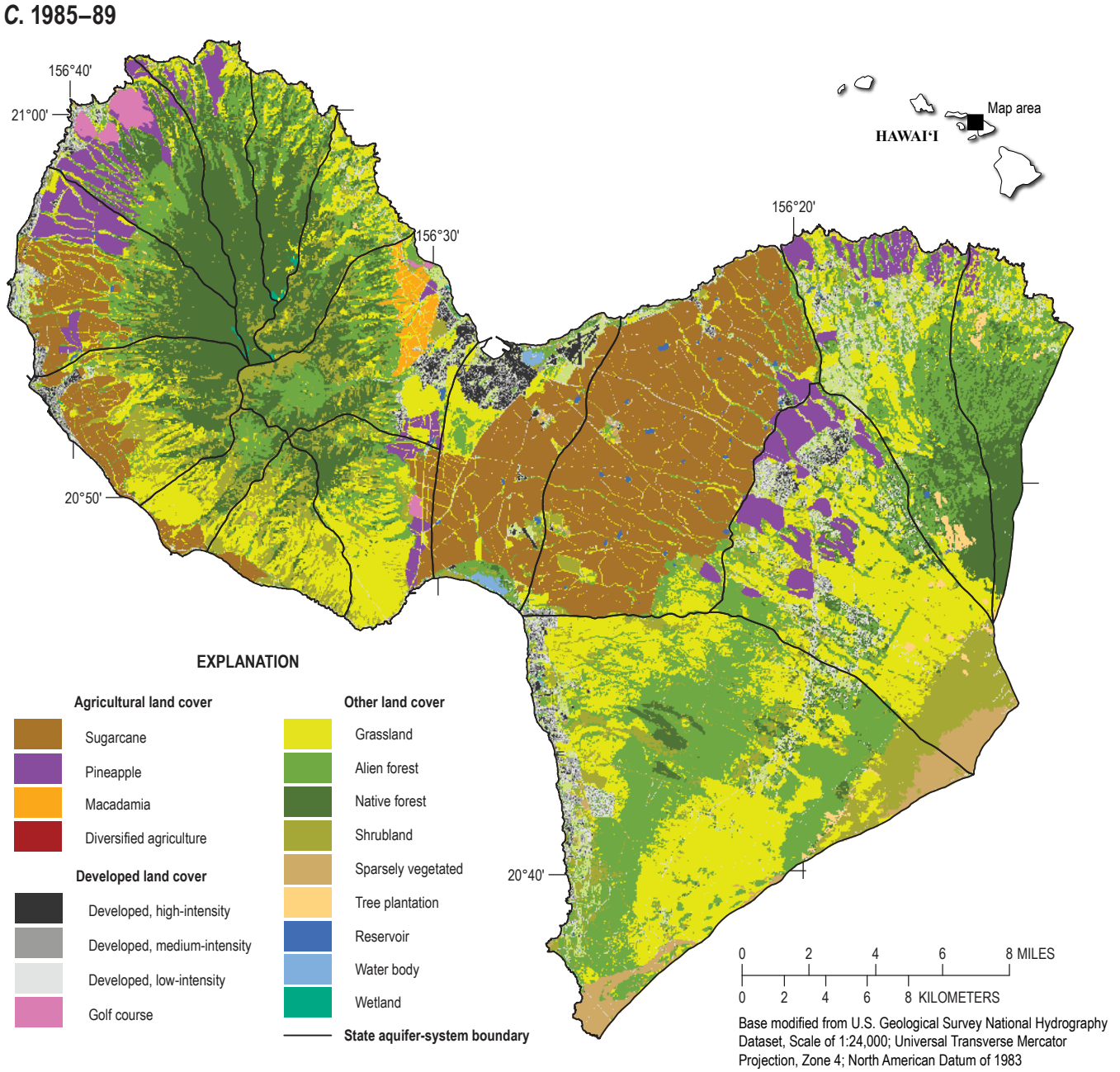

Figure 1.3. —Continued

Alien and native forests were not differentiated in any of the previously mentioned source-land-cover maps, including the 1976 map (State of Hawai‘i, 1976).

Between 1926–79 and 2005–12, the percentage of the water-budget study area with sugarcane decreased from about 18 to 14 percent, whereas the percentage of the water-budget study area with developed land cover increased from 4 to 16 percent (fig. 1.4). The percentage of the water-budget study area with agriculture other sugarcane between 1926–79 and 2005–12 ranged between about 2 and 5 percent.

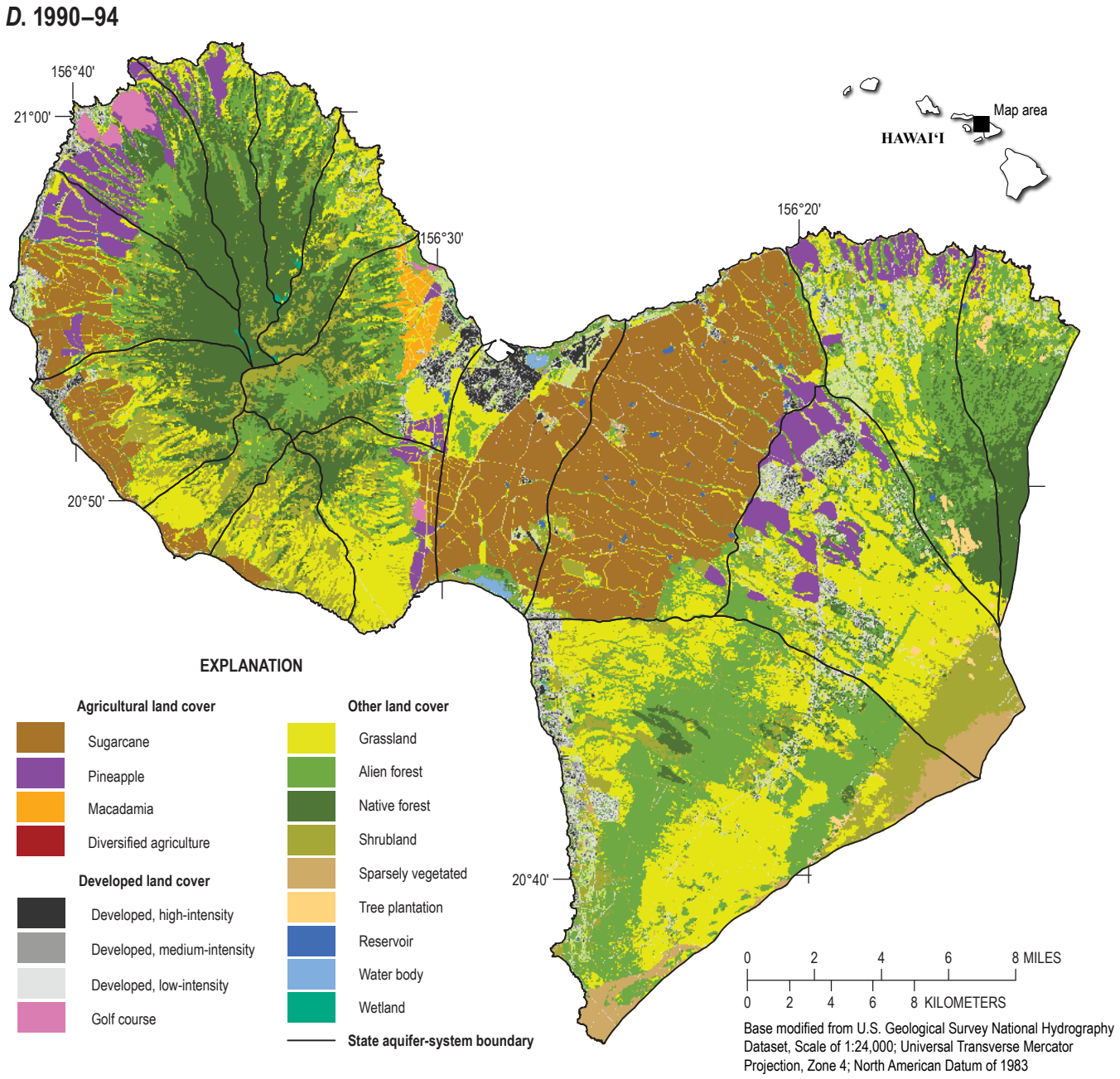

Figure 1.3. —Continued

E. 1995–99

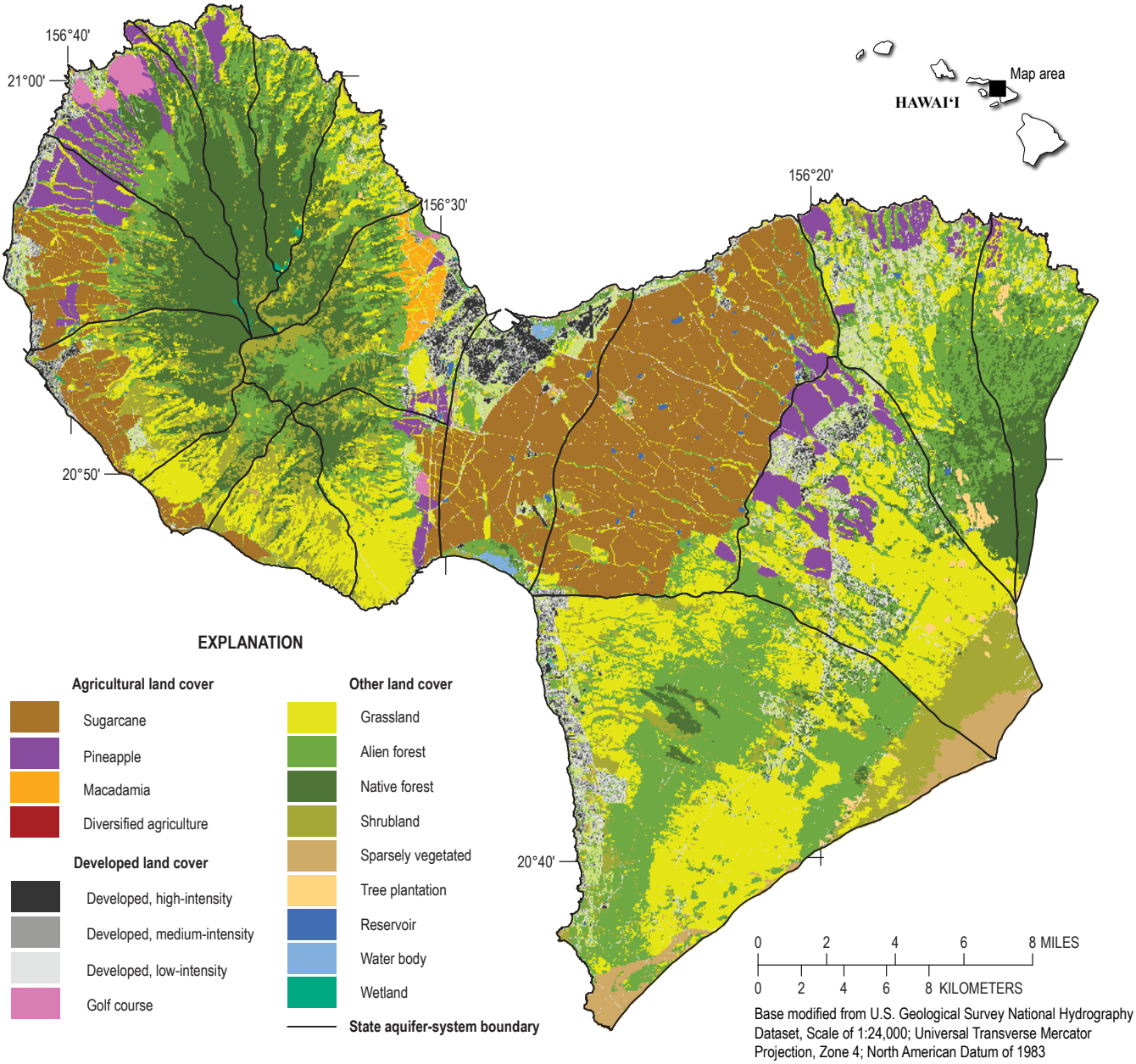

Figure 1.3. —Continued

F. 2000–04

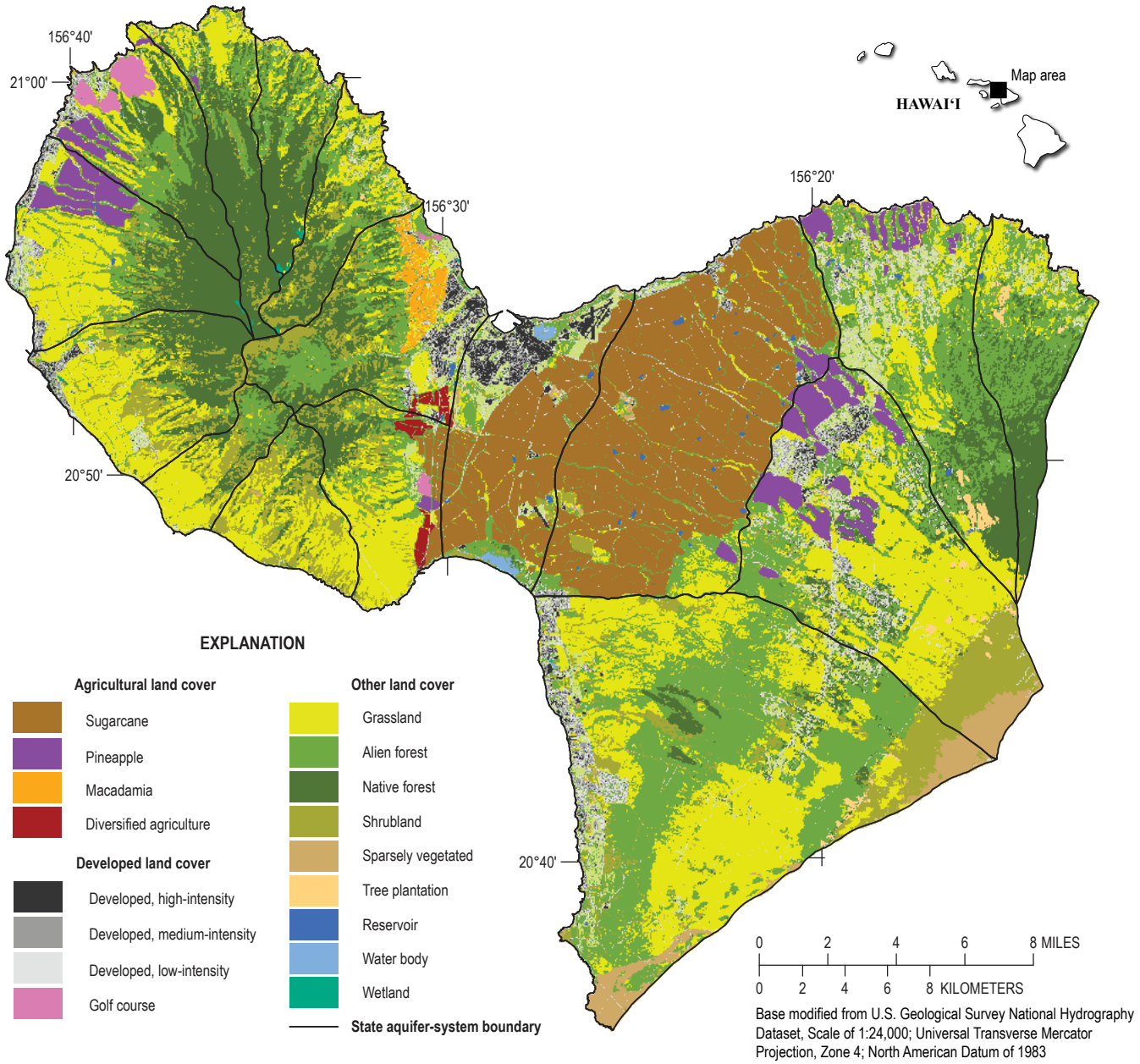

Figure 1.3. —Continued

G. 2005–12

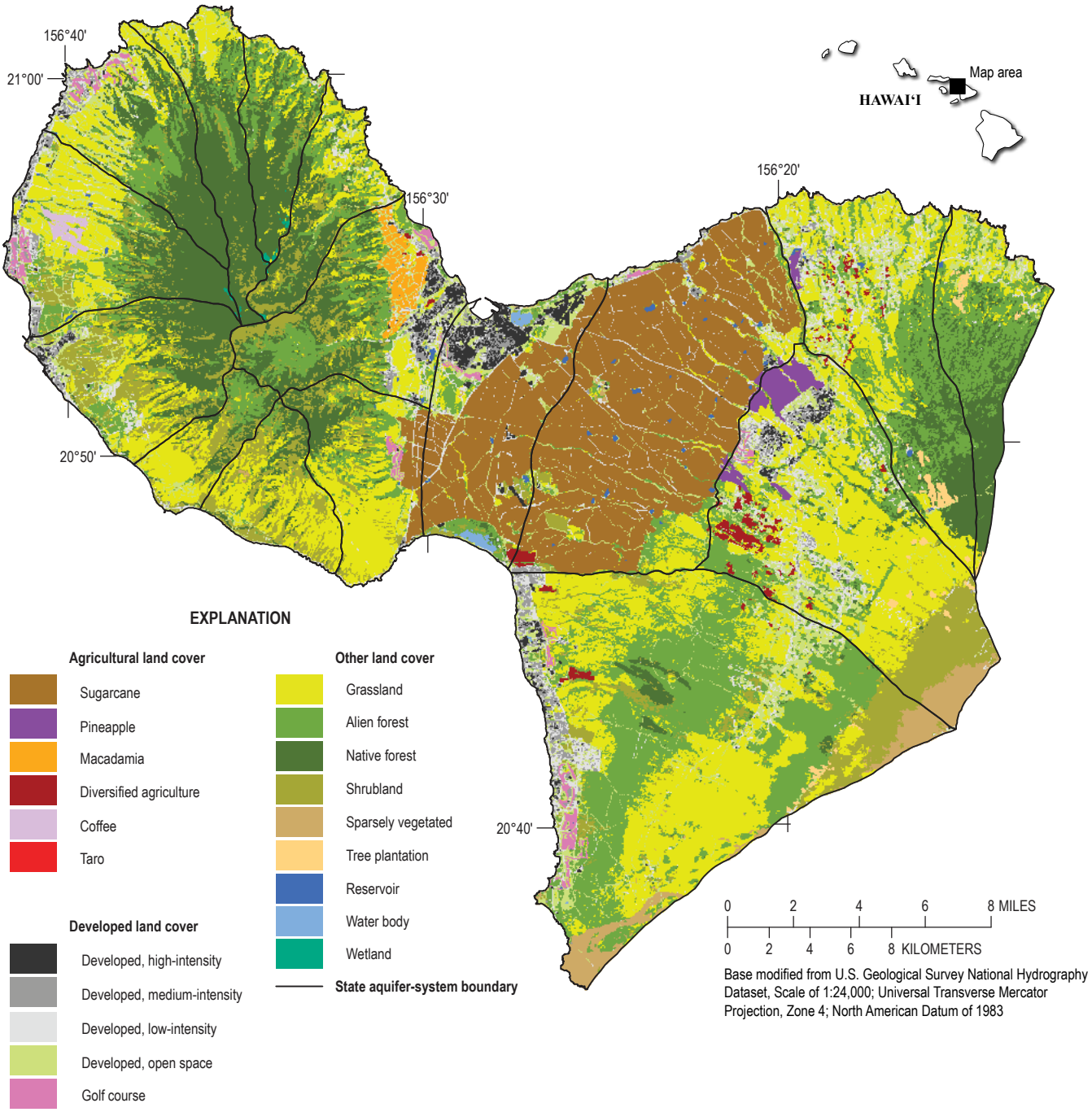

Figure 1.3. —Continued

H. 2017

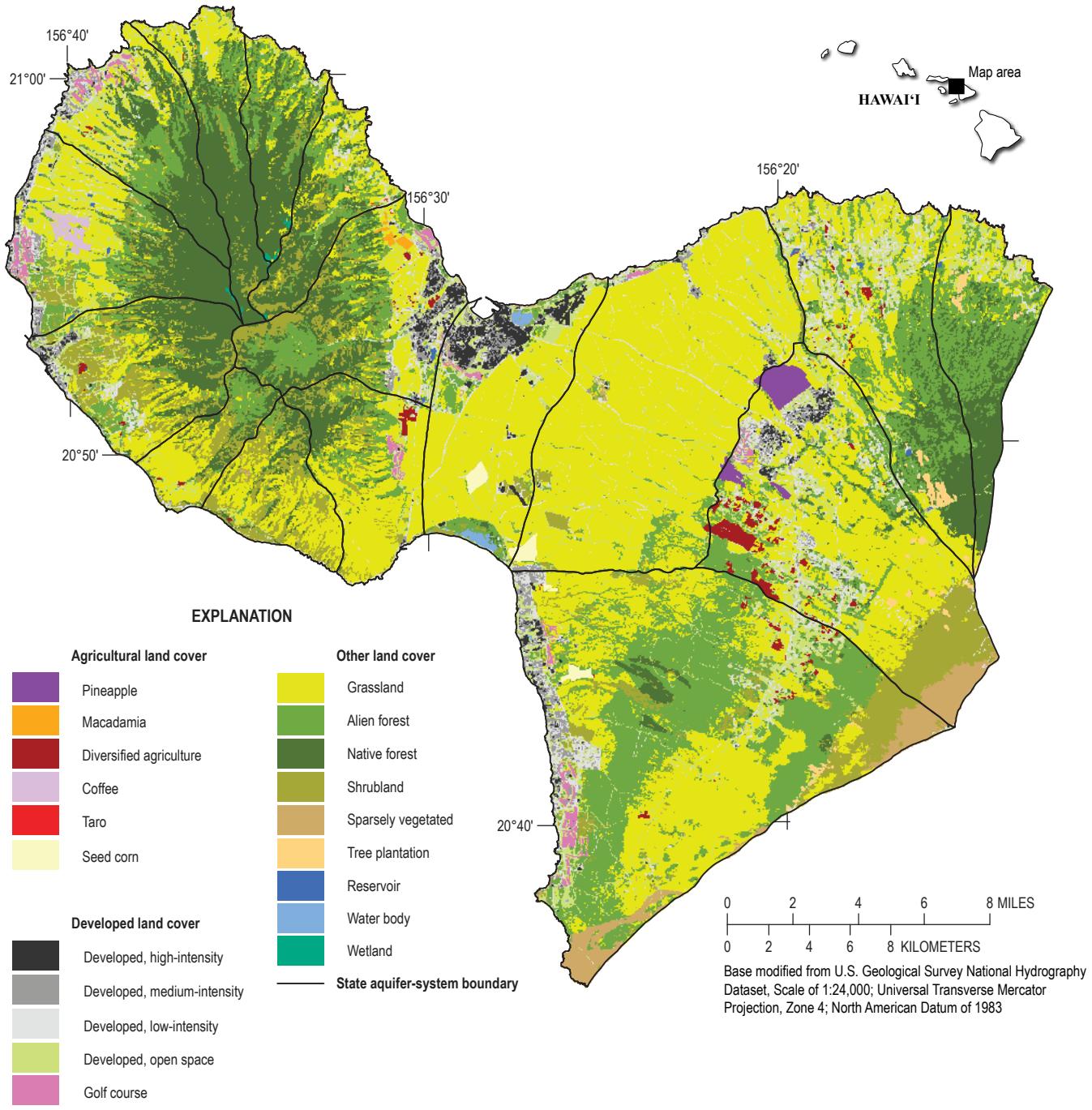

Figure 1.3. —Continued

Land Cover, 2017

A 2017 land-cover map for Maui (Mair, 2018) was used for the hypothetical scenario. Land-cover designations in the 2017 land-cover map were the same as those in the 2005–12 map for the majority (about 84 percent) of the water-budget study area. The 2017 land-cover map differed from the 2005–12 map mainly because it included the agricultural boundaries of a 2015 agricultural land-use map for Maui (Melrose and others, 2016) and because it reflected the cessation of sugarcane cultivation by HC&S in December 2016. As by Mair (2018), all sugarcane from the 2015 agricultural land-use map was reclassified as fallow/grassland, which, for the purpose of simplicity, was included with the grassland land-cover class for this study (fig. 1.3). Additionally, Mair (2018) assigned a grassland designation to areas in the 2017 land-cover map if these areas had received a reservoir designation in 2010 and were in the Waikapū, Kahului, or Pāʻia aquifer systems. The reservoirs in these areas had historically been used to supply irrigation water to nearby sugarcane fields. With the cessation of sugarcane cultivation, Mair (2018) assumed that these reservoirs would no longer be used to store water and would be dry. Less than 2 percent of the water-budget study area contained agriculture in 2017 (fig. 1.4).

The 2017 map included the seed corn land-cover class (fig. 1.3) that Mair (2018) derived from the 2015 agricultural land-use map for Maui. According to the report (Melrose and others, 2016) accompanying the 2015 agricultural land-use map, only about 25 percent of the areas with seed corn have active farming at any given time. Therefore, in the water-budget calculations, each subarea with a seed corn land-cover designation was treated as a spatially undifferentiated mixture of 25 percent seed corn and 75 percent grassland. This approach was used in recent Hawaiʻi water budgets (Engott and others, 2017; Oki and others, 2020) that included the seed corn land-cover class.

Rainfall

Gridded maps of monthly rainfall for each of the 1,044 months during 1926–2012 for Maui (Giambelluca and others, 2013; Frazier and others, 2016) were used to define the spatial and temporal distributions of rainfall in the water-budget calculations. Using Esri ArcGIS software, the monthly rainfall maps were converted from a raster grid to a polygon format for use in the water budget. The rainfall polygons were intersected with the other spatial datasets when creating the subarea maps for the water budget. Monthly rainfall for each subarea was computed by the water budget as the product of monthly rainfall from the gridded maps (Frazier and others, 2016) and a mean monthly adjustment factor. Each rainfall grid cell was assigned a set of 12 mean monthly adjustment factors. The adjustment factors were developed and used by Johnson and others (2018) to ensure that mean monthly rainfall calculated for 1978–2007 from the Frazier and others (2016) dataset would equal mean monthly rainfall in the Rainfall Atlas of Hawaiʻi (Giambelluca and others, 2013).

Estimates of the spatial distribution of daily rainfall on Maui during 1926–2012 were not available and were not developed as part of this study. The water budget synthesized daily rainfall by disaggregating monthly rainfall values during 1926–2012 using the method of fragments (for example, Oki, 2002). This method for computing daily rainfall was also used in recent water budgets for Maui (Engott and Vana, 2007; Gingerich and Engott, 2012; Johnson and others, 2018). The method of fragments creates a synthetic sequence of daily rainfall from monthly rainfall by imposing the rainfall pattern from a rain gage with daily data. The synthesized daily rainfall data approximate the long-term average character of daily rainfall, such as frequency, duration, and intensity, but may not reproduce the true historical daily rainfall record.

Sets of daily rainfall fragments were assigned to the Thiessen polygons of 47 selected rain gages, which consist of all rain gages shown in figure 3 of Johnson and others (2018) except for nine rain gages—with Cooperative Network Index numbers of 510175, 519765, 514634, 511148, 511122, 511125, 517194, 514091, and 511930—whose Thiessen polygons were not in this study's area of interest. The sets of daily rainfall fragments assigned to each Thiessen polygon were the same as those computed and assigned by Johnson and others (2018). In the water-budget calculation, a fragment set assigned to a Thiessen polygon for a given gage and month was randomly selected from among all available sets for that Thiessen polygon and that month of the year. Daily rainfall for a given month was synthesized by multiplying total rainfall computed for that month by each fragment in the set, thereby providing daily rainfall for the water budget.

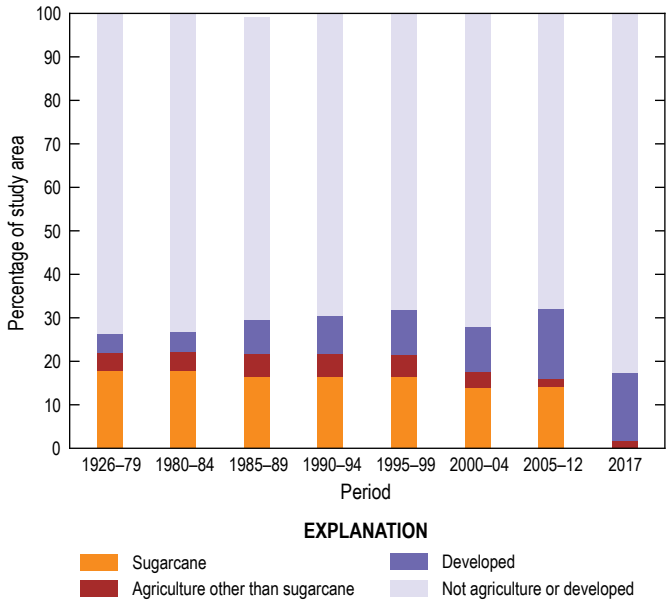

Figure 1.4. Graph of the percentage of 444-square-mile water-budget study area on Maui, Hawaiʻi mapped as sugarcane, agriculture other than sugarcane, developed land cover, and other land cover for eight periods between 1926 and 2017. See figure 1.3 for maps of land cover for each period.

Fog Interception

Fog interception, or cloud-water interception, is moisture from fog and clouds that accumulates on vegetation. Maps of fog-interception rates on Maui were not available for this study. Consequently, fog interception was estimated using the same approach as Johnson and others (2018). Daily fog interception was computed in the water budget as the product of (1) daily rainfall, (2) a mean monthly fog-to-rainfall ratio for the corresponding month, and (3) a fog-catch efficiency factor, which varied by land cover.

Mean monthly fog-to-rainfall ratios varied spatially and were the same as those developed by Johnson and others (2018). The method used to develop these fog-to-rainfall ratios ensured that, for water-budget scenarios that used 1978–2007 rainfall, water-budget estimates of mean annual fog interception in forested areas would be consistent with the fog-interception rates shown in table 3 of Johnson and others (2018). These fog-interception rates, which range from 0 to 30 inches per year (in/yr) and depend on altitude and aspect (leeward or windward), generally represent the midpoint of the ranges in fog-interception measurements reported for Maui (see Scholl and others, 2007; Giambelluca and others, 2011) and elsewhere in Hawai‘i (see DeLay and Giambelluca, 2010). Mean monthly fog-to-rainfall ratios were zero for subareas below altitudes of 2,000 feet (the base of the cloud zone), and greater than zero for subareas at altitudes of 2,000 feet and higher (within the cloud zone on Maui).

A fog-catch efficiency factor was included in the computation of daily fog interception to account for the differences in fog-collecting ability among land-cover types. A land cover's fog-catch efficiency factor represents the quotient of the amount of fog intercepted by the land cover and the amount of fog in a given area. The assigned fog-catch efficiency factor was 1 for forest land covers (alien, native, and tree plantation), 0.5 for shrubland and coffee, and 0 for all remaining land covers, meaning they intercept no fog. The same fog-catch efficiency factors were assigned to the same or similar land covers in recent water budgets for Maui (Engott and Vana, 2007; Gingerich and Engott, 2012; Johnson and others, 2018).

Impervious Surfaces and Storm-Drain Capture

Each water-budget subarea was assigned an impervious-fraction value for each of the eight land-cover map periods (1926–79, 1980–84, 1985–89, 1990–94, 1995–99, 2000–04, 2005–12, and 2017). A subarea's impervious fraction equaled the fraction of its area assumed to be covered by impervious surfaces, such as paved roads and buildings, for the period.

For each land-cover map period, subareas without one of the developed land covers (fig. 1.3) were assigned an impervious fraction of 0, meaning they were 0 percent impervious and 100 percent pervious. Subareas with golf-course land cover also were assigned an impervious fraction of 0. A map of impervious surfaces on Maui for 2010 (National Oceanic and Atmospheric Administration, 2015) was used to compute the impervious fraction of each subarea with one of the remaining developed land covers (open space; and low-, medium-, and high-intensity) in the 2005–12 and 2017 map periods. The computed impervious-fraction values ranged between 0 and 0.99, meaning that their areas were between 0 and 99 percent impervious. Impervious-fraction values assigned to subareas for the 2005–12 map period were used in the pre-2005 map periods for instances when a subarea's developed land-cover class in the pre-2005 map period was the same as that in 2005–12 map period. In all other instances for the pre-2005 map periods, each subarea with a developed land cover was assigned an average impervious-fraction value on the basis of its land-cover class: 0.11 for developed, open space; 0.28 for developed, low-intensity; 0.56 for developed, medium-intensity; and 0.78 for developed, high-intensity. These average values were computed as area-weighted averages of the impervious-fraction values for subareas with these classes of land cover in the 2005–12 map period.

The impervious fraction was used by the water budget to separate a depth of water that was treated computationally as though it fell on an impervious surface from the total rain that fell on a subarea. The rainfall retention-capacity of all impervious surfaces was assumed to be 0.25 inches (in.), meaning that up to 0.25 in. of rain could be stored on an impervious surface, where it could evaporate or be stored until the following day (see equations 6–8 in Johnson and others, 2018). The remaining water, that in excess of 0.25 in., was considered excess water, W_i. For subareas with medium- or high-intensity developed land covers (fig. 1.3), W_i was assumed to be captured by storm-drain systems and was reported as storm-drain capture (fig. 1.1). Subareas with land covers of low-intensity developed or developed open space were assumed to have no storm-drain capture, and W_i was distributed over the pervious fraction of the subarea (see equations 1a and 1b in Johnson and others [2018]). Storm-drain capture and W_i equaled zero for all remaining subareas, which were 100 percent pervious. Storm-drain capture for the scenarios of this study was limited to subareas with medium- or high-intensity developed land covers. Exceptions to this general approach likely exist but would require additional investigations that were beyond the scope of this study.

Irrigation

Irrigation was applied to the agricultural land covers (coffee, corn, diversified agriculture, macadamia, pineapple, sugarcane, and taro) and to three additional land covers (golf course, high-intensity developed, and medium-intensity developed) that were assumed to contain irrigated lawns and landscapes. Two methods were used to estimate irrigation in the model: a constant-value method was used for subareas with taro and a demand-based method was used for the remaining irrigated land covers.

All subareas with taro land cover were assigned a constant-irrigation rate in the water budget because taro was assumed to be grown in flooded pond fields. The constant-irrigation rate assigned to taro for this study, 455 in/yr, was the same as that assigned to taro in recent Hawai‘i water budgets

(Engott and others 2017; Izuka and others, 2018; Johnson and others, 2018). In the water-budget calculations, 455 in/yr of irrigation water was allocated in equal amounts of about 1.25 in. per day to each day of a year. The assigned constant-irrigation rate for taro was meant to represent the recharge rate from pond fields, not the rate of water flowing into pond fields. Water-budget estimates of recharge for taro, however, may exceed 455 in/yr for subareas that have additional water input from septic effluent.

For subareas with one of the remaining irrigated land-cover types, the water budget computed monthly irrigation using a demand-based approach that considered monthly rainfall, runoff, potential ET, and irrigation-method efficiency and uses the following equation:

$$I_m = [(PE)_m + U_m - R_m] / g$$

$$\text{for } (PE)_m + U_m > R_m \text{ and}$$

$$I_m = 0$$

$$\text{for } (PE)_m + U_m \leq R_m \qquad (1.1)$$

where:

$(PE)_m$ is potential ET for month m [unit length, L],
U_m is amount of runoff for month m [L],
R_m is amount of rainfall for month m [L],
I_m is amount of irrigation for month m [L], and
g is irrigation-method efficiency [dimensionless].

Irrigation-method efficiency, the fraction of applied irrigation water that becomes available for plant consumption, varied by irrigation method. Corn, diversified agriculture, and pineapple were assumed to use drip irrigation, which has an irrigation-method efficiency of 0.85 (University of Hawaiʻi, 2008). Coffee and macadamia were assumed to use micro-spray irrigation, which has an irrigation-method efficiency of 0.80 (University of Hawaiʻi, 2008). Golf courses and medium- and high-intensity developed land covers were assumed to use sprinkler irrigation, which has an irrigation-method efficiency of 0.70 (University of Hawaiʻi, 2008).

Each subarea's monthly irrigation rate, calculated using equation 1.1, was allocated in equal amounts for each day of a given month if its land cover was coffee, diversified agriculture, macadamia, golf course, medium-intensity developed, or high-intensity developed. However, for subareas with macadamia land cover, no irrigation was applied in the post-1999 scenarios, an assumption consistent with the approach used in the water budgets of Engott and Vana (2007) and Johnson and others (2018). No irrigation was applied to pineapple in the pre-1980 scenarios because pineapple was not irrigated on Maui before 1980 (Engott and Vana, 2007). Monthly pineapple irrigation for all remaining scenarios was uniformly distributed on days 1, 2, 3, 8, 9, 10, 15, 16, 17, 22, 23, 24, and 28 of each month, consistent with Engott and Vana (2007).

The methods used to estimate sugarcane irrigation in previous water budgets for Maui (Engott and Vana, 2007; Gingerich and Engott, 2012; Johnson and others, 2018) were used in the water-budget calculations for this study. Briefly, sugarcane was assumed to have a 24-month cultivation cycle. Changes in sugarcane's irrigation demand in response to growth changes during its cultivation cycle were accounted for in the water budget by varying sugarcane's crop coefficient (fig. 1.5). A crop coefficient is a vegetation-related factor used to estimate potential ET in the water budget (see "Potential ET" section).

Furrow and drip irrigation were the two primary irrigation methods for sugarcane on Maui (Engott and Vana, 2007). The furrow method was the primary method used before about 1980. The more efficient drip method gradually began replacing furrow irrigation beginning in the mid-1970s (Fukunaga, 1978). During furrow-irrigation periods, large volumes of water were applied about twice a month to furrows dug in the fields. During drip-irrigated periods, relatively small volumes of water were applied to fields for 2–3 consecutive days every week.

In the water-budget calculations for this study, all sugarcane fields were assumed to be furrow irrigated before 1980 and drip irrigated from 1980 to 2012. Sugarcane was absent from the 2017 land-cover map used for the hypothetical scenario. Furrow and drip irrigation of sugarcane were assigned efficiencies of 0.50 and 0.80, respectively; these values were provided to Engott and Vana (2007) by HC&S. For both furrow- and drip-irrigated sugarcane fields, irrigation water was applied during the first 20 months of the 24-month cultivation cycle; no irrigation was applied during the remaining 4 months of the cycle. Monthly irrigation volumes, calculated using equation 1.1, were uniformly distributed on selected days of each month: days 1 and 15 for

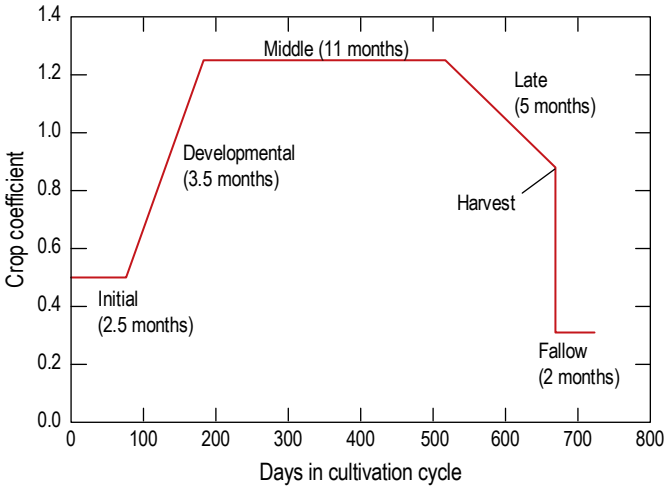

Figure 1.5. Graph of crop coefficients used in the water-budget calculation for different growth stages of sugarcane during its 24-month cultivation cycle (based on data from Fukunaga, 1978).

furrow-irrigated fields and days 1, 2, 3, 8, 9, 10, 15, 16, 17, 22, 23, 24, and 28 for drip-irrigated fields. At the end of the 24-month cycle, the sugarcane was assumed to be harvested, and the field left fallow until the next cycle began. The cultivation cycles of sugarcane fields were staggered such that about half the fields would be harvested in any one year.

The water budget adjusted irrigation estimates from equation 1.1 by applying irrigation-adjustment factors assigned to selected land-cover types for selected periods. The irrigation-adjustment factors were assigned to ensure that the water budget's irrigation estimates were, on average, consistent with reported rates of irrigation and rates of water available for irrigation. An adjustment factor of 0.87 was assigned to sugarcane for scenarios during 1926–79 when the furrow-irrigation method was used. By using an adjustment factor of 0.87, the water budget computed a mean annual furrow-irrigation rate for sugarcane for 1926–79 that was equal to the mean annual rate of water (466 million gallons per day) that Engott and Vana (2007) reported was available for sugarcane irrigation on Maui during 1926–79. The water budget's drip-irrigation estimates for sugarcane during 1980–2012 were not adjusted. No adjustments were made because, for most of the sugarcane in the water-budget study area (about 30,000 acres of HC&S's sugarcane fields in central Maui), the water budget's average drip-irrigation estimate of 6,168 gallons per acre per day (gal/acre/d) during 1984–2007 was less than 6,720 gal/acre/d. The latter value represents the average rate of irrigation water available for these fields, as summarized by Johnson and others (2018), on the basis of water data reported by HC&S (State of Hawai'i, 2010b, p. G-3). For macadamia land cover, an adjustment factor of 0.71 was used for scenarios between 1980 and 1999, when macadamia was assumed to be irrigated in the water budget. A factor of 0.71 ensured that the water budget's irrigation estimates for macadamia during 1984–99 averaged about 52 in/yr, the average of the micro-spray irrigation rates that were provided to Engott and Vana (2007) by Wailuku Water Company. The irrigation adjustment factors used by Johnson and others (2018) for diversified agriculture (0.41) and for medium- and high-intensity developed land covers (0.37) also were used for all scenarios of this study.

Septic Effluent

Septic effluent for this study consisted of cesspool seepage and septic-system leachate. In the water-budget calculations, cesspool seepage was considered direct recharge, whereas septic-system leachate was added to the plant-root zone where it was subject to ET (fig. 1.1). The septic-effluent rates used in water-budget calculations for 2010–12 (fig. 1.6) and for the hypothetical scenario were the same as those used in the water-budget calculations of Johnson and others (2018). Johnson and others (2018) derived the septic-effluent rates from the septic-effluent estimates of Whittier and El-Kadi (2013) for tax map key (TMK) parcels with one or more on-site disposal systems. For TMK parcels containing more cesspool-type disposal systems than other types of septic-disposal systems, septic-effluent estimates were treated as cesspool seepage in the water budget. For all remaining TMK parcels with on-site disposal systems, septic-effluent estimates were treated as septic-system leachate. Owing to uncertainty in the actual disposal locations within TMK parcels, a TMK parcel's septic effluent was applied as a uniform rate, in inches per day, over each subarea within the TMK parcel.

For each subarea that was not within the Pu'unēnē census county subdivision (fig 1.6), septic-effluent rates were estimated as the product of (1) its 2010–12 septic-effluent rate and (2) a septic-adjustment factor assigned to the encompassing census county subdivision for each scenario between 1926 and 2009. Decennial population estimates for census county subdivisions and for Maui during 1920–2010 (table 1.1) were used to compute septic-adjustment factors for each census county subdivision other than Pu'unēnē. For any given census county subdivision, the subdivision's septic-adjustment factor for 2005–09 and 2000–04 equaled the ratio of the subdivision's 2000 population to 2010 population; the ratio of its 1990 population to 2010 population was used as its septic-adjustment factor for 1995–99 and 1990–94; the ratio of its 1980 population to 2010 population was used as its septic-adjustment factor for 1985–89 and 1980–84; and the ratio of its 1970 population to 2010 population was used as its septic-adjustment factor for 1970–79. Each census county subdivision's septic-adjustment factor for 1926–69 equaled the ratio of its 1960 population to 2010 population because population estimates for 1920, 1930, 1940, or 1950 for the census subdivisions shown in fig 1.6 were not found.

The average septic-effluent rate per person for Pu'unēnē for 2010–12, 5,625 gallons per day (gal/d) per person, estimated as the ratio of Pu'unēnē's volumetric septic-effluent rate (about 45,000 gal/d) and its 2010 population (8 people), is more than ten times greater than that of other census county subdivisions in the study area. Therefore, to reduce the risk of overestimating septic effluent, septic-effluent rates in Pu'unēnē during 1926–2009 were not estimated as the product of 2010–12 septic-effluent rates and septic-adjustment factors derived from decennial population estimates, which was the approach used for the other census county subdivisions. If the approach used for other census county subdivisions had also been used for Pu'unēnē, then, for water-budget scenarios between 1926–1999, the range of septic-adjustment factors (between 27.1 and 382) for Pu'unēnē would have been substantially greater than the range of those (between 0.05 and 3.99) for the other census county subdivisions; consequently, the resulting septic-effluent estimates for Pu'unēnē likely would have been unrealistically high during 1926–1999 and would have exceeded the combined septic effluent from the other study area census county subdivisions during 1926–69 and 1970–79.

For subareas within the Pu'unēnē census county subdivision, septic-effluent rates used for the 2010–12 also were used for 2000–04 and 2005–09 because Pu'unēnē's population in 2010 was about the same as it was in 2000

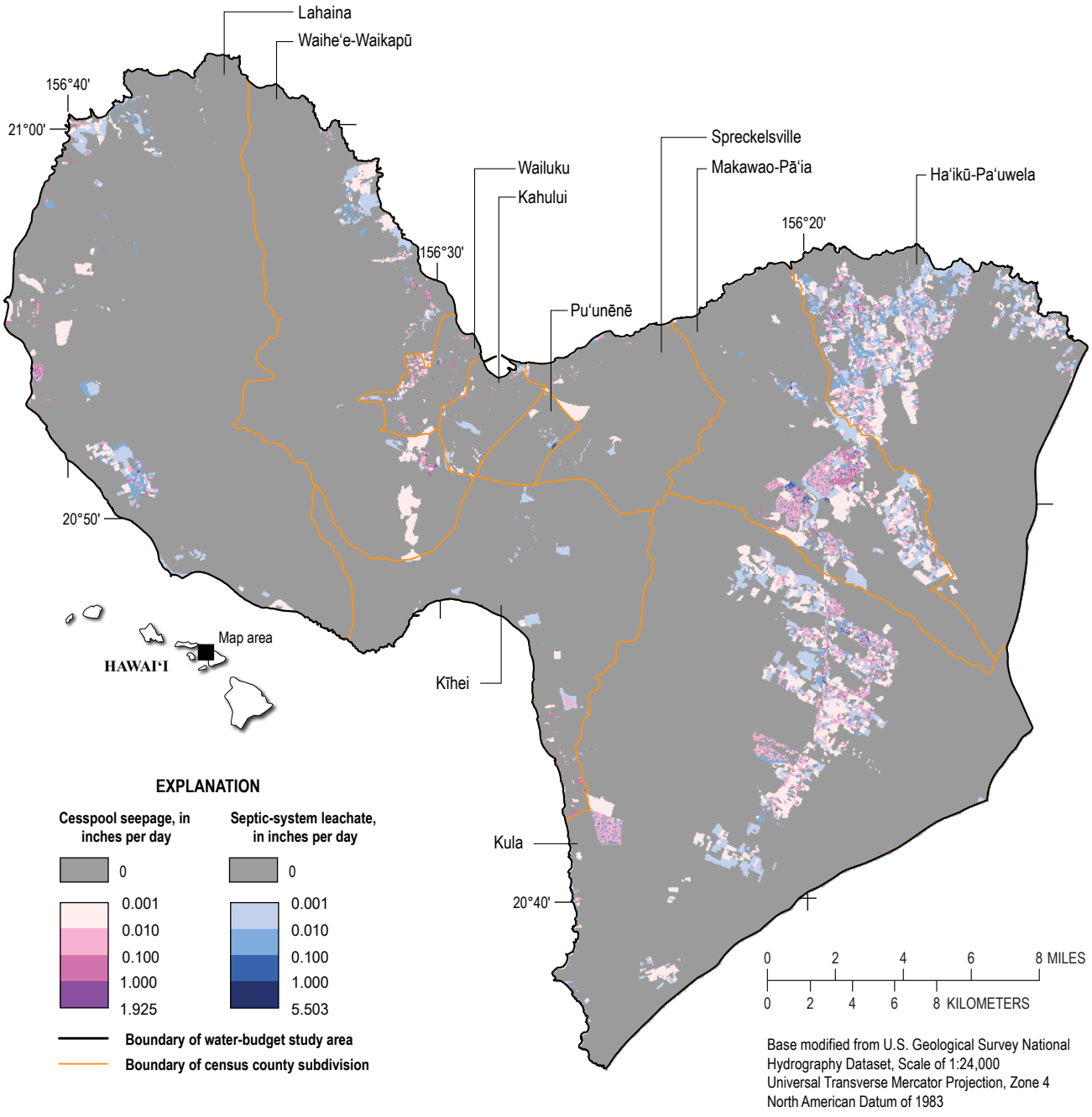

Figure 1.6. Map of septic-effluent rates used in the water-budget calculations for 2010–12 and for parts of census county subdivisions within the water-budget study area on Maui, Hawaiʻi (modified from Whittier and El-Kadi, 2013; U.S. Census Bureau, 2015; Johnson and others, 2018).

(table 1.1). For each historical scenario between 1926 and 1999, Puʻunēnē's total septic effluent rate, in gallons per day, was computed as the product of 200 gallons per person per day (gal/person/d) and an assigned population. Puʻunēnē's 1990 population (table 1.1) was assigned to the 1995–99 and 1990–94 scenarios, its 1980 population was assigned to the 1985–89 and 1980–84 scenarios, and its 1970 population was assigned to the 1970–79 scenario. Puʻunēnē's 1960 population was assigned to the 1926–69 scenario because decennial population estimates for Puʻunēnē during 1920–50 were not found in census documents. The septic rate of 200 gal/person/d was derived from the ratio of combined septic effluent in 2010–12 to the combined population in 2010 for four nearby census subdivisions (Haʻikū-Paʻuwela,

Table 1.1 Decennial populations for census county subdivisions on Maui, Hawai'i, 1920–2010.

[See figure 1.6 for locations of all census subdivisions other than the Hāna subdivision, on eastern Haleakalā, outside the study area. Unless noted otherwise, populations for 2010, 2000, and 1990 were obtained from the U.S. Census Bureau (2012) and populations for 1980, 1970, and 1960 were obtained from the U.S. Bureau of the Census (1981). Populations for 1950, 1940, and 1930 were obtained from U.S. Bureau of the Census (1952), and the population for 1920 was obtained from U.S. Bureau of the Census (1921). N/A, population for census county subdivision was not found.]

Census county subdivision	2010	2000	1990	1980	1970	1960	1950	1940	1930	1920
Haʻikū-Paʻuwela	10,088	8,377	5,695	3,567	2,067	1,943	N/A	N/A	N/A	N/A
Hāna	2,291	1,855	1,895	1,423	969	1,073	N/A	N/A	N/A	N/A
Kahului	26,328	20,134	16,672	13,026	8,287	4,223	N/A	N/A	N/A	N/A
Kīhei	23,677	19,843	12,878	6,035	1,636	1,079	N/A	N/A	N/A	N/A
Kula	11,580	9,729	8,021	5,077	2,124	2,786	N/A	N/A	N/A	N/A
Lahaina	22,156	17,967	14,574	10,284	5,524	4,844	N/A	N/A	N/A	N/A
Makawao-Pāʻia	20,219	18,370	15,491	10,361	5,788	5,680	N/A	N/A	N/A	N/A
Puʻunēnē	8	12	217	572	1,132	3,054	N/A	N/A	N/A	N/A
Spreckelsville	461	337	213	220	781	1,838	N/A	N/A	N/A	N/A
Waiheʻe-Waikapū	6,907	3,397	2,273	1,584	1,299	2,228	N/A	N/A	N/A	N/A
Wailuku	20,729	17,623	13,432	10,674	9,084	6,969	N/A	N/A	N/A	N/A
Island of Maui	**[1]144,444**	**[1]117,644**	**[1]91,361**	**[1]62,823**	**[1]38,691**	**[1]35,717**	**40,103**	**46,919**	**48,756**	**36,080**

[1]Computed as the sum of the values for the eleven census county subdivisions shown in this table.

Kula, Makawao-Pāʻia, and Spreckelsville). Compared with septic rates for Maui's other subdivisions, these four census subdivisions had relatively high septic rates per capita, an attribute that was assumed to pertain to Puʻunēnē during 1926–99. For comparison, Whittier and El-Kadi (2013) used an average daily septic rate of 200 gal per bedroom for residential units in their septic analysis for Kauaʻi, Maui, Molokaʻi, and Hawaiʻi Island. In the water-budget calculations for each scenario between 1926 and 1999, Puʻunēnē's total septic-effluent rate (in gal/person/d) was applied as a uniform rate of septic-system leachate (in inches per day) to the area with developed land cover within the Puʻunēnē subdivision in the 1926–79 land-cover map (fig. 1.3).

Runoff

Direct runoff, hereinafter "runoff," is the fraction of rainfall that does not contribute to net moisture gain within the plant-root zone (fig. 1.1). Runoff of rainfall consists of overland flow and subsurface storm flow that rapidly returns infiltrated water to the stream (Oki, 2003). In the water-budget calculation, runoff was estimated as a fraction of rainfall using runoff-to-rainfall ratios. This approach was also used in previous water-budget studies of Hawaiʻi and other Pacific islands (for example, Izuka and others, 2005; Engott and Vana, 2007; Engott, 2011; Johnson, 2012; Engott and others, 2017; Izuka and others, 2018; Johnson and others, 2018; Mair and others, 2019; Oki and others, 2020) and provides reasonable estimates of regional average runoff using a level of complexity commensurate with the state of knowledge.

In the water budget, daily runoff was calculated by multiplying daily rainfall by a seasonal runoff-to-rainfall ratio, $rr_{t,j}$, where t represents the season (wet or dry) and j represents the year of interest. November through April was considered the wet season, and May through October was considered the dry season. Seasonal runoff-to-rainfall ratios were computed for and assigned to 488 catchment zones (fig. 1.7; minimum, median, and maximum) for each of the 88 wet and 87 dry seasons during 1926–2012. The 488 catchment zones were created by clipping the catchment zones shown in figure 6 of Johnson and others (2018) to the water-budget study area. The boundaries of the catchment zones were included in the subarea maps, so the $rr_{t,j}$ values assigned to a given catchment zone also were assigned to each subarea within the given catchment zone. For the purposes of computing and assigning $rr_{t,j}$ values, each catchment zone was classified as either gaged or ungaged and as either windward or leeward (fig. 1.7). Gaged catchment zones were those that were within one of the twelve gaged drainage basins identified as having sufficient rainfall and streamflow data for computing observed $rr_{t,j}$ values (fig. 1.7). All remaining catchment zones were considered ungaged.

The $rr_{t,j}$ values assigned to catchment zones were either observed or estimated. Observed $rr_{t,j}$ values were determined only for gaged drainage basins and only for seasons when complete six-month rainfall and streamflow data pairs were available (table 1.2). Each observed $rr_{t,j}$ value for a gaged

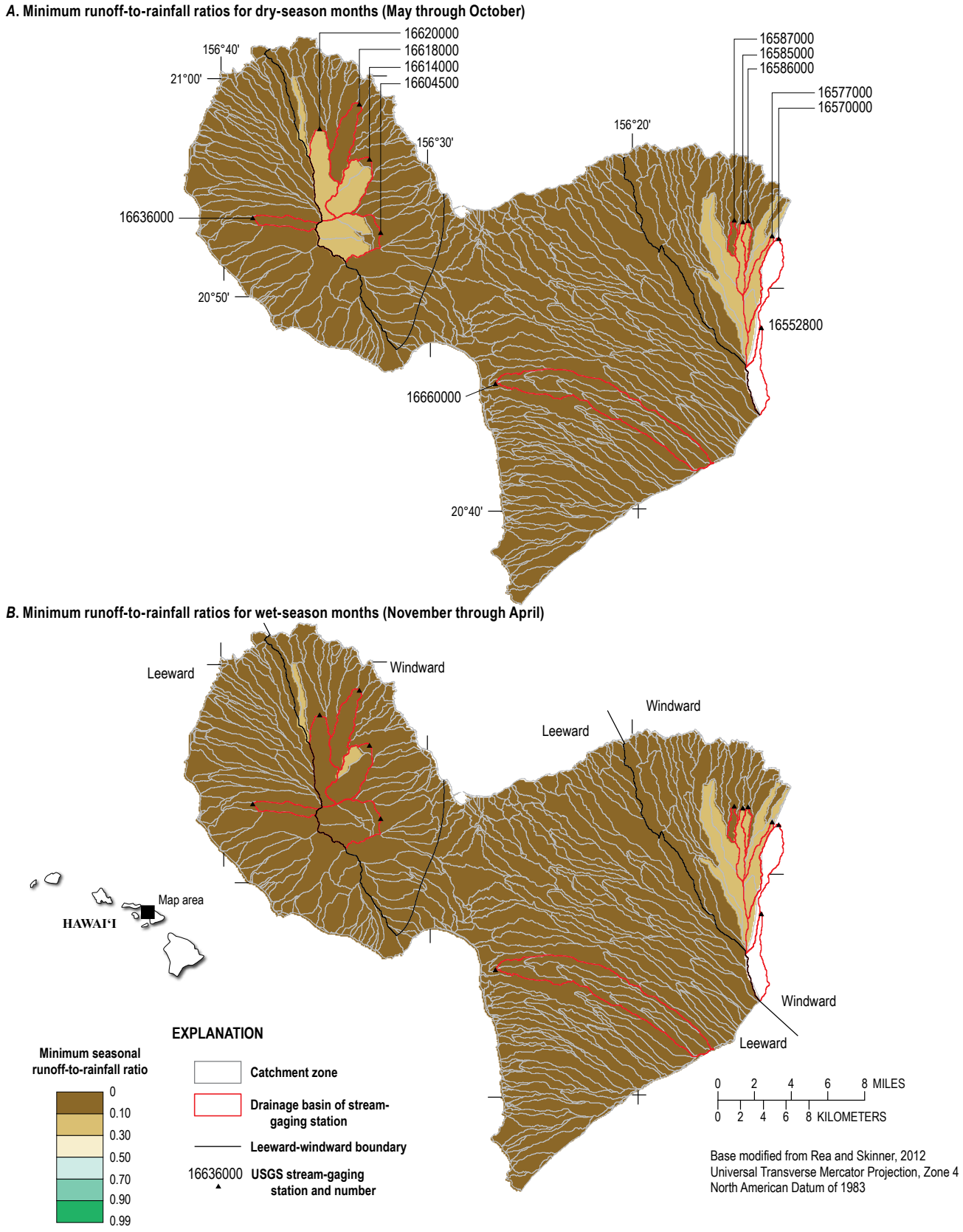

Figure 1.7. Maps of drainage basins of selected stream-gaging stations and summary statistics of runoff-to-rainfall ratios used in the water-budget calculations for the water-budget study area on Maui, Hawaiʻi for the (*A*) minimum runoff-to-rainfall ratios for dry-season months (May through October), (*B*) minimum runoff-to-rainfall ratios for wet-season months (November through April), (*C*) median runoff-to-rainfall ratios for dry-season months, (*D*) median runoff-to-rainfall ratios for wet-season months, (*E*) maximum runoff-to-rainfall ratios for dry-season months, and (F) maximum runoff-to-rainfall ratios for wet-season months during 1926–2012.

C. Median runoff-to-rainfall ratios for dry-season months (May through October)

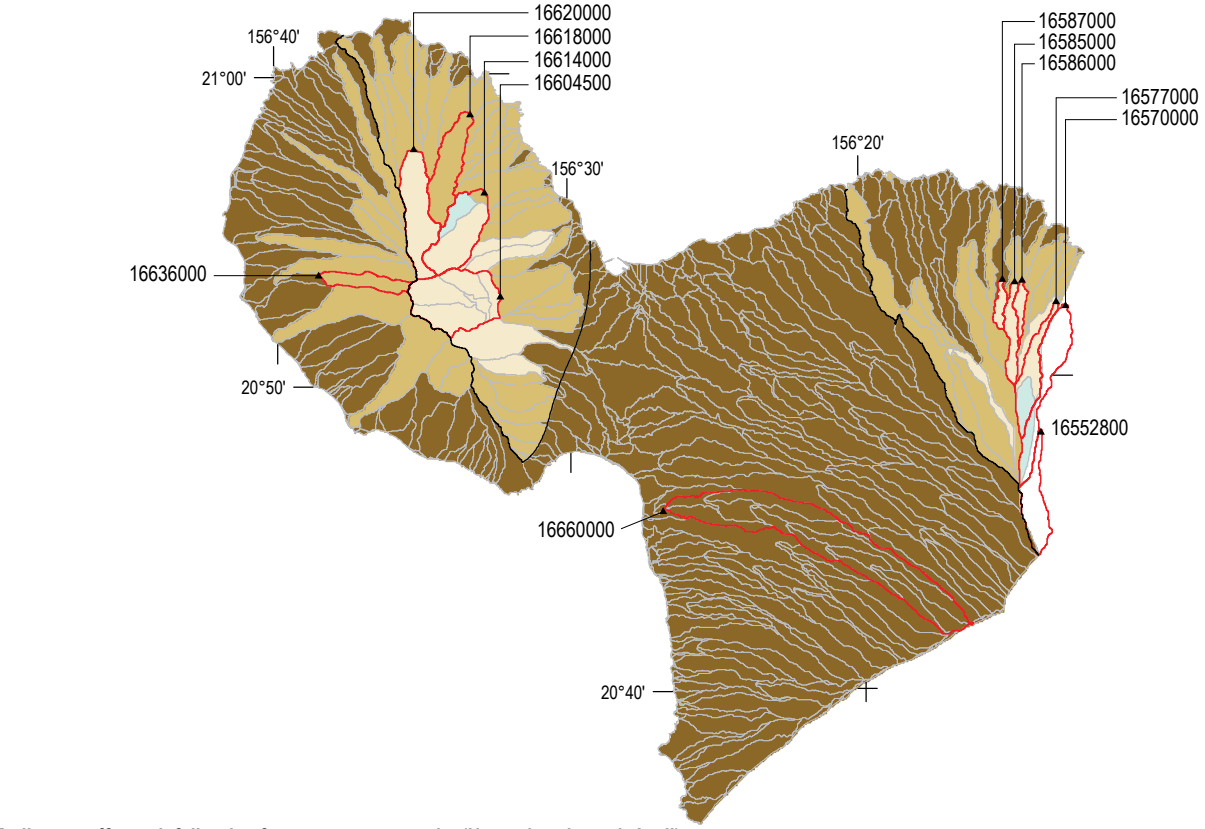

D. Median runoff-to-rainfall ratios for wet-season months (November through April)

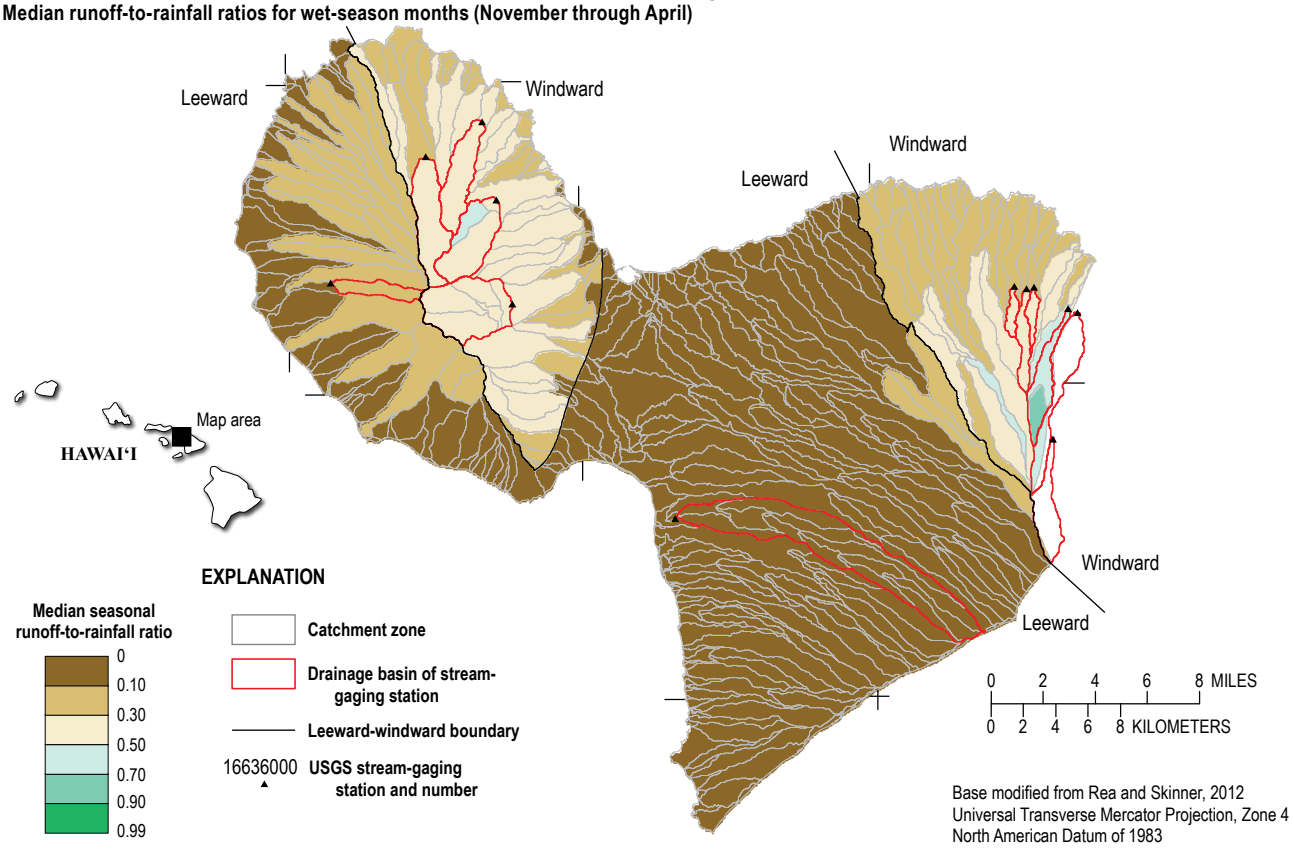

Figure 1.7. —Continued

E. **Maximum runoff-to-rainfall ratios for dry-season months (May through October)**

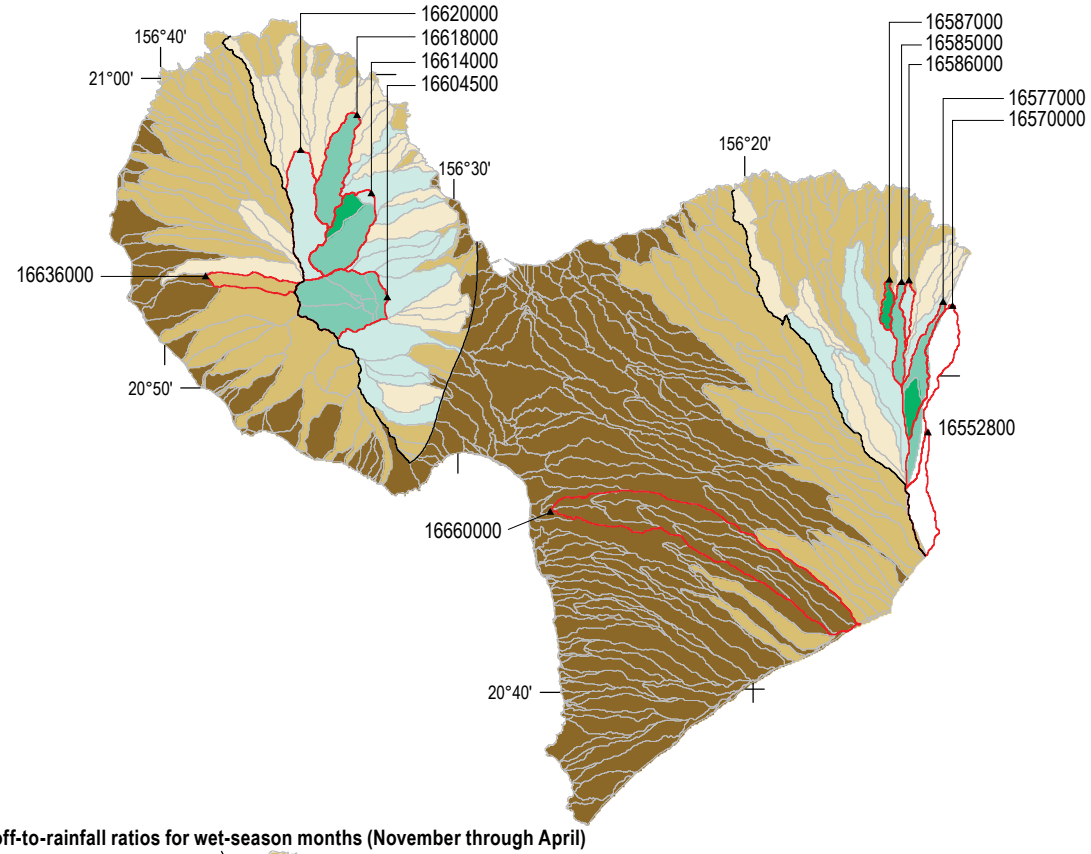

F. **Maximum runoff-to-rainfall ratios for wet-season months (November through April)**

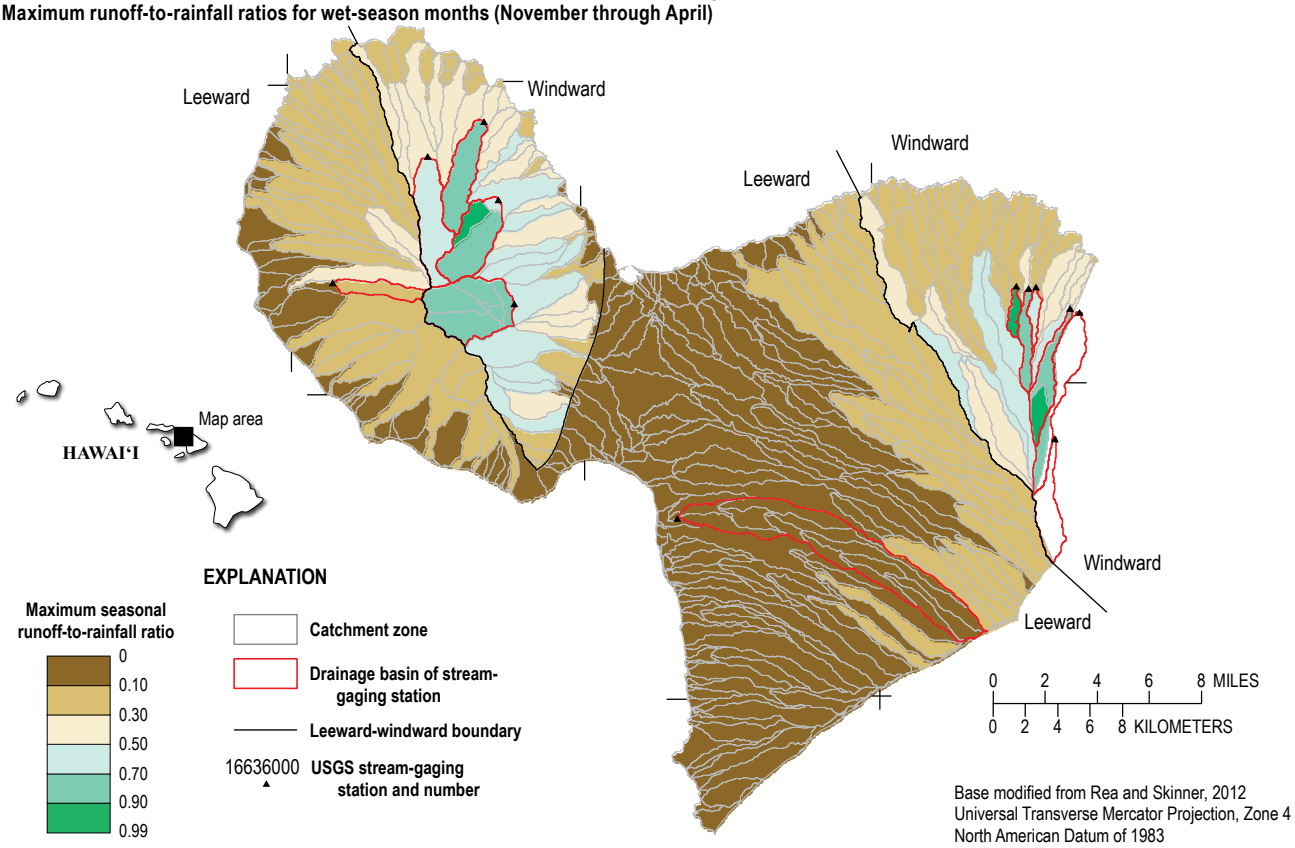

Figure 1.7. —Continued

drainage basin was computed as the quotient of cumulative runoff and cumulative rainfall within the drainage basin during the season. For example, observed $rr_{t,j}$ for the drainage basin of stream-gaging station 16552800 for the dry season of 1954 was computed as the quotient of cumulative runoff and cumulative rainfall in its drainage basin during May–October 1954. Cumulative runoff was computed using the record of daily streamflow values for the stream-gaging station and the methods and parameters to separate runoff from total streamflow as in Johnson and others (2018). Cumulative rainfall was estimated using 1926–2012 monthly rainfall maps (Frazier and others, 2016) and mean monthly rainfall-adjustment factors (see "Rainfall" section).

Of the twelve stream-gaging stations that had sufficient monthly data, seven had drainage basins composed of a single catchment zone and five had drainage basins composed of multiple catchment zones (fig. 1.7). Observed $rr_{t,j}$ values computed for each of the drainage basins of seven stream-gaging stations (16636000, 16570000, 16585000, 16586000, 16587000, 16618000, and 16620000) were assigned to the single-catchment zone within each of these drainage basins. Observed $rr_{t,j}$ values computed for each of the drainage basins of the remaining five stream-gaging stations (16552800, 16577000, 16604500, 16614000, and 16660000) were spatially disaggregated, using equation 17 in Johnson and others (2018), and then assigned to the multiple catchments within each gaged drainage basin.

Table 1-6 in Izuka and others, 2018 was used to compute estimated $rr_{t,j}$ values for all ungaged catchment zones. Equation 7 in Mair and others (2019) was used to adjust $rr_{t,j}$ values for the interannual variability in rainfall compared to the mean seasonal rainfall during 1978–2007. Figure 1.7 depicts the minimum, median, and maximum of the $rr_{t,j}$ values assigned to catchment zones for this study for 1926–2012.

Evapotranspiration

ET is the sum of all water that is evaporated or transpired from a vegetated surface and plant-root zone. ET can be divided into three main evaporative processes (1) canopy evaporation, which is evaporation of intercepted rain and fog from the surface of vegetation; (2) ground evaporation, which is evaporation of water from the soil surface and overlying litter and mulch layers; and (3) transpiration, the process by which soil moisture taken up by vegetation is eventually evaporated through plant pores (Viessman and Lewis, 2003). All three ET processes are represented in the total-ET estimates of the water budget. The methods and much of the input data used to compute canopy evaporation, potential ET, and actual ET for this study, briefly summarized next, are the same as that used in the water-budget calculations in Johnson and others (2018).

Forest-Canopy Evaporation

Canopy evaporation, the fraction of precipitation that accumulates on and then evaporates from vegetation, was computed for subareas with forest land covers (native forest, alien forest, and tree plantation) only. The water budget computed canopy evaporation according to equations 4 and 5 in Johnson and others (2018), which require values for daily rainfall and the following five parameters (1) canopy capacity, (2) trunk-storage capacity, (3) proportion of precipitation

Table 1.2. Periods of record used to compute observed seasonal runoff-to-rainfall ratios for drainage basins of selected stream-gaging stations in the water-budget study area on Maui, Hawai'i, 1926–2012.

[See figure 1.7 for locations of drainage basins of stream-gaging stations.]

Gaging-station number	Drainage system	Period of record used to compute observed seasonal runoff-to-rainfall ratios		Number of observed seasonal runoff-to-rainfall ratios	
		Start	End	Wet season (November through April)	Dry season (May through October)
16552800	Waikamoi Stream	1954	2012	18	17
16570000	Na'ili'ilihaele Stream	1926	1974	49	49
16577000	Kailua Stream	1926	1957	32	32
16585000	Ho'olawanui Stream	1926	1971	46	45
16586000	Ho'olawali'ili'i Stream	1926	1957	32	32
16587000	Honopou Stream	1926	2012	87	87
16604500	Wailuku River	1984	2012	29	29
16614000	Waihe'e River	1984	2012	28	29
16618000	Kahakuloa Stream	1940	2012	64	64
16620000	Honokōhau Stream	1926	2012	85	84
16636000	Kanahā Stream	1927	1932	6	5
16660000	Kūlanihāko'i Gulch	1963	1970	8	7

diverted to stemflow, (4) canopy cover, and (5) the ratio of the mean evaporation rate to mean precipitation rate during saturated conditions, *V*. Canopy capacity (0.05 in), trunk-storage capacity (0.01 in), and the proportion of precipitation diverted to stemflow (4 percent) were assumed to be the same for all forest land-cover classes for recharge scenarios. These values were derived by Johnson and others (2018) on the basis of published data for Hawaiʻi (Gaskill, 2004; DeLay, 2005; Takahashi and others, 2011; Safeeq and Fares, 2014).

Canopy-cover values were assigned to subareas with a forest land-cover class only and canopy-cover values were varied spatially across the water-budget study area. Canopy-cover values assigned to subareas for 2005–09, 2010–12, and for the hypothetical scenario were derived from a map of mean annual vegetation cover for Maui (Giambelluca and others, 2014). The assigned canopy-cover values for subareas ranged from 0.03 (meaning 3-percent canopy cover) to 1.00 (meaning a dense canopy with no gaps). The canopy-cover values assigned in the 2005–09 scenario were also used in each pre-2005 map for subareas that were forested in the pre-2005 scenario and the 2005–09 scenario. For subareas that were forested in a pre-2005 scenario but not in the 2005–09 scenario, the canopy-cover value of the nearest subarea with a forest land-cover class in 2005–09 scenario was used in the pre-2005 scenario. The spatial distribution of *V* (the ratio of the mean evaporation rate to mean precipitation rate during saturated conditions) estimated by Johnson and others (2018) was used for each water-budget scenario within this study. Values of *V* ranged from 0.01 to 0.50, with wetter areas typically having lower *V* values than drier areas.

Potential Evapotranspiration

Estimates of potential ET (the maximum rate of ET from the plant-root zone) were needed to compute the actual rate of ET in the water budget. The water budget computed potential ET for each subarea as the product of its crop coefficient and reference ET. Reference ET, as defined in this study, is the potential ET rate of a hypothetical grass surface with optimum soil-water conditions for given climatic conditions and is equivalent to the Food and Agriculture Organization of the United Nations' Penman-Monteith ET (Allen and others, 1998).

Crop coefficients were assigned to each subarea on the basis of land cover (table 1.3) and were the same as those used in recent Hawaiʻi water budgets (Engott and others, 2017; Izuka and others, 2018; Johnson and others, 2018). Crop coefficients were assumed to be temporally constant for all land covers other than sugarcane (fig. 1.5) and corn. The crop coefficients assigned to seed corn were 0.85, 0.50, 0.29, 0.40, 0.80, 1.20, 0.85, 0.50, 0.29, 0.40, 0.80, and 1.20 for the months of January through December, respectively, and represent a cultivation cycle of two crops per year. For non-forest land-cover classes, crop coefficients integrated the effects of transpiration, ground evaporation, and canopy evaporation. For forest land-cover classes, crop coefficients integrated the effects of transpiration and ground evaporation only because canopy evaporation was accounted for separately (fig. 1.1).

Maps of mean monthly reference ET for Maui (Giambelluca and others, 2014) were used in the water-budget calculations for all scenarios. These maps use the same grid as the monthly rainfall maps. In the water-budget calculation, monthly reference ET was not varied from year to year, and it was assumed to equal mean monthly reference ET. Reference ET was assumed to be the same each day of a given month.

Actual Evapotranspiration

Actual ET results computed by the water budget can represent different ET processes, depending on land cover. For subareas with non-forest land covers, actual ET represents the sum of transpiration, ground evaporation, and canopy evaporation. For subareas with forest land covers, actual ET represents the sum of transpiration and ground evaporation only because canopy evaporation was computed separately (fig 1.1). The method used in the model to compute actual ET, however, was the same for all subareas.

Actual ET for each subarea was computed by the model on the basis of potential ET, moisture storage in the plant-root zone, and threshold-moisture storage, as in Johnson and others (2018). When moisture storage was greater than or equal to the threshold-moisture storage, the actual-ET rate was assumed to equal the potential-ET rate. When moisture storage was less than the threshold-moisture storage, the actual-ET rate was less than the potential-ET rate and declined linearly with soil-moisture content. Threshold-moisture storage was computed on the basis of a depletion fraction and moisture-storage capacity of the plant-root zone (see equation 11 in Johnson and others [2018]). Values for depletion fraction were assigned to each land-cover class (table 1.3), using the same values as Johnson and others (2018).

Moisture-Storage Capacity of the Plant-Root Zone

The moisture-storage capacity of the plant-root zone was calculated as the product of root depth and available water capacity. Root depths were assigned on the basis of land-cover class (table 1.3) and were the same as those used in recent water budgets for Hawaiʻi (Engott and others, 2017; Izuka and others, 2018; Johnson and others, 2018). The available water capacity of soil for each subarea was estimated using the same data and methods as Johnson and others (2018).

Direct Recharge

Direct recharge in the water budget represents water seepage that was not subject to runoff or ET processes because it passed directly to the groundwater system, bypassing the plant-root zone. Direct recharge in this study includes cesspool seepage (fig. 1.6). Direct recharge also was estimated for subareas with land-cover types of water body or reservoir (fig. 1.3). Direct recharge rates assigned to water body (0 in/yr), reservoirs within the Pāʻia, Kahului, Waikapū, and ʻĪao aquifer systems (1,268 in/yr), and all remaining reservoirs in the water-budget study area (528 in/yr) were the same as the rates used in the water-budget scenarios of Johnson and others (2018).

Table 1.3. Selected land-cover parameters used in the water-budget calculations for the water-budget study area on Maui, Hawai'i (modified from Engott and others, 2017; Izuka and others, 2018; Johnson and others, 2018).

[Crop coefficients for forests were used to compute the sum of transpiration and ground evaporation; canopy evaporation was computed separately. Crop coefficients for non-forests were used to compute the sum of all evaporative components; N/A, not applicable.]

Land-cover description	Root depth, in inches	Depletion fraction	Crop coefficient	Canopy capacity, in inches	Trunk-storage capacity, in inches
Forest land covers					
Alien forest	60	0.50	[1]0.33, [2]0.44	0.05	0.01
Native forest	30	0.50	0.30	0.05	0.01
Tree plantation	60	0.50	[1]0.33, [2]0.44	0.05	0.01
Non-forest land covers					
Agriculture					
Coffee	48	0.40	0.91	N/A	N/A
Corn	18	0.60	[3]0.29–1.20	N/A	N/A
Diversified	10	0.35	1.00	N/A	N/A
Macadamia	60	0.50	0.91	N/A	N/A
Pineapple	18	0.50	0.30	N/A	N/A
Sugarcane	24	0.65	[4]0.31–1.25	N/A	N/A
Taro	10	1.05	0.95	N/A	N/A
Developed					
Open space	12	0.50	1.18	N/A	N/A
Low-intensity	12	0.50	1.18	N/A	N/A
Medium-intensity	12	0.50	1.18	N/A	N/A
High-intensity	12	0.50	1.18	N/A	N/A
Golf course	30	0.50	0.85	N/A	N/A
Grassland	39	0.60	0.95	N/A	N/A
Shrubland	12	0.50	1.00	N/A	N/A
Sparsely vegetated	5	0.50	1.18	N/A	N/A
Water body and Reservoir	1	1.00	1.05	N/A	N/A
Wetland	39	0.50	1.18	N/A	N/A

[1]Value used for forests inside the cloud zone, which is between altitudes of 2,000 and 8,200 feet.

[2]Value used for forests outside the cloud zone.

[3]Varies by month (see Potential Evapotranspiration section for explanation).

[4]Sugarcane crop coefficients varied with time, as shown in figure 1.5.

Other Input

In addition to the previously mentioned water-budget inputs to the model, several other parameter inputs were required. The initial moisture storage of the pervious fraction of subareas was set at 50 percent of the soil moisture-storage capacity. The initial moisture storage of the impervious fraction of subareas was set at 0.125 in., equivalent to 50 percent of the rainfall-retention capacity (0.25 in.) of impervious surfaces. These values were used in recent Hawaiʻi water budgets (Engott and others, 2017; Izuka and others, 2018; Johnson and others, 2018).

Water-Budget and Groundwater-Recharge Estimates

Recharge and other water-budget components for the water-budget study area on Maui were estimated for nine historical time periods (1926–69, 1970–79, 1980–84, 1985–89, 1990–94, 1995–99, 2000–2004, 2005–09, and 2010–12) using monthly rainfall and generally representative land-cover conditions for each time period (table 1.4). Recharge and water-budget components also were calculated for a hypothetical scenario that used 1980–2010 rainfall and 2017 land cover.

1926–2012 Conditions

For the water-budget study area, mean annual recharge was highest during 1926–69 and lowest during 2010–12 (table 1.4). Differences in recharge among the historical time periods reflect a shift in the method used to irrigate sugarcane, reductions in irrigation associated with the widespread cessation of sugarcane cultivation, and temporal variations in rainfall. For the water-budget study area, mean annual recharge estimates for all periods after 1979 were less than those for the periods between 1926 and 1979. The shift to lower recharge after 1979 coincides with substantial reductions in irrigation. Mean annual irrigation estimates for periods between 1980 and 2012 were between 30 and 44 percent less than mean annual irrigation estimates for periods between 1926 and 1979 (table 1.4). The decrease in irrigation after 1979 was influenced by the assumed universal shift in the method used to irrigate sugarcane in the study area: the less efficient furrow-irrigation method was used for all sugarcane between 1926 and 1979, whereas the more efficient drip-irrigation method was used for all sugarcane after 1979. Irrigation decreased considerably after 1999 when sugarcane cultivation on leeward west Maui ended (fig. 1.3). The water budget estimated that about 1.9 trillion gallons of water was used to irrigate sugarcane on leeward west Maui between 1926 and 1999, and about 10.7 trillion gallons of water was used to irrigate sugarcane in the remaining part of the water-budget study area on windward west Maui and central Maui between 1926 and 2012. Mean annual rainfall decreased progressively for each historical period after 1985–89, the period with the most rainfall.

For the water-budget study area, mean annual runoff ranged from about 18–25 percent of rainfall. Runoff was highest for periods with relatively high rainfall and was lowest for periods with relatively low rainfall. Septic-system leachate, direct recharge, and storm-drain capture for the water-budget study area were minor relative to rainfall but may have been important components locally. Total ET ranged from 41 to 61 percent of total water inflow, which equals the sum of rainfall, fog, irrigation, and septic leachate. Total ET as a percentage of total water inflow generally was highest for scenarios with relatively low total water inflow and was lowest for scenarios with relatively high total water inflow.

The spatial pattern of mean annual recharge for the water-budget study area for each historical period (fig. 1.8) reflects irrigation and the steep rainfall gradients. The inland parts of west Maui and northern Haleakalā typically had the most rainfall and substantial recharge. Recharge in these areas also was enhanced with fog captured by trees and shrubs and by relatively low potential ET. Most parts of the water-budget study area at lower altitudes had relatively less recharge except in areas that were irrigated. In particular, recharge was high in areas with sugarcane, especially during 1926–1979, when the furrow-irrigation method was used. Seepage from reservoirs, most of which were near sugarcane fields in central Maui during historical periods, also is evident in the recharge maps.

For the seven aquifer systems that contained substantial sugarcane during 1926–1979 (Waikapu, ʻĪao, Honokōwai, Launiupoko, Olowalu, Kahului, and Pāʻia), mean annual recharge was greatest in 1926–69 or 1970–79 (table 1.5), when sugarcane was irrigated with the furrow method. For the remaining aquifer systems in the study area, mean annual recharge was greatest in 1980–84 or 1985–89. Mean annual recharge for the Kahului and Pāʻia aquifers systems was lowest in 2000–04; for the remaining aquifer systems, mean annual recharge was lowest in 2010–12. Mean annual recharge in the ʻĪao aquifer system progressively decreased for each scenario between 1985–89 and 2010–12.

Hypothetical Scenario: 1980–2010 Rainfall and 2017 Land-Cover Conditions

Recharge and water-budget components also were computed for a hypothetical scenario that used 1980–2010 rainfall and 2017 land-cover conditions. In this scenario, all sugarcane as of 2015 was replaced by non-irrigated grassland. Water-budget components estimated for the hypothetical scenario (table 1.4) were compared with averages for 1980–2012 (not shown) that were computed as time-weighted averages of the water-budget components for the seven historical periods between 1980 and 2012. For the water-budget study area, rainfall, fog interception, runoff, and canopy evaporation for the hypothetical scenario were roughly the same as the corresponding averages for 1980–2012. Irrigation, direct recharge, total ET, and recharge for the hypothetical scenario were respectively 90, 60, 27, and 17 percent less than the corresponding averages for 1980–2012. Recharge

Table 1.4. Mean annual water-budget components for the water-budget study area on Maui, Hawai‘i, for nine historical periods between 1926 and 2012 and a hypothetical scenario (1980–2010 rainfall and 2017 land cover).

[Total ET, total evapotranspiration, which includes canopy evaporation. Components may not balance because of rounding and direct recharge.]

Period or scenario	Land-cover period	Rainfall period	Method used to irrigate sugarcane	Water-budget estimate (million gallons per day)									
				Rainfall	Fog	Irrigation	Septic-system leachate	Direct recharge	Runoff	Forest canopy evaporation	Total ET	Storm-drain capture	Recharge
1926–69	1926–79	1926–69	Furrow	1,159.52	75.81	472.09	1.46	50.78	261.22	114.50	702.59	2.04	799.66
1970–79	1926–79	1970–79	Furrow	998.00	62.05	489.14	1.01	50.63	214.85	103.36	661.26	1.80	728.76
1980–84	1980–84	1980–84	Drip	1,193.72	76.66	332.15	1.61	52.04	268.80	116.39	802.92	2.14	588.85
1985–89	1985–89	1985–89	Drip	1,365.73	87.40	305.75	1.61	49.31	334.63	130.30	823.11	3.94	651.67
1990–94	1990–94	1990–94	Drip	1,154.09	76.53	323.39	2.34	50.99	274.42	117.20	783.81	2.74	553.21
1995–99	1995–99	1995–99	Drip	1,020.02	64.69	321.17	2.34	50.99	214.65	107.21	752.41	3.18	494.12
2000–04	2000–04	2000–04	Drip	991.99	65.34	275.87	3.03	52.27	213.47	111.13	721.85	2.97	456.70
2005–09	2005–12	2005–09	Drip	971.38	62.00	297.72	3.03	52.28	199.23	97.49	728.68	2.24	462.10
2010–12	2005–12	2010–12	Drip	750.07	48.48	307.34	3.59	53.50	137.60	86.47	675.97	1.28	357.77
Hypothetical	2017	1980–2010	None; no sugarcane	1,104.60	69.68	32.04	3.59	20.67	247.30	108.21	555.15	3.26	429.33

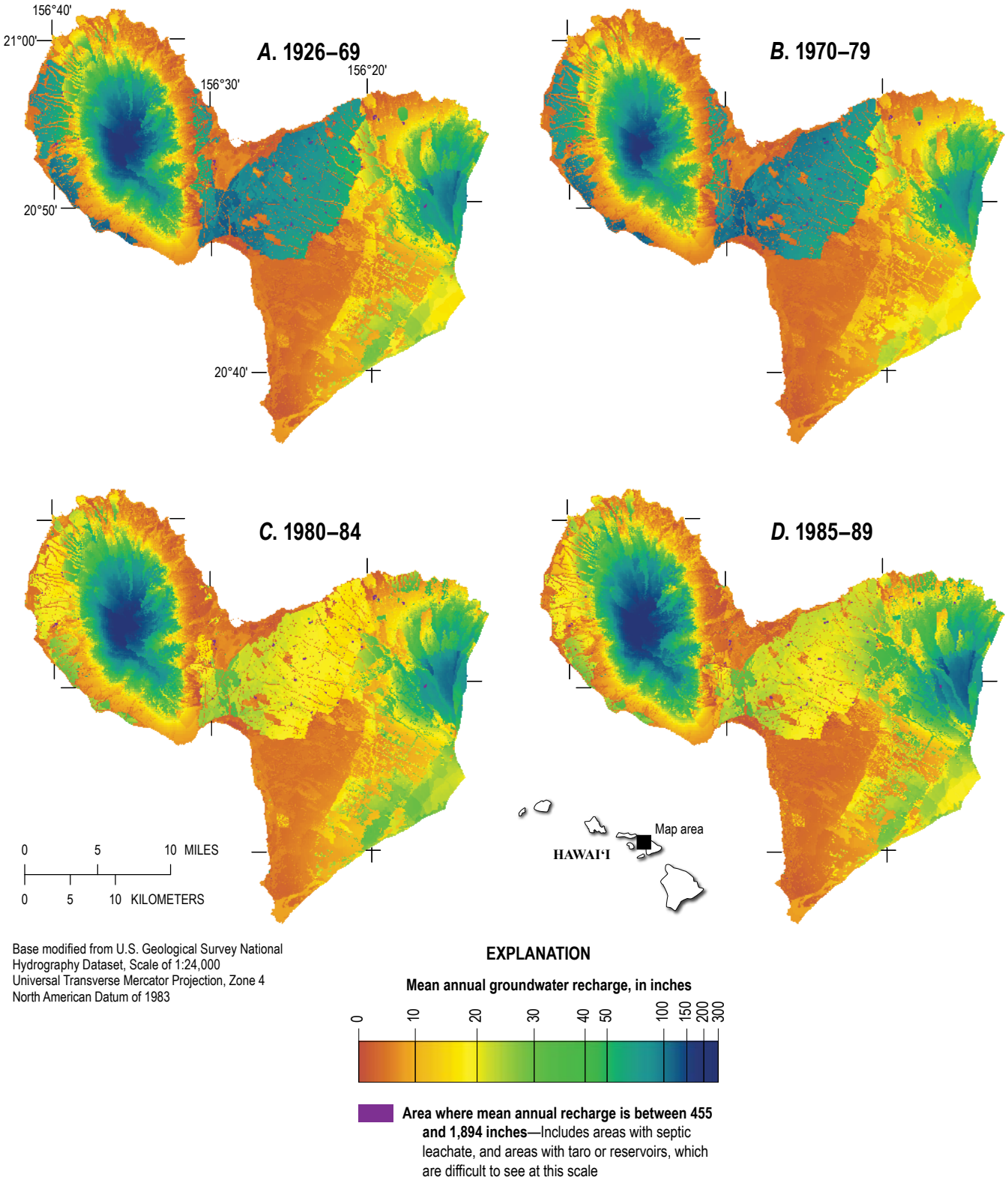

Figure 1.8. Maps of the water-budget study area on Maui, Hawaiʻi, showing the distribution of mean annual recharge for (*A*) 1926–69, (*B*) 1970–79 (*C*) 1980–84, (*D*) 1985–89, (*E*) 1990–94, (*F*) 1995–99, (*G*) 2000–04, (*H*) 2005–09, (*I*) 2010–12, and (*J*) a hypothetical scenario (1980–2010 rainfall and 2017 land cover).

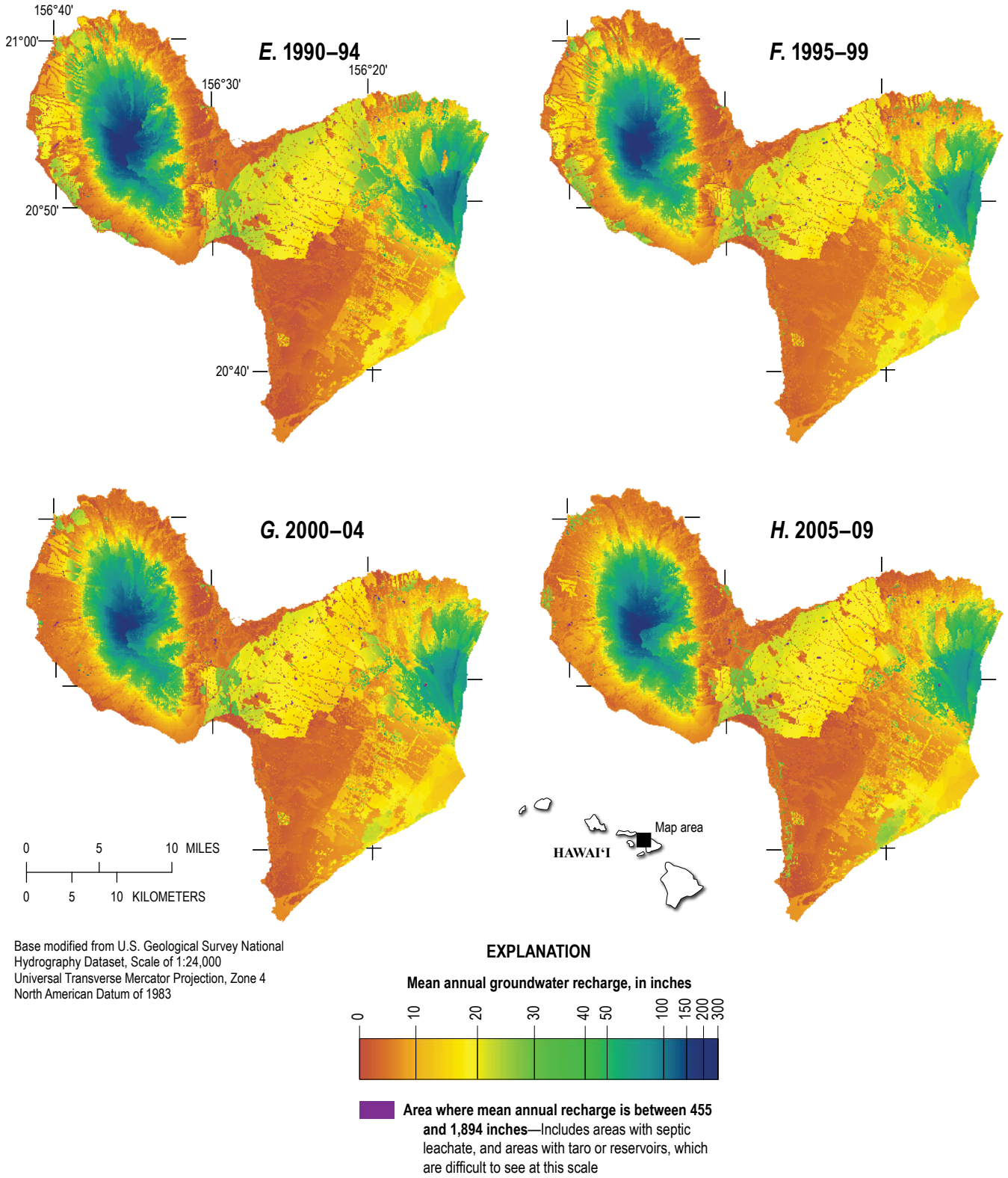

Figure 1.8. —Continued

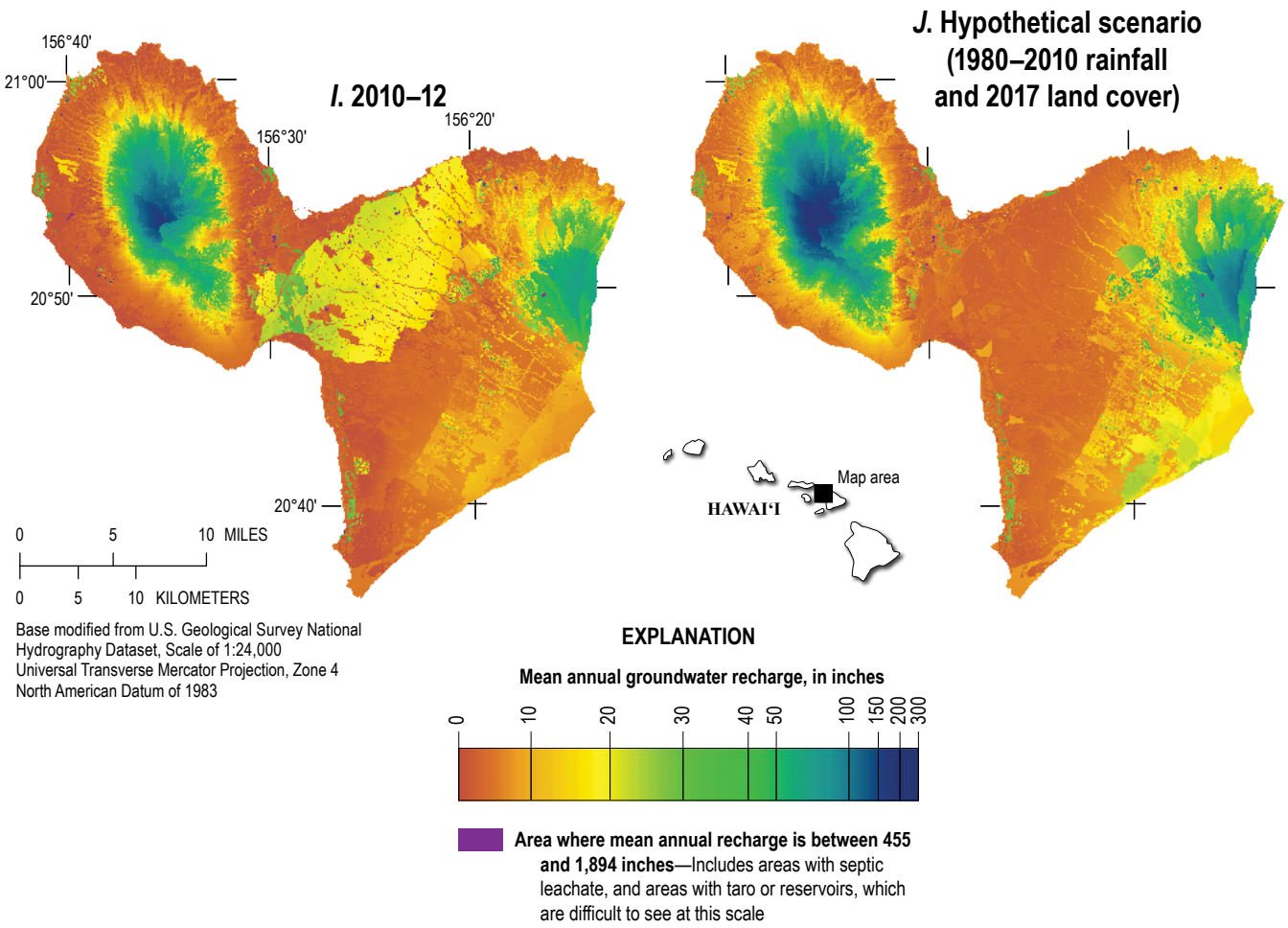

Figure 1.8. —Continued

for the hypothetical scenario was lower than the average for 1980–2012 mainly because the hypothetical scenario (1) had no sugarcane or associated irrigation water and (2) had no direct recharge (water seepage) from dozens of reservoirs that were assumed to be dry, owing to the absence of sugarcane cultivation.

Exclusions and Limitations

Several exclusions were made to simplify the water budget. Re-infiltration of runoff (water that runs off one subarea and then infiltrates the plant-root zone of a different subarea) was not explicitly considered in the water budget. Re-infiltration of runoff within gaged basins was assumed to be included in streamflow records that were used to derive runoff-to-rainfall ratios. Spatial variations in the re-infiltration of runoff within a drainage basin, however, were not accounted for in this study. For example, if re-infiltration of runoff was considerable within streambeds, then recharge may have been underestimated in intra-channel (streambed) areas. Additionally, runoff from upland areas that seeps into the streambed of lower reaches near the coast was not quantified.

Because of the lack of complete daily information and the use of synthesized daily rainfall, the water budget did not reconstruct the actual distributions of the water-budget components (rainfall, fog interception, irrigation, septic-system leachate, runoff, ET, and recharge) within the water-budget study area on Maui for each simulated day. The reconstruction of actual daily runoff was also precluded by the use of seasonal runoff-to-rainfall ratios. Additionally, runoff may have been overestimated by the water budget on days with light rain and underestimated on days with intense rain.

Some parameters and conditions not included in the calculations of the water budget were inherent in other parameters used in the water budget. For example, the permeability and vertical hydraulic conductivity of the plant-root zone and underlying substrate were not included in the water-budget calculations. Their effect on runoff, however, would be inherent in streamflow records used to derive runoff-to-rainfall ratios that the water budget used to calculate

Table 1.5. Mean annual recharge estimates for 16 aquifers systems in the water-budget study area on Maui, Hawai'i, for nine historical periods between 1926 and 2012 and for a hypothetical scenario (1980–2010 rainfall and 2017 land cover).

[See figure 1.2 for locations of aquifer systems; N/A, not applicable]

Aquifer system	Aquifer code	Mean annual recharge estimate (million gallons per day)									
		1926–69	1970–79	1980–84	1985–89	1990–94	1995–99	2000–04	2005–09	2010–12	Hypothetical scenario (1980–2010 rainfall and 2017 land cover)
Waikapū	60101	28.46	24.71	21.12	24.73	18.27	16.63	17.71	18.07	13.81	16.63
ʻĪao	60102	52.33	48.01	43.27	51.87	39.52	37.58	33.90	31.38	25.02	39.45
Waiheʻe	60103	23.17	19.79	22.41	24.94	21.46	20.29	20.64	22.10	15.52	22.21
Kahakuloa	60104	16.74	12.83	16.15	18.08	16.74	13.18	11.07	13.04	9.62	14.65
Honokōhau	60201	35.73	28.59	35.71	39.27	37.82	31.40	26.77	26.76	21.87	32.13
Honolua	60202	31.63	25.74	32.16	35.83	32.81	25.37	23.26	21.43	17.93	25.48
Honokōwai	60203	64.40	58.21	44.37	46.67	42.10	37.62	30.37	31.32	25.52	34.83
Launiupoko	60204	60.72	52.69	48.33	50.14	43.20	41.49	32.82	39.81	22.97	39.82
Olowalu	60205	18.23	15.31	15.00	17.62	12.89	12.31	10.39	12.63	6.00	12.59
Ukumehame	60206	18.19	14.03	15.52	19.42	12.16	11.62	11.86	13.49	6.47	13.24
Kahului	60301	78.32	79.93	24.94	24.63	23.68	23.84	23.00	23.88	23.26	2.37
Pāʻia	60302	192.31	199.51	71.52	77.70	73.15	71.41	66.87	69.52	69.95	6.55
Makawao	60303	41.19	33.97	49.75	60.47	43.00	39.16	36.03	30.64	19.08	40.97
Kamaʻole	60304	35.52	29.09	42.35	35.30	21.24	27.29	27.49	28.01	17.95	31.41
Haʻikū	60401	59.94	50.66	64.31	77.92	70.23	51.80	50.59	46.39	37.67	58.19
Honopou	60402	42.78	35.69	41.94	47.08	44.94	33.13	33.93	33.63	25.13	38.81
Study area total	**N/A**	**799.66**	**728.76**	**588.85**	**651.67**	**553.21**	**494.12**	**456.70**	**462.10**	**357.77**	**429.33**

runoff. For subareas with forest land covers, a reduction in the potential ET of the plant-root zone in response to evaporation from the forest canopy was not included in the water-budget calculations. However, the effects of forest-canopy evaporation on the potential-ET rate likely were accounted for in the forest crop coefficients, which were calibrated to the estimates of mean transpiration and ground evaporation produced by Giambelluca and others (2014).

Some processes and conditions were excluded from the water-budget calculations. The land-cover maps developed for this study account for identifiable changes in agricultural and developed areas but generally do not account for other types of land-cover changes, such as changes to the spatial extents of alien and native forests. This study did not account for interannual variations in monthly reference ET or spatial variations in reference ET at resolutions finer than the spatial resolution of the reference-ET maps. Potential ET was assumed to be uniform each day of the month and consequently may have been overestimated on cloudy days and underestimated on clear days. For subareas with impervious surfaces, potential ET was not reduced to account for evaporation from impervious surfaces.

Other conditions not considered in the water budget include the variability of soil moisture as a function of depth within the soil root zone, the effect of soil texture on irrigation demand, and removal of water from saturated groundwater zones by transpiration. Additionally, daily irrigation estimates were based on monthly variations in rainfall, runoff, and potential ET instead of daily variations. The daily irrigation estimates of the water budget may also differ from actual irrigation rates because, in addition to the water budget not reproducing actual daily rainfall, the water budget does not account for other factors—field observations, non-irrigation water needs, and water availability—that may be considered by irrigation managers each day. Fog interception in a given area was limited to days with rain owing to the use of fog-to-rainfall ratios in the water budget. Spatial variations in the fog-catch efficiencies assigned to forests and shrubland were not accounted for. Direct recharge from injection wells and leakage from water-transmission systems were excluded from the analysis. The water budget did not allocate storm-drain capture to runoff, ET, or recharge.

Owing to a dearth of available information, this study did not account for temporal changes in sewage-related infrastructure, including temporal changes related to sewage-treatment plants, sewage-transmission systems, and on-site sewage-disposal systems. Also, this study's septic-effluent estimates did not account for temporal changes in (1) the percentage of people using sewage-treatment plants, (2) the percentage of people using on-site sewage-disposal systems, (3) septic effluent generated by non-residents, or (4) daily septic effluent. Because septic effluent was a relatively minor water-budget component for the water-budget study area (table 1.4), the effect of these limitations likely was minor for regional-scale recharge estimates but could be important locally.

References Cited

Allen, R.G., Pereira, L.S., Raes, D., Smith, M., 1998, Crop evapotranspiration—Guidelines for computing crop water requirements: Food and Agriculture Organization of the United Nations, FAO Irrigation and Drainage Paper 56, 300 p., accessed June 9, 2011, at http://www.fao.org/docrep/X0490E/X0490E00.htm.

DeLay, J.K., 2005, Canopy water balance on an elfin cloud forest at Alakahi, Hawaiʻi: Honolulu, University of Hawaiʻi, M.S. thesis, 78 p., accessed May 22, 2020, at http://hdl.handle.net/10125/11633.

DeLay J.K., and Giambelluca, T.W., 2010, History of fog and cloud water interception research in Hawaiʻi, in Bruijnzeel, L.A., Scatena, F.N., and Hamilton, L.S., eds., Tropical montane cloud forests —Science for conservation and management: New York, Cambridge University Press, p. 332–341.

Dorrance, W.H., and Morgan, F.S., 2000, Sugar islands—The 165-year story of sugar in Hawaiʻi: Mutual Publishing, Honolulu, Hawaiʻi, 282 p.

Engott, J.A., 2011, A water-budget model and assessment of groundwater recharge for the Island of Hawaiʻi: U.S. Geological Survey Scientific Investigations Report 2011–5078, 53 p., accessed September 13, 2011, at https://pubs.usgs.gov/sir/2011/5078/.

Engott, J.A., and Vana, T.T., 2007, Effects of agricultural land-use changes and rainfall on ground-water recharge in central and west Maui, Hawaiʻi, 1926–2004: U.S. Geological Survey Scientific Investigations Report 2007–5103, 56 p, accessed April 24, 2020, at https://pubs.usgs.gov/sir/2007/5103/.

Engott, J.A., Johnson, A.G., Bassiouni, M., Izuka, S.K., and Rotzoll, K., 2017, Spatially distributed groundwater recharge for 2010 land cover estimated using a water-budget model for the island of Oʻahu, Hawaiʻi (ver. 2.0, December 2017): U.S. Geological Survey Scientific Investigations Report 2015–5010, 49 p., accessed April 24, 2020, at https://doi.org/10.3133/sir20155010.

Frazier, A.G., Giambelluca, T.W., Diaz, H.F., and Needham, H.L., 2016, Comparison of geostatistical approaches to spatially interpolate month-year rainfall for the Hawaiian Islands: International Journal of Climatology, v. 36, no. 3, p. 1459–1470, accessed May 22, 2020, at https://doi.org/10.1002/joc.4437.

Fukunaga, L.K., 1978, Some agroclimatic, economic, ecological, and site considerations that condition the practice of drip irrigation in Hawaii's sugar industry: Honolulu, University of Hawaiʻi, M.S. thesis, 181 p.

Gaskill, T.G.R., 2004, Hydrology of forest ecosystems in the Honouliuli Preserve—Implications for groundwater recharge and watershed restoration: Honolulu, University of Hawai‘i, Ph.D. dissertation, 177 p., accessed May 22, 2020, at http://hdl.handle.net/10125/12116.

Giambelluca, T.W., DeLay, J.K., Nullet, M.A., Scholl, M.A., and Gingerich, S.B., 2011, Canopy water balance of windward and leeward Hawaiian cloud forests on Haleakalā, Maui, Hawai‘i: Hydrological Processes, v. 25, p. 438–447, accessed June 1, 2020, at https://doi.org/10.1002/hyp.7738. [Special issue on the Hydrometeorology of tropical montane cloud forests.]

Giambelluca, T.W., Chen, Q., Frazier, A.G., Price, J.P., Chen, Y.-L., Chu, P.-S., Eischeid, J.K., and Delparte, D.M., 2013, Online rainfall atlas of Hawai‘i: Bulletin of the American Meteorological Society, v. 94, no. 3, p. 313–316, accessed December 30, 2016, at https://doi.org/10.1175/BAMS-D-11-00228.1.

Giambelluca, T.W., Shuai, X., Barnes, M.L., Alliss, R.J., Longman, R.J., Miura, T., Chen, Q., Frazier, A.G., Mudd, R.G., Cuo, L., and Businger, A.D., 2014, Evapotranspiration of Hawai‘i—Final report: Honolulu, University of Hawai‘i at Mānoa, Department of Geography, Submitted to the U.S. Army Corps of Engineers–Honolulu District and Commission on Water Resource Management, 178 p.

Gingerich, S.B, and Engott, J.A., 2012, Groundwater availability in the Lahaina District, West Maui, Hawai‘i: U.S. Geological Survey Scientific Investigations Report 2012–5010, 90 p., accessed April 24, 2020, at https://pubs.usgs.gov/sir/2012/5010/.

Izuka, S.K., Oki, D.S., and Chen, C.-H., 2005, Effects of irrigation and rainfall reduction on ground-water recharge in the Lihue Basin, Kauai, Hawaii: U.S. Geological Survey Scientific Investigations Report 2005-5146, 48 p, accessed June 11, 2020, at https://pubs.usgs.gov/sir/2005/5146/.

Izuka, S.K., Engott, J.A., Rotzoll, K., Bassiouni, M., Johnson, A.G., Miller, L.D., and Mair, A., 2018, Volcanic aquifers of Hawai‘i—Hydrogeology, water budgets, and conceptual models (ver. 2.0, March 2018): U.S. Geological Survey Scientific Investigations Report 2015–5164, 158 p., accessed April 24, 2020, at https://doi.org/10.3133/sir20155164.

Johnson, A.G., 2012, A water-budget model and estimates of groundwater recharge for Guam: U.S. Geological Survey Scientific Investigations Report 2012–5028, 53 p., accessed July 24, 2020 at http://pubs.usgs.gov/sir/2012/5028/.

Johnson, A.G., 2014, Land use for the island of Maui, Hawaii, circa 2010: U.S. Geological Survey digital data, accessed May 22, 2020, at http://water.usgs.gov/lookup/getspatial?maui_land_use_circa_2010.

Johnson, A.G., Engott, J.A., and Bassiouni, M., 2018, Spatially distributed groundwater recharge estimated using a water-budget model for the Island of Maui, Hawai‘i, 1978–2007 (ver 2.0, February 2018): U.S. Geological Survey Scientific Investigations Report 2014–5168, 53 p., accessed April 24, 2020, at https://doi.org/10.3133/sir20145168.

Mair, A., 2018, Land-cover map for the Island of Maui, Hawaii, 2017 (ver. 1.2, November 2018): U.S. Geological Survey data release, accessed November 30, 2018, at https://doi.org/10.5066/F7DF6PPB.

Mair, A., Johnson A.G., Rotzoll, K., and Oki, D.S., 2019, Estimated groundwater recharge from a water-budget model incorporating selected climate projections, Island of Maui, Hawai‘i: U.S. Geological Survey Scientific Investigations Report 2019–5064, 46 p., accessed August 23, 2019, at https://doi.org/10.3133/sir20195064.

McJannet, D., Wallace, J., Fitch, P., Disher, M., and Reddell, P., 2007, Water balance of tropical rainforest canopies in north Queensland, Australia: Hydrological Processes, v. 21, p. 3,473–3,484.

Melrose, J., Perroy, R., and Cares, S., 2016, Statewide agricultural land use baseline 2015: University of Hawai‘i at Hilo Spatial Data Analysis and Visualization Research Lab, 101 p., accessed May 22, 2020 at http://hdoa.hawaii.gov/wp-content/uploads/2016/02/StateAgLandUseBaseline2015.pdf. [Prepared for the Hawai‘i Department of Agriculture]

National Oceanic and Atmospheric Administration, 2009a, C-CAP Maui county 1992-era land cover: National Oceanic and Atmospheric Administration, digital file, accessed August 21, 2015 at http://coast.noaa.gov/ccapftp/.

National Oceanic and Atmospheric Administration, 2009b, 2001 Hawaii land cover, Maui and Kahoolawe islands: National Oceanic and Atmospheric Administration, digital file, accessed August 21, 2015 at http://coast.noaa.gov/ccapftp/.

National Oceanic and Atmospheric Administration, 2015, C-CAP land cover, Maui, Hawaii: National Oceanic and Atmospheric Administration, digital file, accessed September 1, 2015, at http://coast.noaa.gov/ccapftp/.

Oki, D.S., 2002, Reassessment of ground-water recharge and simulated ground-water availability for the Hawi area of North Kohala, Hawaii: U.S. Geological Survey Water-Resources Investigations Report 02–4006, 62 p.

Oki, D.S., 2003, Surface water in Hawaii: U.S. Geological Survey Fact Sheet 045–03, accessed November 15, 2018, at https://doi.org/10.3133/fs04503.

Oki, D.S., Engott, J.A., and Rotzoll, K., 2020, Numerical simulation of groundwater availability in central Moloka‘i, Hawai‘i: U.S. Geological Survey Scientific Investigations Report 2019–5150, 95 p., accessed February 4, 2020 at https://doi.org/10.3133/sir20195150.

Rea, A., and Skinner, K.D., 2012, Geospatial datasets for watershed delineation and characterization used in the Hawaii StreamStats web application: U.S. Geological Survey Data Series 680, 20 p., accessed at http://pubs.er.usgs.gov/publication/ds680.

Safeeq, M., and Fares, A., 2014, Interception losses in three non-native Hawaiian forest stands: Hydrological Processes, v. 28, p. 237–254, accessed May 22, 2020, at https://doi.org/10.1002/hyp.9557.

Scholl, M.A., Giambelluca, T.W., Gingerich, S.B., Nullet, M.A., and Loope, L.L., 2007, Cloud water in windward and leeward mountain forests—The stable isotope signature of orographic cloud water: Water Resources Research, v. 43, W12411, 13 p, https://doi.org/10.1029/2007WR006011.

State of Hawaiʻi, 1976, Land use and land cover of the main Hawaiian Islands as of 1976, accessed July 22, 2015 at http://planning.hawaii.gov/gis/download-gis-data-expanded/.

State of Hawaiʻi, 2010a, Aquifer boundaries for the island of Maui, Hawaii: Department of Land and Natural Resources, accessed May 20, 2020 at http://planning.hawaii.gov/gis/download-gis-data/.

State of Hawaiʻi, 2010b, Compilation of data submissions, Part II, PR-2010-01: Department of Land and Natural Resources, Commission on Water Resource Management.

Takahashi, M., Giambelluca, T.W., Mudd, R.G, DeLay, J.K., Nullet, M.A., and Asner, G.P., 2011, Rainfall partitioning and cloud water interception in native forest and invaded forest in Hawaiʻi Volcanoes National Park: Hydrological Processes, v. 25, p. 448–464, accessed May 22, 2020 at https://doi.org/10.1002/hyp.7797. [Special issue on the Hydrometeorology of tropical montane cloud forests.]

Territorial Planning Board, 1939, An historic inventory of the physical, social, and economic and industrial resources of the Territory of Hawaii, First progress report: Advertiser Publishing Co. Ltd., Honolulu.

Thornthwaite, C.W., and Mather, J.R., 1955, The water balance: Publications in Climatology, v. 8, no. 1, 104 p.

U.S. Bureau of the Census, 1921, Fourteenth Census of the United States taken in the Year 1920, Population 1920, Number and Distribution of Inhabitants, Vol. 1, pg. 682, Government Printing Office, Washington, accessed September 1, 2015 at http://www.census.gov/prod/www/decennial.html.

U.S. Bureau of the Census, 1952, U.S. census of population—1950—number of inhabitants: Washington, D.C., U.S. Government Printing Office, v. 1, p. 52–57, accessed September 1, 2015 at http://www.census.gov/prod/www/decennial.html.

U.S. Bureau of the Census, 1981, 1980 census of population—vol. 1—Characteristics of the population, ch. A, number of inhabitants, part 13, Hawaii: U.S. Census Bureau, accessed September 1, 2015, at http://www.census.gov/prod/www/decennial.html.

U.S. Census Bureau, 2012, Population and housing unit counts—2010 census of population and housing: Hawaii, U.S. Government Printing Office, Washington, D.C., CPH-2-13, accessed September 1, 2015, at http://www.census.gov/prod/cen2010/cph-2-13.pdf.

U.S. Census Bureau, 2015, 2015 State geodatabase for Hawaii: U.S. Census Bureau, accessed September 1, 2015, at https://catalog.data.gov/dataset/2015-state-geodatabase-for-hawaii.

U.S. Geological Survey, 2010, LANDFIRE data distribution site: U.S. Geological Survey, Earth Resources Observation and Science Center, at http://landfire.cr.usgs.gov/viewer.

University of Hawaiʻi, 2008, Hawaii agricultural water use and development plan: report submitted to Hawaiʻi Department of Agriculture by College of Tropical Agriculture and Human Resources, Department of Natural Resources and Environmental Management, University of Hawaiʻi at Mānoa, Honolulu, Hawaiʻi, 108 p.

Viessman, W., Jr., and Lewis, G.L., 2003, Introduction to hydrology (5th ed.): Upper Saddle River, N.J., Prentice Hall, 612 p.

Whittier, R.B., and El-Kadi, A.I., 2013, Human and environmental risk ranking of onsite sewage disposal systems for the Hawaiian Islands of Kauai, Maui, Molokai, and Hawaii (draft report January 2013): Honolulu, Hawaiʻi, University of Hawaiʻi at Mānoa, Department of Geology and Geophysics.

Moffett Field Publishing Service Center, California
Manuscript approved September 23, 2021
Edited by Mitchell Phillips and Conner Fisher
Illustrative support by JoJo Mangano
Layout by Kimber Petersen

ISSN 2328-0328 (online)
https://doi.org/10.3133/sir20215113